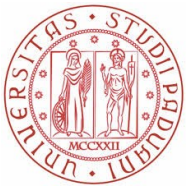

UNIVERSITÀ DEGLI STUDI DI PADOVA

DIPARTIMENTO DI SCIENZE CHIMICHE

CORSO DI LAUREA MAGISTRALE IN CHIMICA

TESI DI LAUREA MAGISTRALE

Exploiting Confined Catalysts in Atom Transfer Radical Polymerization

Relatore: Prof. Cristiano Zonta

Correlatore: Prof. Marco Fantin

Controrelatore: Prof. Alessandro Aliprandi

Laureando: Sebastiano Darè

ANNO ACCADEMICO 2023/2024

INDEX

1 INTRODUCTION 3
1.1 Polymerization reactions 3
1.1.1 Free Radical Polymerization 4
1.1.2 Controlled/Living Radical Polymerization 7
1.1.3 From Atom Transfer Radical Addition to Atom Transfer Radical Polymerization 9
1.1.4 Electrochemically mediated atom transfer radical polymerization 13
1.2 Role of ligands in coordination chemistry 16
1.2.1 Tris(2-pyridilmethyl)amine (TPMA) complexes 16
1.2.2 Application of TPMA complexes in catalysis 19
1.3 Organic cage compounds 19
1.4 Reactivity in molecular and supramolecular cages 21
1.5 TPMA based cage 24
1.5.1 Molecular recognition properties of the novel cage structure 25
1.5.2 Supramolecularly templated cage assembly 26
1.5.3 Chiral Diaza-Cope rearrangement for the preparation of novel macromolecular cages 27
1.5.4 Preparation of the novel cage complex catalyst 30
2 AIM OF THE THESIS 33
3 RESULTS AND DISCUSSION 35
3.1 Characterization of the copper complexes 35
3.1.1 Cyclic voltammetry of Cu2IICAGE(OTf)4 35
3.1.2 Effect of Bromide anions 37
3.1.3 Comparison between Br2Cu2IICAGE2+ and $[BrCu^{II}TPMA]^{+}$ 39
3.1.4 Determination of equilibrium constants for Br^{-} addition to Cu2IICAGE4+ 40
3.1.5 Determination of diffusion coefficients for the Cu-CAGE complexes 41

3.1.6 Determination of the standard rate constant for electron transfer (k^0) for Br2Cu2IICAGE2+ 43

3.2 Application of the Cu/CAGE electrochemically mediated atom transfer radical polymerization 45

3.2.1 Evaluation of the electrocatalytic activation of carbon-bromine bonds in a typical atom transfer radical polymerization initiator 45

3.2.2 eATRP of butyl acrylate in DMF catalysed by Br2Cu2IICAGE2+ 46

3.2.3 Role of the degree of polymerization on butyl acrylate polymerization 49

3.2.4 Measurement of catalyst activity during polymerization 51

3.3 Investigation of the reactivity of the Cu^{I}/CAGE complex with (macro)initiators and of increasing molecular weight 54

3.3.1 Synthetic approach 55

3.3.2 Determination of the diffusion coefficients of the (macro)initiators 59

3.3.3 Voltammetry of Br2Cu2IICAGE2+ and $[BrCu^{II}TPMA]^{+}$ in the presence of the (macro)initiators 60

4 CONCLUSIONS 63

5 EXPERIMENTAL SECTION 65

5.1 Materials and reagents 65

5.2 Instrumentation 66

5.2.1 Potentiostats 67

5.2.2 Gel permeation chromatography (GPC) 67

5.2.3 Nuclear magnetic resonance (NMR) spectrometer 68

5.3 Experimental procedures 68

5.3.1 Electrochemical cell 68

5.3.2 Cyclic voltammetry 69

5.3.3 eATRP 70

5.3.4 Normal ATRP (macroinitiators' synthesis) 71

5.3.5 Macroinitiators purification 72

6 APPENDIX 81

6.1 Appendix A 81

6.1.1 Effect of monomer choice on key polymerization parameters 81

6.1.2 Role of the polymerization initiator 82

6.2 Appendix B 84

6.2.1 Cyclic voltammetries of Cu_2CAGE at varying concentration of bromide anions 84

ABSTRACT

Atom Transfer Radical Polymerization (ATRP) is a powerful method for obtaining highly controlled polymers through the concepts of living polymerization, established via an equilibrium between active radical species and dormant, halogen-capped species. This study aims to explore the application of a novel ligand for the metal catalyst, comprised of two identical tripodal tris(2-pyridilmethyl)amines linked together to form a chiral cage. The goal is to determine how this confined chiral nanospace influences the control and selectivity of ATRP, with the hypothesis that it will enhance selectivity due to the properties of confined spaces. The copper catalyst used operates in its (I) oxidation state for activation and in its (II) oxidation state for deactivation. Activation of the copper (II) catalyst was achieved via potentiostatic chronoamperometry. Voltammetric methods, primarily linear sweep and cyclic voltammetry, were utilized to analyse the behaviour of these complexes. Both analysis and polymerizations were conducted in a 5-necked, jacketed electrochemical cell maintained at 50°C under an inert atmosphere. Kinetic constants of the polymerization of butyl acrylates indicated that the kinetic activation of the halogen-capped, dormant growing chains decreased as the length of these molecules increased. Further studies on polystyrene initiators of different molecular weight showed that as the size of the initiator increased, the catalytic effect of the novel cage catalyst decreased drastically. These findings corroborate the initial hypothesis of dimensional selectivity of the catalytic complex, paving the way for further exploration of the unique possibilities offered by this kind of catalyst.

1 INTRODUCTION

1.1 Polymerization reactions

Polymers are essential materials for modern society. Polymerization mechanisms are crucial in determining the properties of the resulting polymers, such as:

- the number average molecular weight (M_n), that is the statistical average of the polymer chain's molecular weight;
- the weight average molecular weight M_w, which represents the average molecular weight of the polymer chains weighted for their molecular mass, meaning that higher molecular weight species have greater significance on the average;
- the degree of polymerization (*DP*), that is the number of repetitive units constituting a macromolecule;
- tacticity, the organization of eventual stereogenic centres on the chain;
- dispersity (*Đ*), defined as the ratio between weight average molecular weight (M_w) and the M_n.

There are two primary polymerization mechanisms: step growth and chain growth. Step growth or polyaddition proceeds via successive additions between molecules of all degrees of polymerization, the most common example being a series of condensation reactions such as in the production of PET (Polyethylene terephthalate) or nylon polymers. In chain growth, instead, the reaction proceeds between the monomer molecule and a reactive site on the polymer chain with a regeneration of the reactive site at the end of the growth step[1]. Chain growth methods can be anionic, cationic, and radical.

In an anionic polymerization the growth is driven by negatively charged species, usually generated by an initiator such as strong nucleophiles (like *n*-C_4H_9Li) that can attack the C=C bond in the monomer molecules and produce a carbanion which will then start the chain reaction, usually via addition to an electrophilically activated double bond. This method is widely used thanks to the great control over the degree of polymerization and the dispersity of the obtained polymer due to the lack of effective termination and chain transfer processes in most cases.

A cationic polymerization instead is generally started by strong Lewis or Bronsted acids like $AlCl_3$, BF_3 or H_2SO_4 and proceeds by electrophilic attack to the C=C bond in the monomer, forming a carbocation that will act as an electrophile on another monomer molecule,

propagating the polymerization. Due to the extremely high reactivity of the propagating species, trace impurities can lead to significant termination effects, also the inherent instability of the cationic macromolecules increases the likelihood of rearrangements and isomerizations. The cationic mechanism often leads to less controlled polymerizations, subjected to a wide variety of side reactions.[2]

A radical polymerization is characterised by the presence of a radical initiator, which is a specie capable of generating radicals, either via thermal or photochemical homolytic scission of bonds or via redox processes. These primary radicals add to carbon-carbon double bonds of monomer resulting in propagating radicals that further propagate chain growth. Generally, the propagation proceeds in a highly regioselective manner to yield a polymer chain comprised of head-tail linkages. In the absence of catalysts, it is also not a highly stereospecific reaction, except for sophisticated structurally designed monomers. Dispersity of the resulting polymers depends on the possible side reactions and on the mode of termination of the observed process[3].

1.1.1 Free Radical Polymerization

Free radical polymerization (FRP) is widely used in various industrial polymerization processes, particularly in the production of high molecular weight polyolefins. Its versatility allows it to be applied to a wide range of monomers (**Figure 1** under relatively mild conditions, making it a cost-effective method. Additionally, this type of polymerization has a high tolerance for impurities, making it simpler to implement since it is less dependent on highly purified solvents and reagents. However, a significant downside of free radical polymerization is the difficulty in controlling the growth of polymer chains due to the high reactivity of the radicals involved. This leads to very high propagation rates which, combined with the slow rate of initiation, cause the polymers to grow rapidly before complete initiation can occur, and terminating at different times and lengths. As a result, the polymers produced often have irregular structures and broad molecular weight distributions.

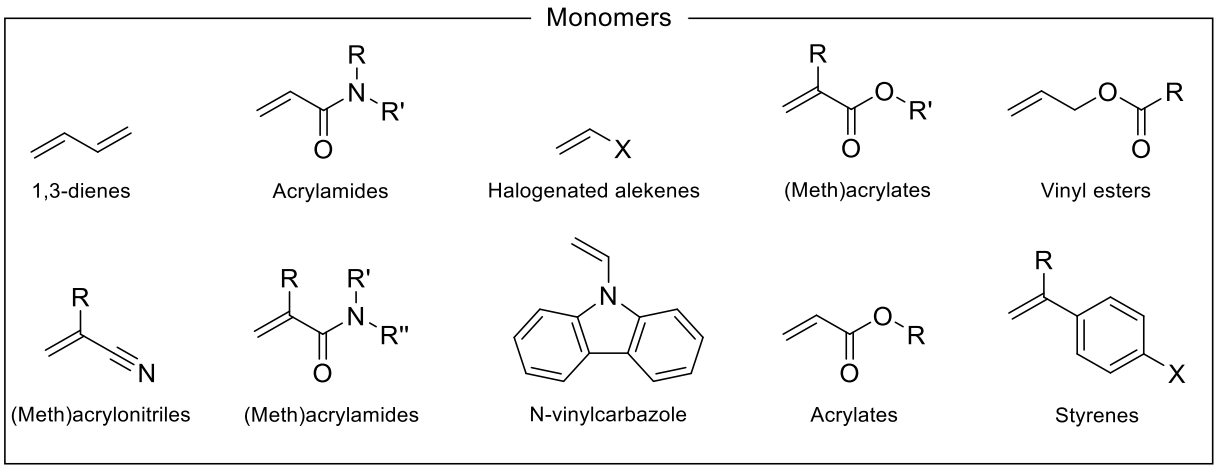

Figure 1 Typical monomer choices for radical polymerizations.

A free radical polymerization is comprised of three main phases:

- The initiation, which involves two distinct steps, of which the chemical reactions are described in (1.1) and (1.2), together with the corresponding expression for the reaction rate. The first step is the homolytic cleavage of a bond, leading to the formation of two radical species and can be induced mainly thermically, photochemically or electrochemically. The second step consists of the reaction between the newly generated radical specie with the monomer to form a propagating radical (P_n).

$$\mathrm{In} \longrightarrow 2\mathrm{R}^{\bullet} \qquad v_{\mathrm{d}} = 2 f k_{\mathrm{d}}[\mathrm{In}] \tag{1.1}$$

$$\mathrm{R}^{\bullet} + \mathrm{M} \longrightarrow \mathrm{P_n}^{\bullet} \qquad v_{\mathrm{i}} = k_{\mathrm{i}}[\mathrm{R}^{\bullet}][\mathrm{M}] \tag{1.2}$$

  The *f* factor in the expression for the rate of initiator dissociation represents the initiation efficiency, which is the ratio between the number of radicals that actually propagate the polymerization and the total number of radicals that are generated. Typical *f* factors are 0.5 - 0.8.

  The rate determining step consists in the first reaction (1.1) and has a much smaller rate constant than that of the second step. Usually, the rate constants have values of $k_d \approx 10^{-5}$ s^{-1} and $k_i > 10^4$ $M^{-1}s^{-1}$, allowing the system to reach a stationary state regarding the concentration of R•, keeping its concentration very small and approximately constant.

- The second phase is propagation, where the generated radicals grow via radical addition to the monomer in a chain reaction.

$$P_n^{\bullet} + M \longrightarrow P_{n+1}^{\bullet} \qquad v_p = k_p[P_n^{\bullet}][M] \tag{1.3}$$

The propagation rates heavily depend on monomer choice but typically k_p assumes values around 10^2 – 10^4 $M^{-1}s^{-1}$.

- Termination is the irreversible conclusive step of a free radical polymerization. These reactions have two main mechanisms, which are coupling and disproportionation respectively:

$$P_m^{\bullet} + P_n^{\bullet} \longrightarrow P_m{-}P_n \qquad v_{tc} = 2k_{tc}[P_m^{\bullet}][P_n^{\bullet}] \approx 2k_{tc}[P_n^{\bullet}]^2 \tag{1.4}$$

$$P_m^{\bullet} + P_n^{\bullet} \longrightarrow P_m(-H) + P_n(+H) \qquad v_{td} = 2k_{td}[P_m^{\bullet}][P_n^{\bullet}] \approx 2k_{td}[P_n^{\bullet}]^2 \tag{1.5}$$

The coupling mechanism involves the reaction between two radical species forming a σ bond. The disproportionation also occurs between two growing chains but it results in the abstraction of an hydrogen atom from a growing macromolecule forming a π bond on one chain, and a C−H bond in the other. The termination reaction rate constants are extremely high, usually close to the diffusive limit, with values spanning from 10^7 to 10^9 $M^{-1}s^{-1}$. The termination rates depend on a variety of factors, like monomer type and conversion. As the reaction proceeds, the concentration of available monomer decreases, decreasing the propagation rate. This causes a relative increase in termination reactions. Usually less sterically hindered monomers, like styrene, favour the coupling termination while poly-substituted molecules, such as methyl methacrylate (MMA), have much higher rates of disproportionation.

The measured average molecular weights of macromolecules generated by free radical polymerization are often lower than predicted by accounting for initiation, propagation and termination processes. This experimental observation can be attributed to chain transfer reactions, described as follows:

$$P_n^{\bullet} + T \longrightarrow P_n + T^{\bullet} \qquad v_{CT} = k_{CT}[P_n^{\bullet}][T] \tag{1.6}$$

Where the transfer agent (T) can be the monomer, the initiator, the solvent, another macromolecule or other deliberately added transfer agents. The reaction consists of an abstraction of a weakly bonded atom from the T to a growing chain radical, causing the formation of a dead chain (without an active growing site) and a new free radical, which might in turn react with other molecules like the monomer. These processes cause the macromolecules generated to branch out (if a chain transfer reaction involves an internal hydrogen on a chain it generates a non-terminally positioned active site, causing the polymer to form a branch) or to be shorter due to their termination by hydrogen or halogen abstraction, capping the active

site.[4] Since the radical concentration is constant, chain transfer reactions typically do not retard the polymerization rate.

1.1.2 Controlled/Living Radical Polymerization

The concept of living polymerization is known since 1956, when it was first reported by Szwarc[5] regarding an anionic polymerization of styrene in a non-protic solvent (THF), impeding the termination of the reactive, carbanionic, chain-end with a proton donation from the solvent. This causes the polymerization to proceed up to theoretically a conversion of 100% without termination; if further monomer were to be added the polymerization would start again, hence the term “living”, meaning that providing food (monomer) to the polymeric chain would keep it growing.

A living polymerization is characterized by five main properties:

i) a fast and complete initiation,
ii) low polydispersity ($Đ < 1.5$),
iii) a high control on the resulting molecular weight,
iv) a linear relationship between M_n and monomer consumption
v) first order kinetics, meaning that the active chains concentration is constant.

In order to obtain these conditions a variety of methods can be designed, spanning from anionic mechanisms, as discussed above, to cationic or radical polymerizations.[6] Since the main objective of this work is the study of a living radical polymerization method, only this kind of process will be discussed further.

Obtaining a controlled/living radical polymerization (CRP) means, in a simplified way, avoiding the possibility of side reactions and termination of the growing chains. To achieve this, great success has been found in exploiting equilibriums between active and dormant species, preferably shifted towards the latter in order to obtain a low concentration of active radical species at any given moment. This allows the polymerization to proceed while reducing the likelihood of termination or chain transfer since all those reactions scale with increasing concentration of radicals.

CRPs often rely to an effect called the persistent radical effect (PRE), a feature that allows a sort of self-regulating capacity to certain controlled radical polymerization systems. As shown in **Scheme 1**, the propagating radicals are quickly trapped by the deactivation

process (k_{deact}) by a specie X, which is typically a stable radical such as nitroxide or organometallic compounds. The dormant species P_n-X are instead activated (k_{act}) either with the usual mechanism of initiation (thermal, photochemical or redox) or thanks to an appropriate catalyst to reform the growing centres. Due to the reversibility of the trapping mechanism, this process is also called reversible deactivation radical polymerization (RDRP). The persistent radicals X cannot undergo termination but can only reversibly cross-couple with the growing species. This causes an accumulation of X for every radical-radical termination event, leading to an increase in persistent radicals as the polymerization proceeds, following a peculiar 1/3 power law.[7] Consequently the concentration of radicals and the probability of termination decreases at increasing conversion.

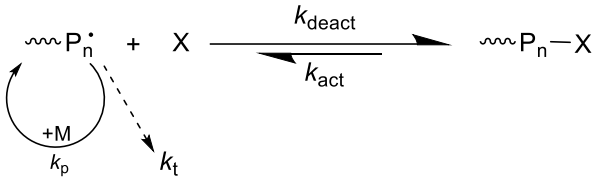

Scheme 1 Reversible activation/deactivation equilibrium allowing the establishment of a persistent radical effect.

The dynamic equilibrium between dormant and active species allows the establishment of a PRE, while the rates of initiation sought after in CRP are often very high. These conditions practically result in the following characteristics:

- Increase in average life of the propagating chain, from the few seconds of a traditional free radical polymerization to several hours or days.
- The fast initiation allows for almost instantaneous activation of all growing chains, ultimately leading to controlled architecture and molecular weight.
- Termination and intermolecular chain transfer events are drastically reduced directly thanks to the PRE, which minimizes the concentration of active radicals at any given moment, highly reducing the likelihood of reaction between radical species.
- The degree of polymerization (*DP*) increases linearly with conversion, since all chains are activated simultaneously and there are no termination reactions, the number of growing chains is equal to the number of added initiator's molecules. Consequently, considering that all chains have the same probability and rate of growth, it is easy to determine the *DP* at any given point of the polymerization as the ratio between consumed monomer and initiator numbers of moles.

$$\mathrm{DP} = \frac{\mathrm{MM_p}}{\mathrm{MM_m}} = \frac{\Delta[\mathrm{M}]}{[\mathrm{In}]_0} = \frac{[\mathrm{M}]_0}{[\mathrm{In}]_0} \times \frac{[\mathrm{M}]}{[\mathrm{M}]_0} = \frac{[\mathrm{M}]_0}{[\mathrm{In}]_0} \times \mathrm{conversion} \qquad (1.7)$$

Where MM_p and MM_m are the molecular masses of the polymer and the monomer respectively, while [M] is the concentration of monomer, [In] is the concentration of initiator and the zero at the subscript refers to the initial concentrations.

- All these qualities combined often allow to achieve narrow molecular weight distributions ($Đ$ < 1.2) which are much better than the usual free radical polymerization polydispersities of 1.5 to 2, depending on the prevalent mechanisms of termination.
- Finally, thanks to the protective effect of the deactivating species, which allows minimized termination events, the chain-end functionalities can be preserved. In CRP usually only about 10% of the chains terminate, so adding further monomer at the end of the polymerization should restart it, enabling a high degree of control on molecular weights and composition of block copolymers or other complex structures.

Other than the RDRP mechanism in **Scheme 1**, another possibility to obtain a controlled radical polymerization is found in degenerative transfer processes (**Scheme 2**), where the system follows typical FRP kinetics, constituted by slow initiation and fast termination. However, the transfer agent is much more concentrated than the radical initiator, thus playing the role of dormant specie. A fast exchange between active and dormant species is required to allow high control over the polymerization. In this way, there is a low but constant concentration of active radicals, reducing termination and intermolecular chain transfer reactions and making the polymerization “living”.

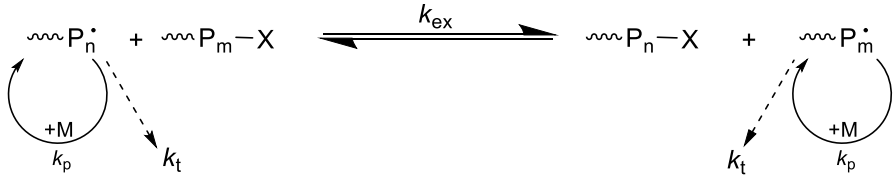

Scheme 2 Degenerative transfer equilibrium.

1.1.3 From Atom Transfer Radical Addition to Atom Transfer Radical Polymerization

Atom transfer radical addition (ATRA) is a widely used reaction in organic synthesis[8] to addition a halogenated compound to an alkene or alkyne. In this technique, an atom transfer from an organic halide to a transition metal complex occurs to form organic radicals, quickly deactivated by back transfer to the oxidized metal complex. The conditions are carefully

chosen to inhibit propagation reactions (k_p << k_{deact}) and so that the activation of the mono-adducted product is much less favourable than that of the initial alkyl halide, allowing to obtain mainly the halide functionalized monoadduct.[9] The optimization of this process during the years lead to results that paved the way for the development of controlled radical polymerizations, like the optimization of the metal catalysts, ligands and alkyl halides.

Following this results, in 1995 Matyjaszewski[10] and Sawamoto[11] independently reported for the first time one of the now most widely used CRP methods, revolutionizing the field of radical polymerization. This process, known as atom transfer radical polymerization (ATRP), is based on a reversible activation/deactivation equilibrium enabled by a transition metal catalyst, establishing a PRE as discussed in the previous section (**Scheme 1**).

The ATRP equilibrium is established between initiating alkyl halides/macromolecular species (P_n-X) and their respective active radical form, and it is promoted by a transition metal catalyst which can expand its coordination sphere and increase its oxidation state. The metal centre is complexed to a ligand (M^n/L), and is responsible for the cleavage of an alkyl halogen bond RX, generating the radical specie R• and the higher oxidation state (XM^{n+1}/L) metal complex. The organic radical formed can then react with the vinyl monomer to propagate the polymerization, terminate as in conventional free radical polymerization or be reversibly deactivated in the same ATRP equilibrium, to form a halide-capped dormant chain. The equilibrium constant (K_{ATRP}) is defined as:

$$K_{\mathrm{ATRP}} = \frac{k_{\mathrm{act}}}{k_{\mathrm{deact}}} \tag{1.8}$$

where k_{act} ($M^{-1}s^{-1}$) is the activation rate constant and k_{deact} ($M^{-1}s^{-1}$) is the deactivation rate constant. Typically, the most used metal catalysts involve the Cu^{II}/Cu^{I} couple in the presence of an amine ligand.

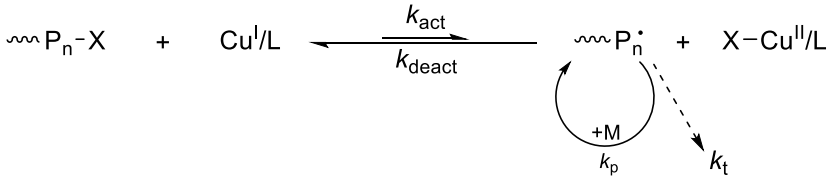

Scheme 3 Copper mediated atom transfer radical polymerization equilibrium.

In ATRP, the equilibrium between active and dormant species is heavily shifted towards the latter ($k_{act} << k_{deact}$), allowing the persistent radical effect to take place and as such minimizing termination reactions and favouring simultaneous growth of all the chains. The key components of an ATRP are the monomer (M), the initiator (RX), the metal catalyst (usually copper or iron), the ligand necessary to form the active metal complex (L), the counterion (X) for the metal complex and the solvent. Typically, the initiator is an alkyl halide "activated" by an electron attractive group (COOR, CN…) attached to the halogenated carbon in the α position, but it could also be a radical stabilizing group like a phenyl. The most widely used halogens for ATRP are chlorine and bromine; iodine can also be used but its extremely high activity, stemming from the weaker C-X bond, makes it difficult to utilize successfully. The structure-activity relationship in initiators has been thoroughly studied and resulted in the empirical order reported in **Figure 2**.[12]

The ligand chosen to form the catalytic complex is also a crucial factor in ATRP kinetics, and it has been in turn widely studied. A strong correlation between the reduction potential of the copper(II) complex and its K_{ATRP} has been reported for numerous commonly used ligands (**Figure 3**).[13]

The general order of activity for the copper complexes seems to follow the order: tetradentate (branched) > tridentate > tetradentate (linear) > bidentate. A higher activity copper complex (lower K_{ATRP}) is best paired with less reactive monomers, while a less active catalyst is more suited to highly reactive monomers, which would otherwise form an excessive amount of radical species, compromising the persistent radical effect required to obtain a controlled polymerization.

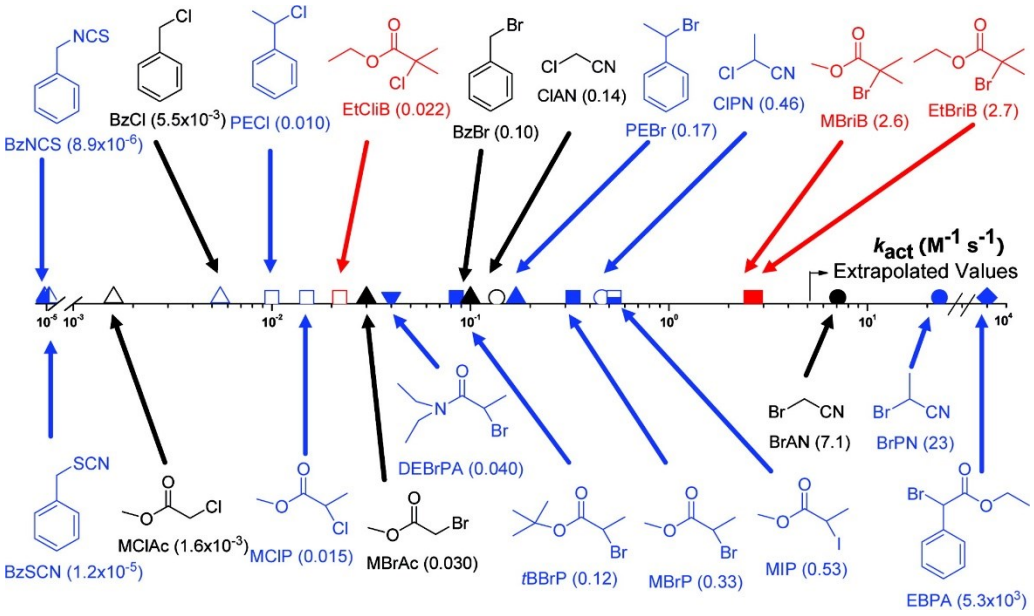

Figure 2 ATRP activation rate constants for various initiators with Cu^{I}X/PMDETA (X = Br or Cl) in MeCN at 35 °C: 3°, red; 2°, blue; 1°, black; isothiocyanate/thiocyanate, left half-filled; chloride, open; bromide, filled; iodide, bottom half-filled; amide, ▾; benzyl, ▴; ester, □; nitrile, ○; phenyl ester, ◇. Figure adapted from reference [12].

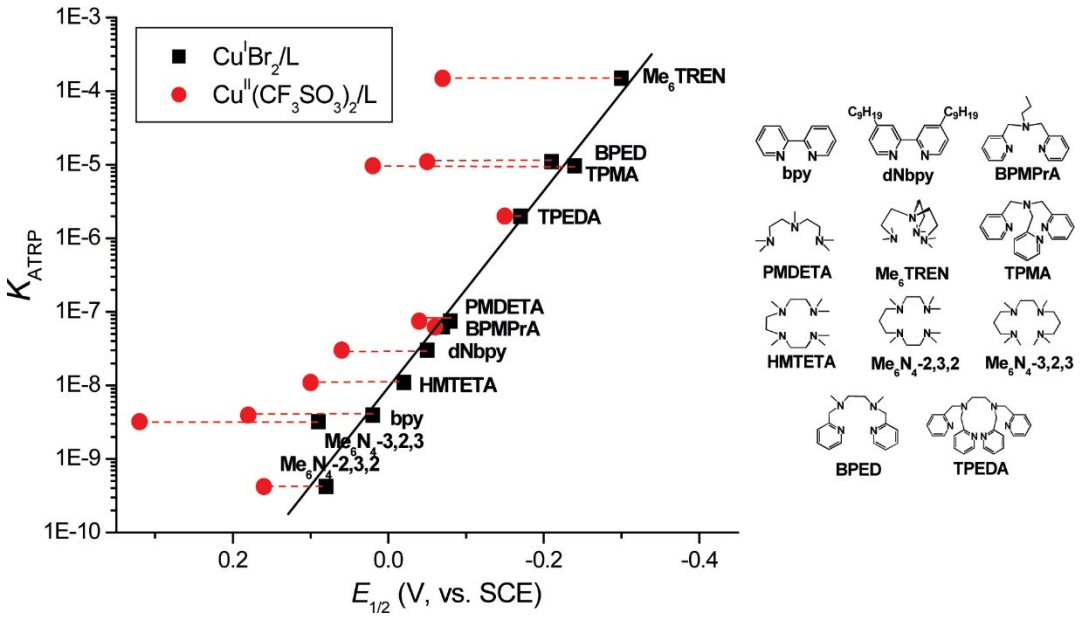

Figure 3 Correlation of K_{ATRP} (measured with ethyl 2-bromoisobutyrate) with the redox potentials ($E_{1/2}$) of Cu^{II}(CF$_3$SO$_3$)$_2$/L and Cu^{II}Br$_2$/L in CH$_3$CN.[14]

A broad range of solvents has been successfully utilized to perform ATRP, discovering it also plays a crucial role in the reaction kinetics. A general trend observed is that the catalyst

increases its activity (higher k_{act}) as the polymerization medium (solvent + monomer) increases in polarity.[15] A qualitative explanation of this phenomenon is that the copper(II) formed during the activation of the RX species is strongly stabilized in more polar solvents due to its higher charge and more "polar" character, ultimately leading to a higher rate of activation and an overall higher K_{ATRP}. The actual parameters factoring in this behaviour are more complex and include the solvent dependence on the affinity of the copper complexes for halide anions (halidophilicity), on the electron transfer to the copper complexes, and on the electron affinity of the utilized halogen atoms. [14]

The ATRP's rate of polymerization is expressed as the following equation:

$$R_{\mathrm{p}} = k_{\mathrm{p}}[\mathrm{M}][\mathrm{P_n}^{\bullet}] = k_{\mathrm{p}}[\mathrm{M}]K_{\mathrm{ATRP}}[\mathrm{P_nX}]\frac{[\mathrm{Cu^I/L}]}{[\mathrm{XCu^{II}/L}]} \qquad (1.9)$$

where k_p ($M^{-1}s^{-1}$) is the propagation rate constant of the monomer in conventional radical polymerization, [M], [P_n•] and [P_nX] are respectively the concentrations of monomer, active radicals and alkyl halides, which is theoretically the same as the concentration of initiator added. [Cu^I/L] and [XCu^{II}/L] are the concentrations of copper complexes in the respective oxidation state.

1.1.4 Electrochemically mediated atom transfer radical polymerization

Even though the catalyst concentration does not influence the rate of polymerization, as expressed in equation 1.9, a significant amount of metal complex is still required. This is caused by the termination events of the polymerization, which lead to irreversible accumulation of deactivating Cu(II) complex since the radicals formed via the activation reaction can terminate and can no longer engage in the opposite, deactivating, reaction. Although the termination reaction typically involves only about 10% of the chains, the concentration of initiator is usually relatively high, leading to the necessity of increasing the amount of catalyst to exceed the concentration of terminated chains expected. To overcome this problem, a variety of methods mainly based on the regeneration of Cu(I) during the polymerization have been developed and are summarized in **Figure 4**.[16]

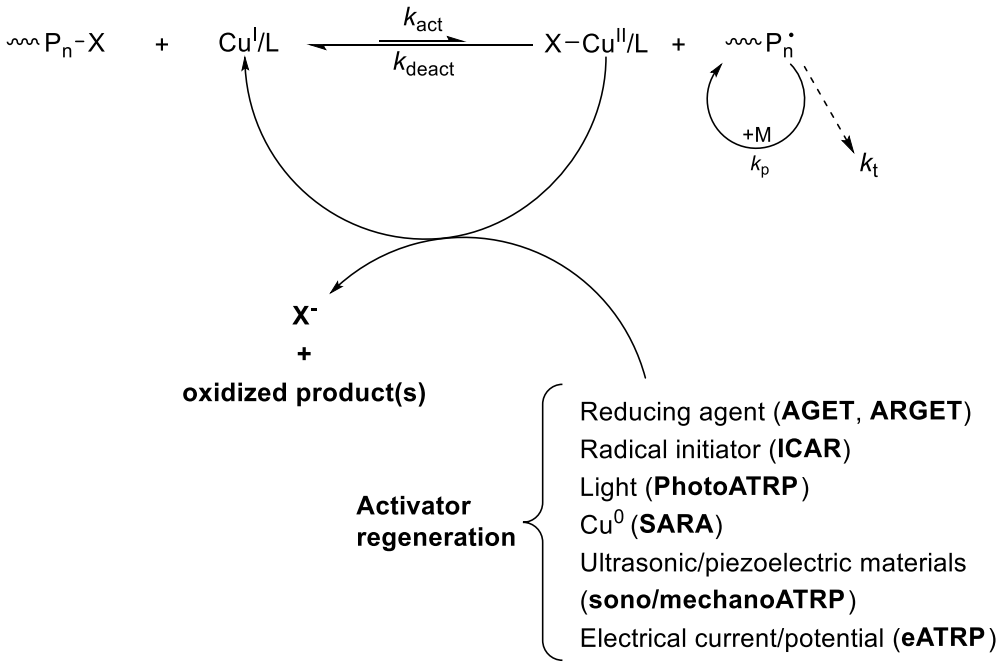

Figure 4 Mechanism of ATRP with regeneration of activating [Cu^{I}/L]. Image adapted from reference [16].

This allows to reduce catalyst loading to ppm amounts, making the reaction cheaper and more practical to purify. Of the possible methods of Cu(I) regeneration one of the more promising and recently developed is electrochemically mediated ATRP.[17,18] This involves the regeneration of the activating form of the catalyst by reducing it at an electrode. One of the upsides of this method is the possibility of setting up the experiment starting from the air stable Cu(II) complex, reducing it in situ to its active form and starting the polymerization.

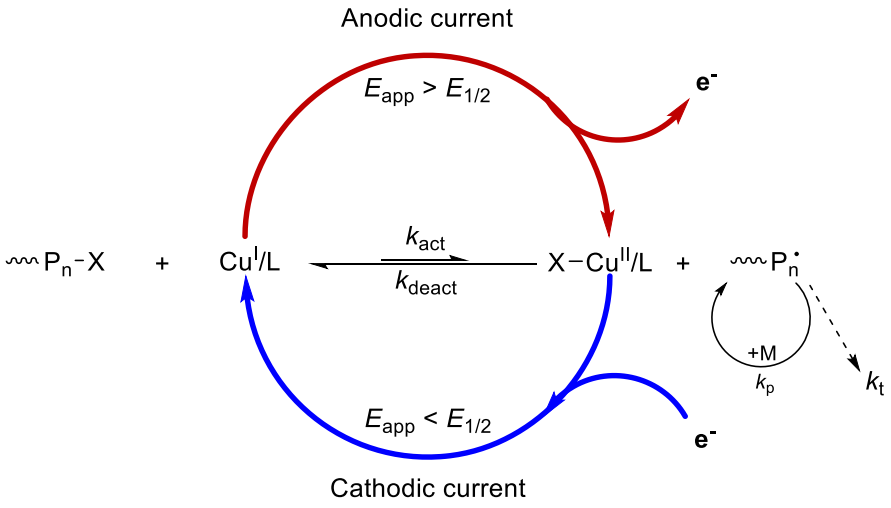

Figure 5 General mechanism for electrochemically mediated ATRP.

Once the chosen potential is applied, the ratio between activating Cu(I) and deactivating Cu(II) complexes is determined by the Nernst equation:

$$E_{\mathrm{app}} = E^0 + \frac{RT}{nF}\ln\frac{[\mathrm{Cu^{II}}]}{[\mathrm{Cu^{I}}]} \tag{1.10}$$

which can easily be rearranged in equation 1.11.

$$\frac{[\mathrm{Cu^{II}}]}{[\mathrm{Cu^{I}}]} = \exp\left[\frac{nF}{RT}(E^0 - E_{\mathrm{app}})\right] \tag{1.11}$$

where [Cu^x] is the concentration of copper complex in the respective oxidation state, n is the number of electrons transferred in the redox process, F is the Faraday constant (96485 C/mol), R is the universal gas constant (8.314 J K^{-1} mol^{-1}), T is the temperature (K), E_{app} is the potential applied at the electrode (V) and E^0 is the standard reduction potential of the [XCu^{II}/L]$^+$/[Cu^I/L]$^+$ couple (V). This choice of E_{app} in electrochemical ATRP, in absence of mass transport limitations (stirring is needed to diffuse the Cu(I) catalyst in the whole reaction mixture), allows precise control of the [Cu^{II}]/[Cu^I] ratio, where a higher value of this parameter (induced by a more positive applied potential) leads to slower polymerizations and eventually, by raising further the potential, to stopping it completely. The opposite scenario, induced by a more negative E_{app} makes the polymerization faster, at the cost of progressively inferior control as the applied potential becomes more negative, due to decreasing concentrations of Cu(II) deactivator and loss of the persistent radical effect.

A relatively important downside of eATRP is the need to add a relatively high concentration of supporting electrolyte to the polymerization medium, which is required to allow the electric current to flow through the solution.

A typical eATRP setup includes an electrochemical cell in which the polymerization takes place, three electrodes including a working (WE), a reference (RE) and a counter electrode (CE), and a potentiostat instrument. The WE is the component where the catalyst undergoes reduction. It typically features a high surface area to facilitate rapid electron transfer to the metal complex. The WE is commonly made from a noble or non-reactive metal, such as platinum mesh, though various more cost-effective alternatives are currently being explored.[19] The RE is a separated electrode containing an electrochemical couple having a well-defined and stable redox potential and its used to measure accurately the potential applied at the WE. The counter electrode has the role of closing the circuit, allowing the current emitted from the working electrode a way out of the electrolytic solution and it's also

in a separated cell to prevent contamination of the reaction mixture with the products of the anodic reaction. The setup can be significantly simplified by applying a constant current instead of a constant potential, eliminating the need for a reference electrode. A further simplification consists in the use of a sacrificial counter electrode, like an aluminium wire, removing the need for a separated cell at the cost of the dissolution of Al^{3+} ions in the polymerization medium.[18]

1.2 Role of ligands in coordination chemistry

As previously discussed, the ligand selected for the ATRP catalyst plays a crucial role in its reactivity and behaviour. In coordination chemistry, ligands are often employed as a mean to manipulate the reactivity and behaviour of the complexes by tuning the environment around the metal centres to obtain precise modifications on their electronic and steric properties.[20] One of the main challenges in the scientific community is the synthesis of molecular structures mimicking and improving on the characteristics of their biological equivalents.

Synthetic complexes represent a broad category of catalysts constituted by metal centres surrounded by organic ligands and the activity of these compounds relies on both the metal ion and the ligands. Besides catalyst's activity, metal complexes have also been used as building blocks for supramolecular structures capable of molecular recognition[21] and catalysis.[22] A large group of well-studied polydentate ligands is found in polypyridines, particularly a large fraction of these is constituted by tripodal ligands having three pyridyl cycles linked to a central nitrogen atom. These tris-pyridyl amines have been widely studied in catalysis, particularly on the possibility of modulating steric and electronic properties of the ligand by modifying the substituents on the pyridyl units.[23]

1.2.1 Tris(2-pyridilmethyl)amine (TPMA) complexes

The simplest version of this class of compounds is the tris(2-pyridylmethyl)amine (TPMA), that has been extensively employed thanks to the capability to form stable complexes with a wide range of metals.

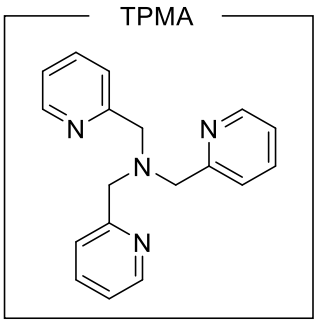

The first synthesis of TPMA was reported in 1977 by Anderegg et al.[24] and was obtained via the reaction reported in the left of scheme 4. While this method remains the prevalent synthetic route to obtain TPMA, in recent years a valuable alternative was found in the reductive amination of an aldehyde precursor with ammonium acetate to furnish the nitrogen atom and sodium tryacetoxyborohydride as the mild reducing agent.[25] This method is most useful in the presence of sensitive functional groups since its more tolerant than the previous.

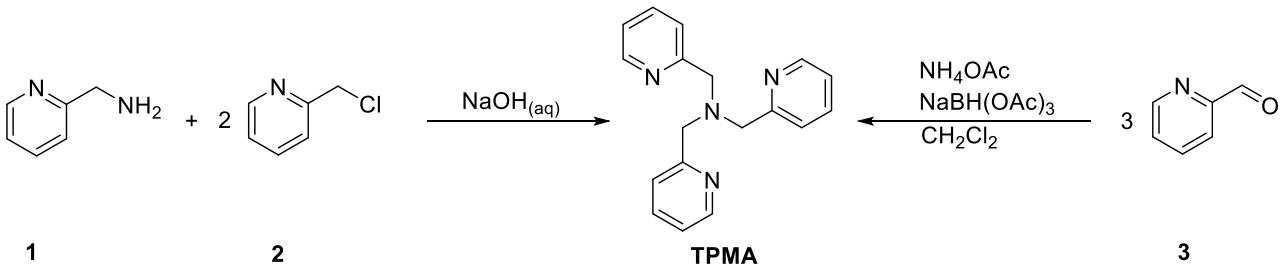

Scheme 4 Two possible strategies for the synthesis of the tris(2-pyridylmethyl)amine. On the right the synthesis reported by Anderegg[24], on the right the reductive amination based synthetic route.

This ligand usually binds in a 1:1 stoichiometry metal to ligand, and assumes a trigonal bipyramidal complexation geometry, where one apical position is occupied by the aminic nitrogen, while the other by a solvent molecule or a counterion.[26] There are some less common exceptions, like the ones displayed in **Figure 6**, where the complex can also assume an octahedral or tetrahedral configuration.

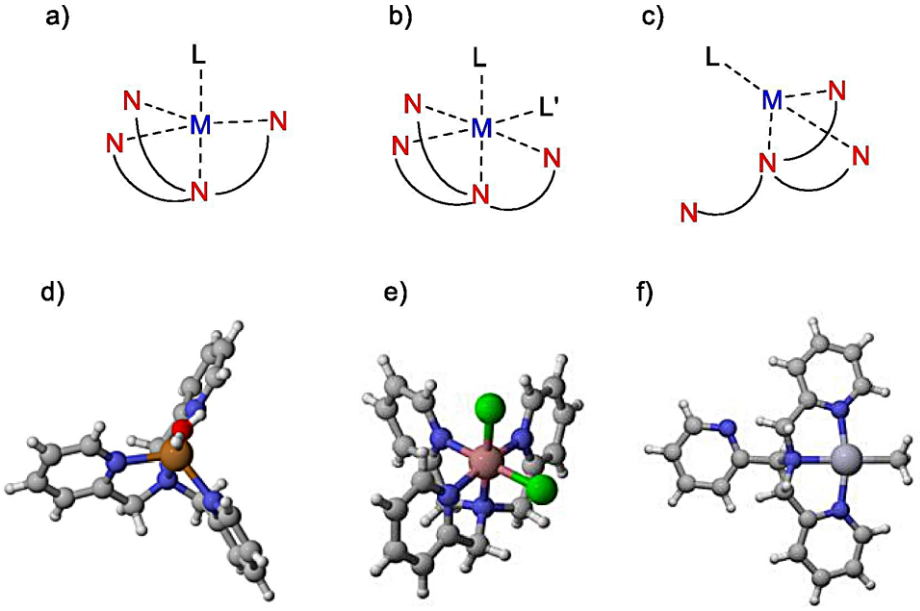

Figure 6 Common coordination geometries in **TPMA** complexes. a) trigonal bipyramidal; b) octahedral and c) tridentate and corresponding examples of d) Copper(II)[27], e) Cobalt(III)[28], f) Platinum(II) complexes[29]. Figure adapted from reference [26].

Other very interesting properties arise from the stereochemical arrangement of the ligand, which in its trigonal bipyramidal geometry assumes a propeller-like configuration (**Figure 7**). At room temperature, in solution, the ligand constantly interchanges between the two helical enantiomeric forms (Δ ⇌ Λ). Addition of a second stereogenic element, linked either covalently or non-covalently, leads to two different diasteroisomers that can therefore lead to a preferential helical arrangement based on their different stability.

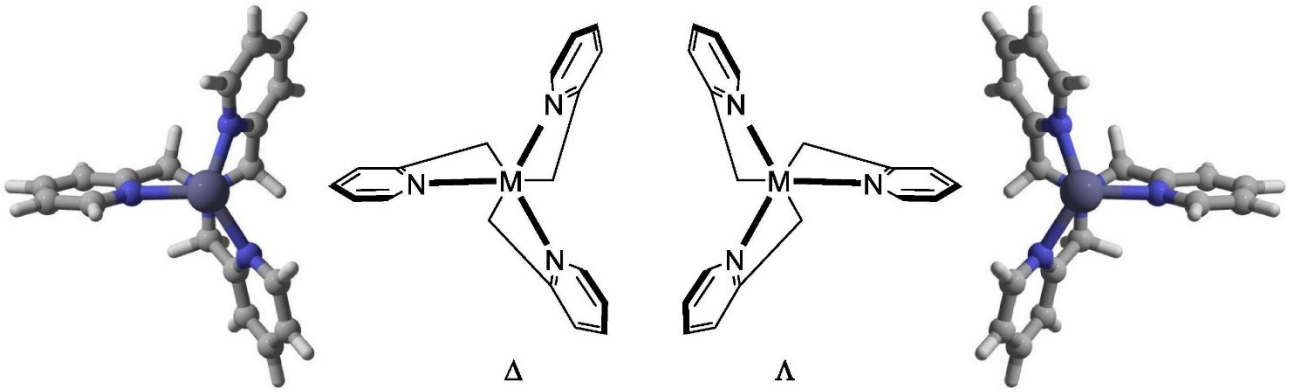

Figure 7 Δ (clockwise) and Λ (counterclockwise) conformation of TPMA ligands wrapped around a metal centre. Figure adapted from reference [26].

1.2.2 Application of TPMA complexes in catalysis

TPMA metal complexes have been extensively employed for catalytic purposes, like nickel(II), iron(II) or cobalt(II) complexes with TPMA have been studied for the hydrogen evolution reaction[30,31]; carbon dioxide reduction employing cobalt(II)-TPMA[32–34] and lastly ATRA and ATRP using copper(II)-TPMA.[23] Zinc(II)-TPMA systems have also been studied for their properties of molecular recognition if paired with an exciton coupled circular dichroism analysis.[35]

1.3 Organic cage compounds

According to the IUPAC, a cage compound is a polycyclic compound shaped as a cage.[1] Over the last decade, a series of species with well-defined inner void spaces, defined as cages and capable of accommodating molecular guests, have been prepared and studied. The first reported example of organic cage compound having a clear function is dated 1984, when Vögtle's group published the synthesis of a shape-persistent cage which was a better ligand to Fe^{3+} ions than EDTA.[36] Shape-persistent means that the obtained cage compound has a large and defined interior capable of hosting other molecules and it does not collapse to a more dense or twisted structure.[37] Synthesis of these compounds can be carried out in two main routes: using irreversible bond formation, i.e. amidation and cross-coupling, which robustly results in highly chemically stable compounds in often low yields; the other route is through synthesis of the thermodynamically preferred product by reversible bond formation, resulting in higher yields and facile synthesis from relatively simpler molecular precursors but the obtained cage compound has a lower chemical stability.[37] The second route is now the most widely applied and is based on the work of Marie Lehn, who first introduced the concept of dynamic covalent chemistry (DCC), allowing to exploit a virtual combinatorial library to obtain the most thermodynamically favoured product.[38] In more recent years, chemists have increasingly adopted the use of DCC to synthesize organic cage compounds with covalent bonds.[39]

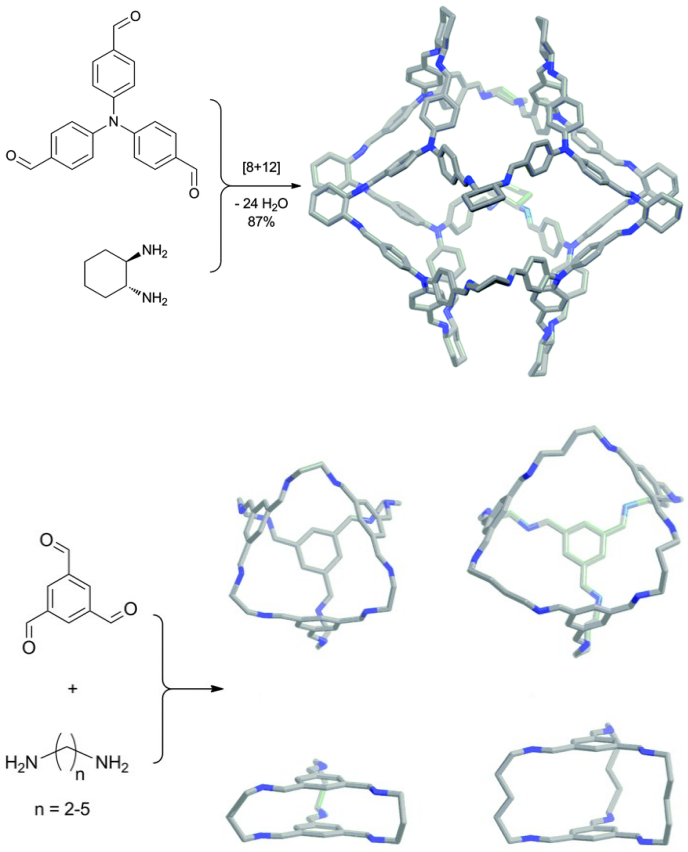

Figure 8 Examples of imine condensation-based synthesis of molecular cages. Images adapted from reference [37].

Among this broad range of possible reactivities, reversible imine bond formation takes on the main role of most commonly applied method of organic cage compounds' synthesis.

These compounds can express multiple useful properties, the most characteristic of which is molecular recognition of specific guests, made possible by the "void" space present within the cage compound. Selective recognition is still a topic of interest as shown in relatively recent publications, spanning from differential binding of simple ions to recognition of dicarboxylic guest of different alkyl chain length through a chiral organic cage compound.[37,40,41] Other useful applications of the molecular cages are found in stabilization of reactive compounds, as shown by Warmuth and co-workers, which managed to *in-situ* encapsulate an highly strained Bredt olefine via imine bond formation of a precursor, successively irradiated rendering the highly reactive polycyclic Bredt alkene which was then stable for days at room temperature.[42]

(a)

(b)

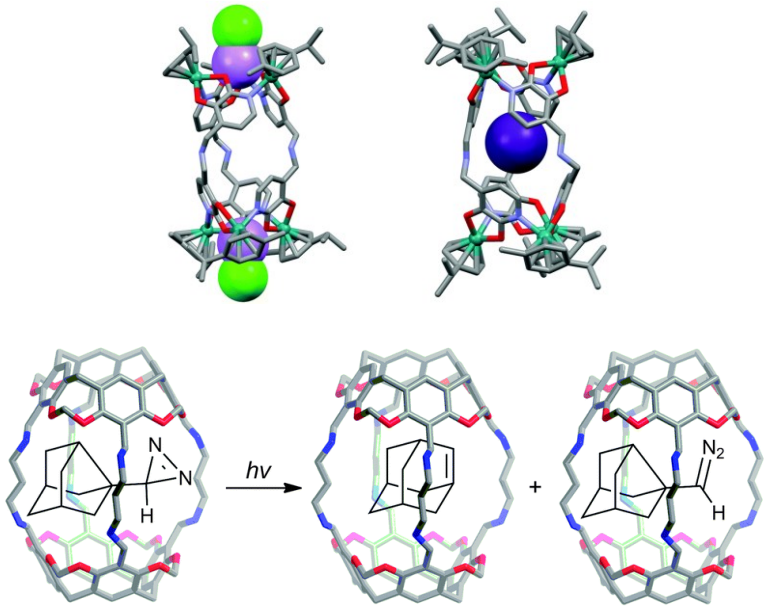

Figure 9 (a) Molecular structures of the Cs^+ (left) and the bis-LiCl (right) adducts of cage in the solid state.[40] (b) Photochemistry of encapsulated 3-noradamantyldiazirine (Bredt olefin).[42] Images adapted from reference [37].

1.4 Reactivity in molecular and supramolecular cages

As previously discussed, the cavity within the organic cage compounds is characterized by unique properties, allowing for interesting effects on the reactivity of various compounds. The confined and isolated environment provided inside the cage is often completely different from the one found in the bulk solution. The confined microenvironment can govern the host-guest interaction in terms of substrate orientation and reactive conformation. This specific interaction can modulate the reactivity in a few different ways: reducing the reaction free energy by stabilization of the transition state, increasing the local concentration of reactants, impeding unfavourable reaction pathways. An examples is the cage-catalysed Micheal addition reported in a recent paper of Lusby and colleagues, showing an up to six orders of magnitude improvement in the reaction rate, mainly thanks to pre-orientation effects and stabilization of the anionic intermediate.[43] Looking at the chemistry of supramolecular cages, which are cage compounds held together and organized by means on intermolecular interactions, we can find many more examples of reactivity in confined spaces. Namely, metal organic cages (MOCs) are discrete molecular architectures with well-defined shape, size and geometry, obtained through self-assembly of multiple metallic ions and multidentate ligands.[44]

These systems are widely studied for their catalytic properties, which follow the same mechanistic principles mentioned above. A series of notable examples will be now presented in order to best clarify how each mechanism can play a role in catalysis.

Numerous reports of metal organic cages catalytic effects is found in the literature,[45] starting from simpler reactions, like MOC-catalysed amide hydrolysis. This process is based on the preorganization of the amidic substrate guest, which causes it to twist inside the cavity and inducing a strain on the amide's structure, enhancing its reactivity towards the base catalysed hydrolysis of amides.[46]

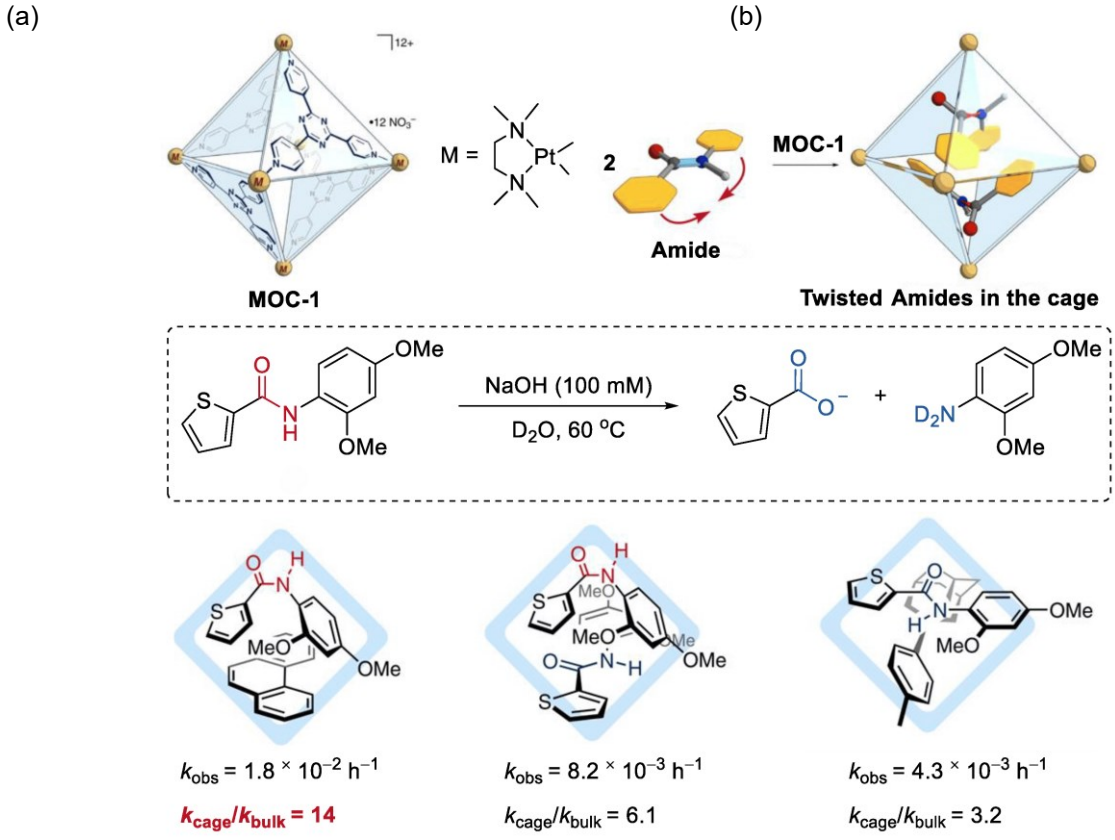

Figure 10 Hydrolysis of amides catalysed by **MOC-1** by mechanically twisting them within the cavity of the cage. Reaction additions: Amide (2.4 mM), co-encapsulated guest agent (Phenanthrene) (1.05 eq.), MOC-1 (2.4 mM), NaOH (100 mM), 60 °C, D_2O. Image adapted from reference [46].

Another viable catalytic route is based on the increase in local concentrations, like the metal-organic cage proposed by Reek and colleagues managed to accomplish.[45] **MOC-3** is a cage ($Pd_{12}L_{24}(OTf)_{24}$) with tuneable high concentrations (0.05 M to 1.1 M) of gold(I) catalyst within the cavity. In fact the $M_{12}L_{24}$ nanosphere strongly encapsulates gold complexes

functionalized with sulfonate group, up to 24 gold centres per cage, drastically increasing the local concentration of catalyst for hydroalkylation of allenols and enabling a strong catalytic effect, as demonstrated by the fact that in the same conditions the same gold complex is inactive in absence of the **MOC-3**.[47]

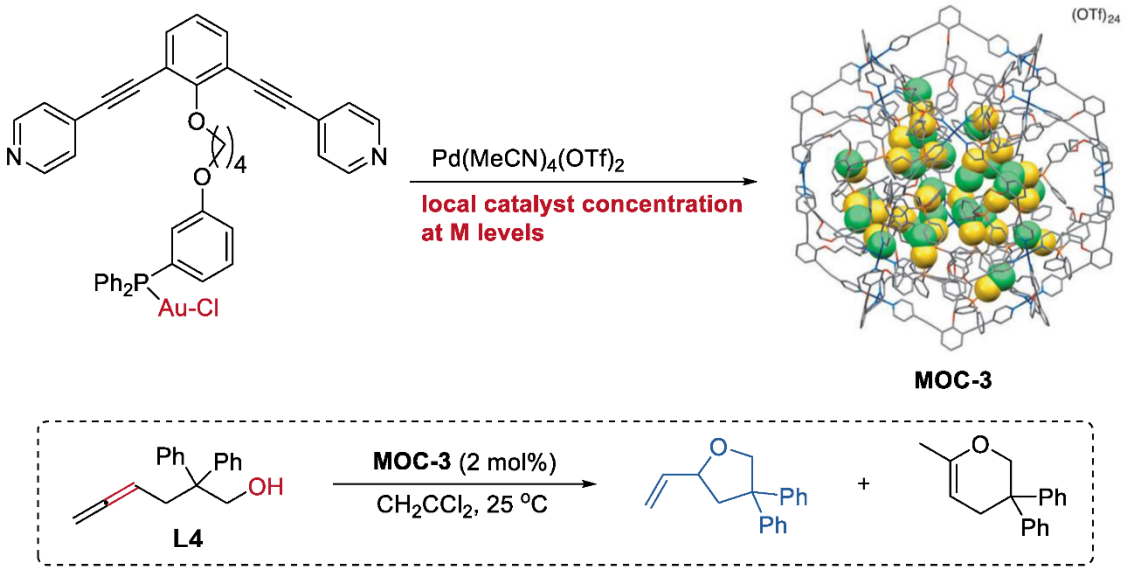

Figure 11 Hydroalkoxylation of the g-allenol catalysed by **MOC-3** with a high local Au catalyst concentration. Reaction additions: **L4** (10.4 mM), **MOC-3** (2 mol%), CH_2CCl_2, 25 °C. Figure adapted from refence [47].

More complex and exotic processes are also enabled by the confined spaces provided by the cavity inside the MOCs. A notable example of this is the catalysed cyclopropane demethylenation. This reaction is enabled by the highly electron deficient nature of **MOC-2**, which promotes a photoinduced guest to host electron transfer, leading to an highly chemoselective reaction (**Figure 12**).[48]

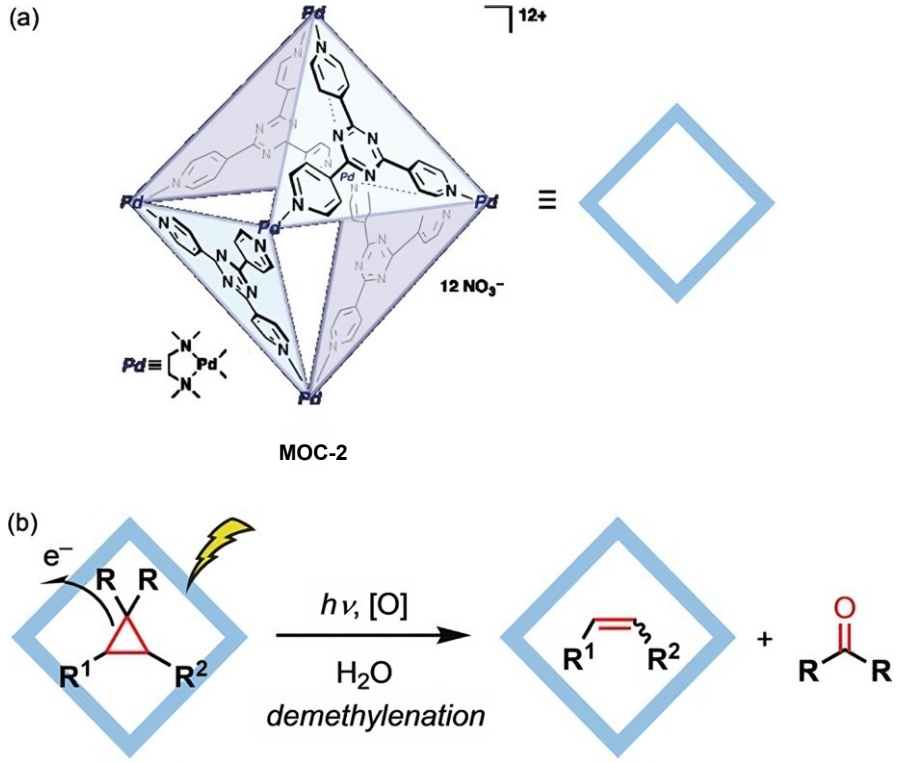

Figure 12 Demethylenation of cyclopropane catalysed by **MOC-2**. Reaction additions: 15 (0.136 mmol), MOC (100 mol%), UV light, H2O, r.t. Adapted from reference [48].

1.5 TPMA based cage

The research group in which this work was carried out already reported the possibility of using TPMA as a building block to obtain a metal-organic cage compound with a well-defined internal cavity.[49] The molecular cage was obtained by exploiting the above discussed concepts of dynamic covalent chemistry, starting from relatively simple building blocks to create a large, three-dimensional architecture.[50] In this context, the reversible imine condensation reaction (**Scheme 5**) was exploited by adding ethylenediamine to the zinc complex (**4**), leading to the formation of the molecular cage structure (**5**).

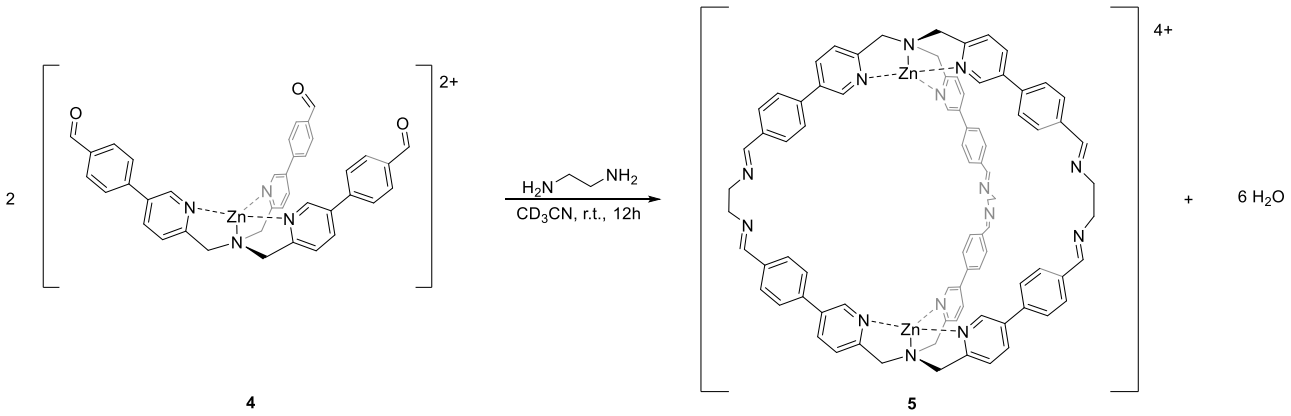

Scheme 5 Formation of the supramolecular cage 5 starting from complex 4 and using ethylenediamine as linker. The reaction was performed in CD_3CN at room temperature obtaining the product after 12 hours. Perchlorate counter anions are removed for clarity.

1.5.1 Molecular recognition properties of the novel cage structure

The recognition properties of this novel cage structure were then investigated, inspired by the work of Anslyn and colleagues on the determination of enantiomeric excess and identity of chiral dicarboxylates based on copper-TPMA complexes.[51] Similarly, a study of molecular recognition of cage **5** towards dicarboxylate anions was initially investigated by the group.[49] Confined space processes are ruled by the interplay of the size and shape adaptability of hosts and guests, which in turn determine the thermodynamic and kinetic behaviour of the process. To a solution of empty cage **5**, the addition of a sub-stoichiometric amount (0.2 to 0.9 equiv.) of suberic acid ($HOOC(C_6H_{12})COOH$) lead to the appearance of a new set of ^{1}H-NMR signals and, after reaching an excess of dicarboxylic acid (1.3 equiv.), it resulted in the complete conversion to the filled cage (**Figure 13**). These observations lead to hypothesizing the formation of a 1:1 host-guest complex, successively confirmed by two-dimensional NMR spectroscopy (ROESY, DOSY) and ESI-MS experiments.

The successful results achieved with the binding of suberic acid (C_8) within cage **5** prompted the study of other diacids, ranging from succinic acid (C_4) to tetradecanoic acid (C_{14}) to determine the correlation between free energy of complexation to aliphatic chain length of the guest (The resulting binding constants are reported in **Figure 13**). Successive studies on the distance between zinc atoms within the cage at varying guest size (C_4 to C_{14}) simulated through semiempirical computational methods, showed a trend of increasing distance with increasing alkyl chain length of the dicarboxylate up to the suberic acid (C_8), followed by a plateau with Zn-Zn distance approximately constant with further increases in guest

sizes. Dicarboxylates with alkyl chains longer than that of suberic acid tended to coil inside the cage's cavity.

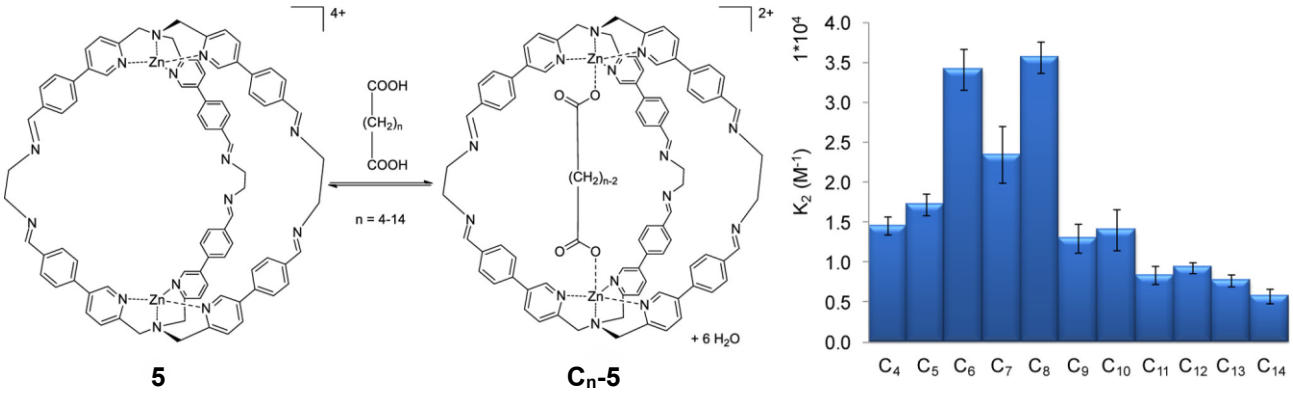

5 **C_n-5**

Figure 13 ^{1}H NMR binding constants (K_2) for the inclusion of diacids C_4–C_{14} within cage **5** (embedded ethylenediamine and perchlorate counter anions are removed for clarity). Figure adapted from reference [49].

1.5.2 Supramolecularly templated cage assembly

Having studied the binding of dicarboxylic guests to cage **5**, rate constants for the formation (assembly) and hydrolysis (disassembly) have been measured in the presence of the various diacids. A remarkable effect of the presence of these acids on the initial rate constants, determined through ^{1}H-NMR, was observed. This result suggests a templating effect promoted by the dicarboxylate anions to the cage formation, with a trend very similar to that of the binding constants, with the highest favourable effect once again caused by addition of suberic acid, which enhanced the assembly's rate of almost 12 times relative to the cage formation without templating agents. The initial hydrolysis rate constants instead follow an unexpected trend of increasing disassembly rate with increasing alkyl chain length of the guest molecules, with suberic acid showing a hydrolysis rate constant comparable to that of the empty cage (**Figure 14**).[49] Likely, the shorter chain diacids (C_4-C_6) tend to keep the two tripodal Zn-TPMA units together, adding an additional strain in the opening of the cage to maintain the guest to bind both metal centres and reducing the initial hydrolysis rate constant up to 2.5 times that of the empty cage for the succinic acid. Diacids with longer alkyl chains (C_7-C_9) show an effect similar to that of solvent molecules, meaning that no particular straining is observed in the cage's architecture and the initial rate of disassembly is comparable to that of the empty cage. Increasing the chain length further (C_{10}-C_{14}) causes the hydrolysis of the cage to accelerate, up to two times faster for the longest chain C_{14}. This is likely due to the conformation that the longer chain guests are forced to attain in order to bind inside

the cage. This coiled up configuration is likely to behave like a spring, tending to push away the two Zn-TPMA units. Upon hydrolysis, the strain forced on the long diacids is released, leading to a better binding once the two halves of the cage are separated and more mobile.

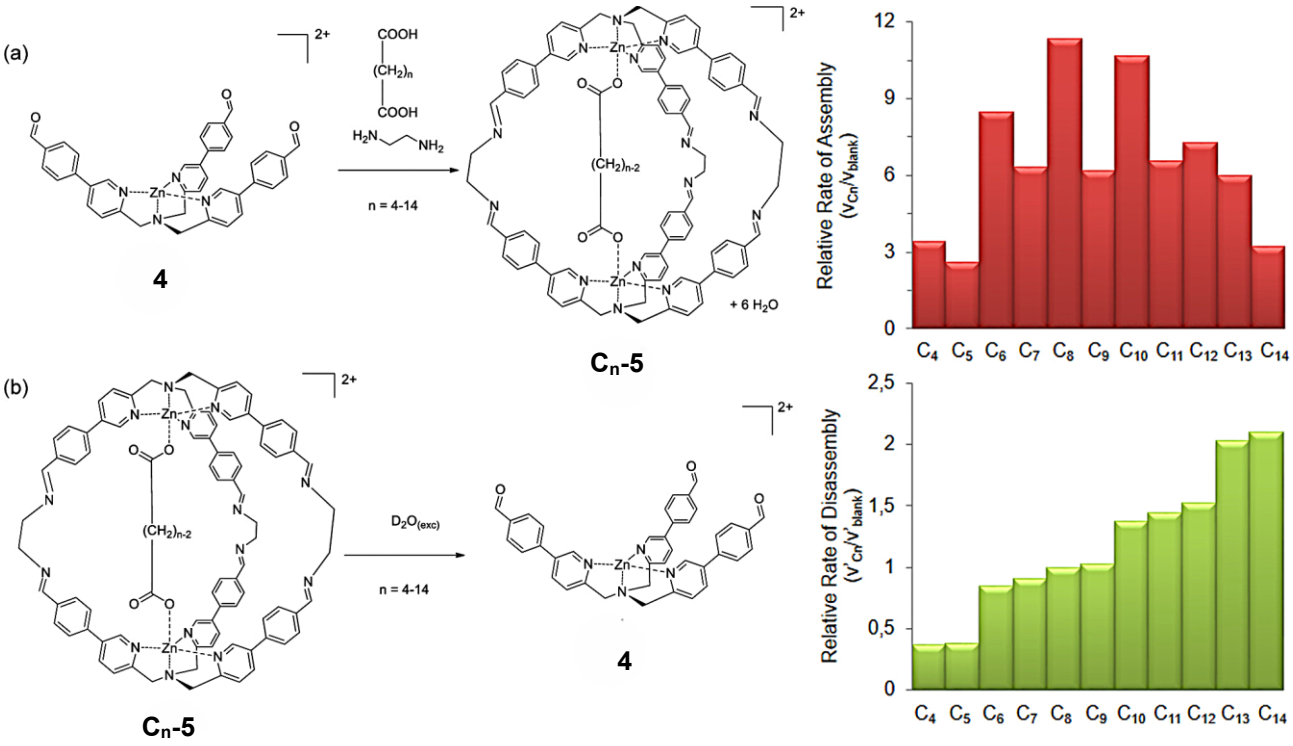

Figure 14 Initial relative rates of assembly (a) and disassembly (b) of cage **5** in the presence of diacids C_4–C_{14}. Initial rates for the formation and hydrolysis of the cages have been measured using ^{1}H NMR, and they have been compared with the rates of the empty cage 5. Initial conditions for (a) assembly $[4]_0$ = 1.50 mM (1.0 equiv), [ethylenediamine]$_0$ = 2.25 mM (1.5 equiv), [**C$_n$**] = 0.75 mM (0.5 equiv) and (b) disassembly [**C$_n$-5**]$_0$ = 0.30 mM, $[D_2O]_0$ = 16 M. In all the structures, the counter anions are perchlorates and are omitted for clarity. Figure adapted from reference [49].

1.5.3 Chiral Diaza-Cope rearrangement for the preparation of novel macromolecular cages

The dynamic covalent chemistry, as mentioned above, allows for simple synthesis of complex molecular architecture through formation of thermodynamically stable reversible bonds. In the case of cage **5**, the concept of DCC was applied to the imine condensation and although the method has a high versatility, the inherent hydrolytic lability of the imine bond precludes many possible applications for the synthesized cage **5**. In order to overcome this limitation, it was decided to combine the imine DCC with a [3,3]-sigmatropic rearrangement, leading to the formation of a hydrolytically stable C-C bond.[52]

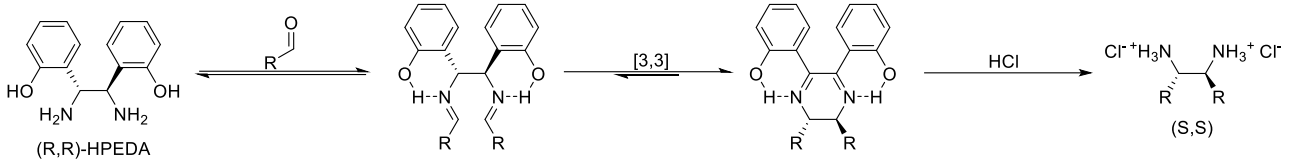

Scheme 6 [3,3]-sigmatropic Diaza-Cope rearrangement for the synthesis of chiral amines.

The Diaza-Cope rearrangement (**Scheme 6**) is shifted towards the product thanks to the (R,R)-HPEDA phenols, which favour the formation of strong resonance-assisted hydrogen bonds.[53,54] This powerful process was then applied to the synthesis of the cage architecture, by using (R,R)-HPEDA as a diamine linker instead of ethylenediamine (**Scheme 7**).

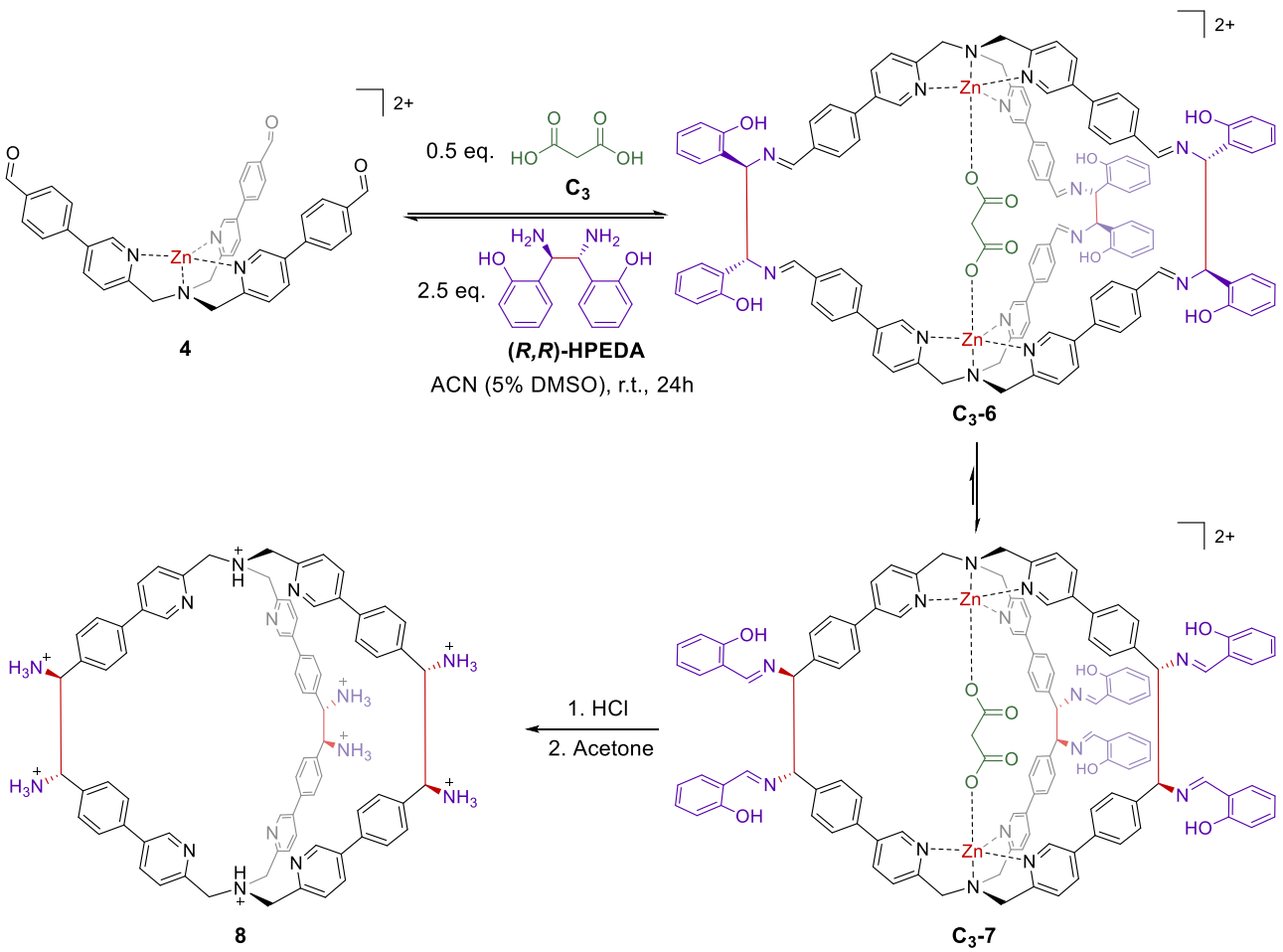

Scheme 7 Reaction scheme for the synthesis of chiral TPMA-based cage **8**. Perchlorate and pyridine counter ions are omitted for clarity. Figure adapted from reference [52].

Also, after a preliminary study on the effect of templating agents (dicarboxylates) of various chain length was conducted, indicating in the malonic acid (C_3) the optimal guest for the templation. After the Diaza-Cope rearrangement takes place and the newly formed imine bond is hydrolysed by using concentrated aqueous hydrochloric acid, interestingly resulting also in the complete decomplexation of the zinc cations. The obtained product was then isolated via acetone solubilization and recrystallization. Repeating the synthesis with (S,S)-HPEDA yields the opposite enantiomer of cage **8**, as confirmed via circular dichroism spectra.

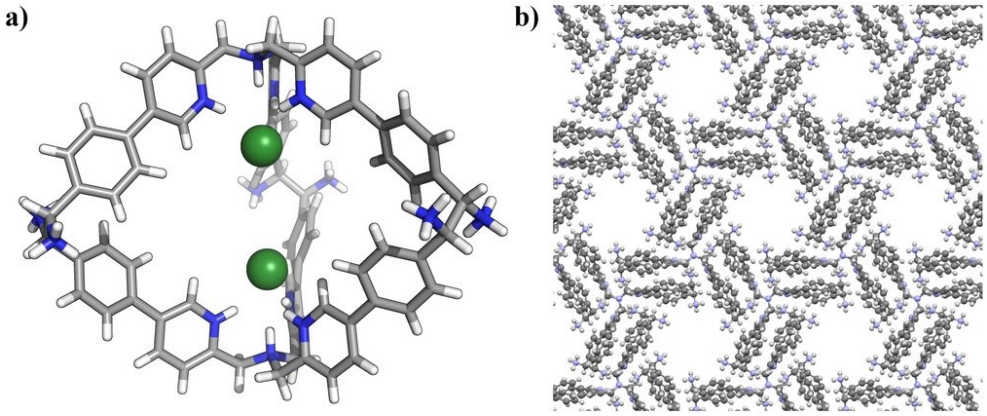

Figure 15 (a) Single-crystal X-ray structure of cage **8**; (b) Pore system of cage **8** in the crystal structure. Chloride ions and solvent molecules are removed for clarity. Figure adapted from reference [52].

X-Ray analysis of a single crystal of cage **8** obtained through slow evaporation of a solution of **8** in H_2O/DMSO disclosed a C_3 symmetry for the molecular cage in the solid state, in which the two TPMA units adopt an opposite propeller arrangement (**Figure 15a**). Interestingly, the crystal packing of the solid reveals an intrinsic porosity with a honeycomb disposition of the cages, driven by salt bridges between chloride anions and the cage's ammonium cations (**Figure 15b**).

1.5.4 Preparation of the novel cage complex catalyst

The novel chiral covalent cage **8** obtained by the diaza-Cope rearrangement has interesting characteristics that could lead to new applications currently under investigation in the group. In order to broaden its range of potential applications, a *post-functionalization* reaction has been performed to go from a water-soluble cage to a structure soluble in most organic solvents. An amidation reaction was chosen in order to incorporate six pivaloyl functional groups into the cage: the presence of amide and *tert*-butyl groups can increase the structure solubility and reduce aggregation phenomena.

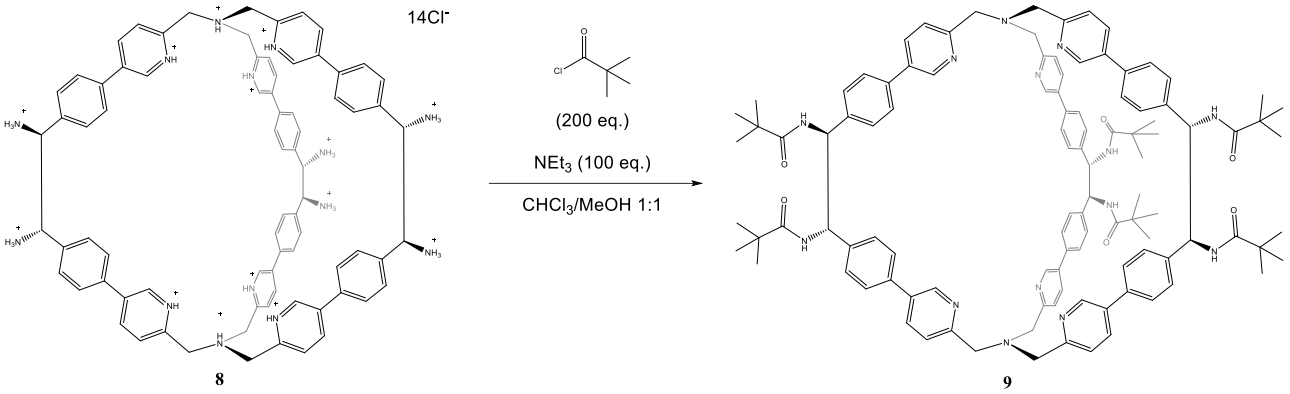

Scheme 8 Amidation of cage **8** with pivaloyl chloride

An excess of triethylamine was used as a mean to neutralize the numerous free protons present in **8** and the ones generated by the amidation reaction. The obtained cage **9** is capable of coordinating various transition metals, like zinc(II) and copper(II).

Knowing most of the literature work on ATRP catalysis is based on copper complexes, the preparation of a Cu(II) based cage complex was designed as follows:

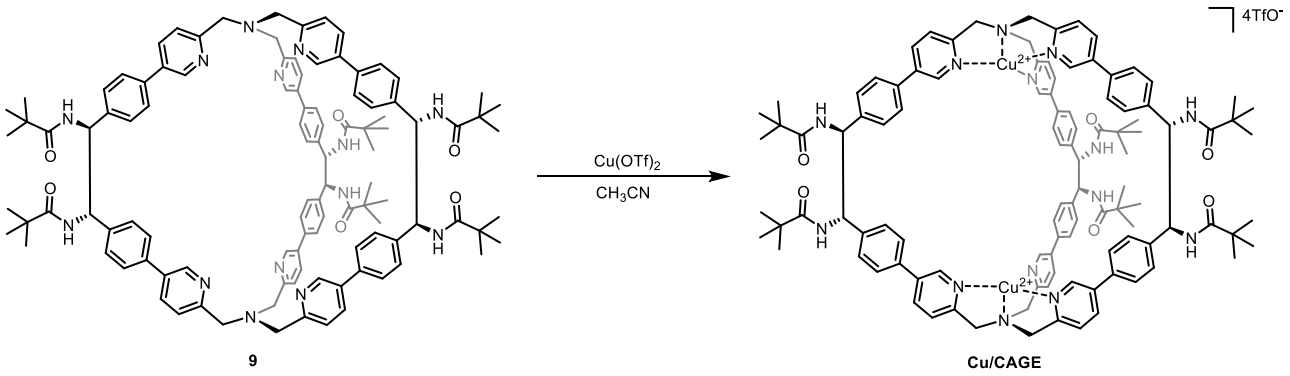

Scheme 9 Preparation of the novel complex **Cu/CAGE** from organic cage compound **9** and copper (II) triflate.

The **Cu/CAGE** system was obtained via simple complexation of a copper (II) triflate salt using cage **9** as a ligand. The novel complex **Cu/CAGE** was then precipitated using diethyl

ether and collected as a powder, which proved to be soluble in polar organic solvents such as acetonitrile and dimethylformamide, enabling the exploration of its potential applications.

2 AIM OF THE THESIS

In recent years, in the research group in which this work was carried out, a variety of TPMA based molecular cages has been developed, studied and employed for molecular recognition applications.[55] The catalytic properties and applications of these cage architectures remain however unexplored. This thesis aims to assess the capability of the modified cage structures discussed above, when complexed with Cu ions, to perform electrochemically catalysed C-Br scission, in order to evaluate the system's ability to initiate and catalyse eATRP processes. This novel confined space complex is a variation of cage **8** prepared by amidation of the primary ammonium groups with pivalic acid and by complexation of the empty molecular cage resulting with copper (II) cations (**Cu/CAGE**).

Furthermore, a special consideration will be given to potential influences of the presence of a confined environment within the catalyst by comparing its behaviour to that of a well-known ATRP catalyst like copper-TPMA (**Cu/TPMA**).

The study will be directed towards the characterization of electrochemical properties and speciation in the DMF electrolytic solution of the novel **Cu/CAGE** complex in order to better investigate and evaluate its electrocatalytic properties. Successively, eATRP of various monomers at various targeted DPs will be explored and the kinetics of the polymerization and initiator's activation will be determined to evict the possible role of the confined environment provided by the novel complex.

3 RESULTS AND DISCUSSION

3.1 Characterization of the copper complexes

As expressed in the aim of the thesis, objective of this study is to investigate the Cu(II) molecular cage architecture in electrochemically-mediated Atom Transfer Radical Polymerization (ATRP). The cage, which have been synthesized in the group where this work was carried out, has been initially characterized electrochemically. In the second part of this work preliminary ATRP experiments have been carried out.

3.1.1 Cyclic voltammetry of $[Cu^{II}_2CAGE(OTf)_4]$

Considering that the literature on ATRP indicates that the electrochemical properties of the copper catalysts are fundamental to understanding their reactivity, the first investigation focused on the cyclic voltammetry (CV) of the cage complex $[Cu^{II}_2CAGE(OTf)_4]$, synthesized in the group (**Figure 16**).[52]. Unless specified, all the CVs were performed in a 5-necked, jacketed electrochemical cell at a temperature of 50 °C in dimethylformamide (DMF) with 0.1 M *n*-Bu_4NPF_6 as a supporting electrolyte and at a concentration of copper centres of 10^{-3} M and concentration of CAGE = 5×10^{-4} M. The working electrode was a glassy carbon disk and the counter electrode was a platinum wire. An Ag wire coated in AgI in a separate cell containing 0.1 M *n*-Bu_4NI served as the reference electrode. The potential of the reference electrode was calibrated at the end of each CV experiment by adding ferrocene (Fc) to the cell. The half wave potential ($E_{1/2}$) of the Fc^+/Fc couple was measured and used as a reference point for the experiment's potential values. This ensures reproducible potential values, as the reference electrode's redox potential can shift over time (days) and with usage due to changes in the electrolytic solution's composition.

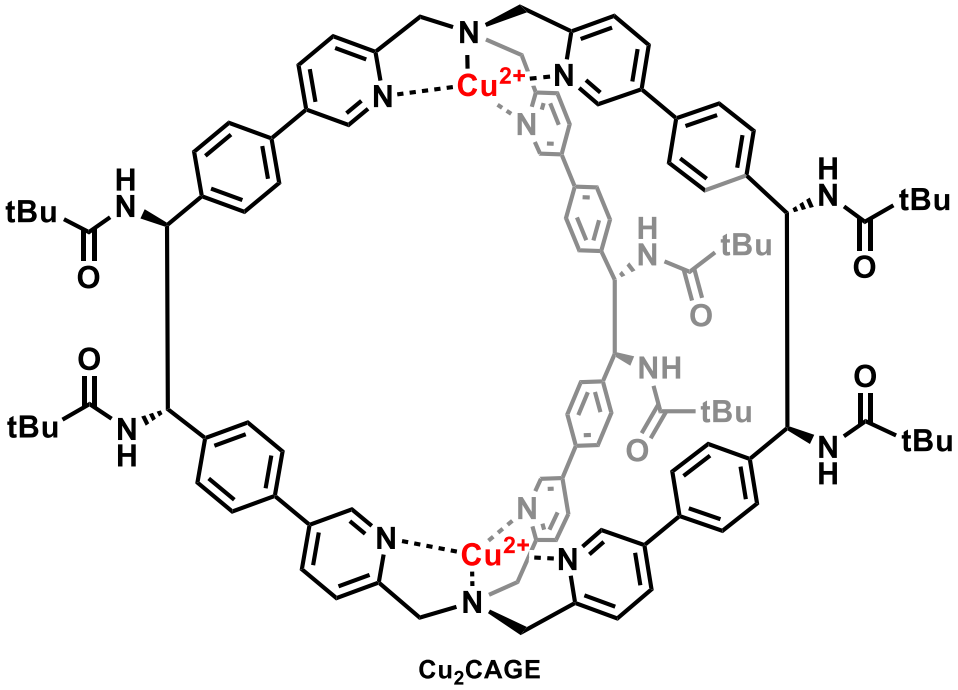

Figure 16 Molecular structure of the novel confined space complex $[Cu^{II}_2CAGE]^{4+}$ characterized and studied in this work.

The CV of $[Cu^{II}_2CAGE(OTf)_4]$ showed a quite complex voltammetric pattern, with an odd-shaped cathodic peak, and a sharp anodic peak (**Figure 17**). However, clear evidence of a reversible reduction of Cu^{I} to Cu^{II} was observed, via the following electron transfer reaction:

$$[Cu^{II}_2CAGE]^{4+} + 2e^- \rightleftharpoons [Cu^{I}_2CAGE]^{2+} \quad (3.1)$$

(It should be noted that, for simplicity, non-coordinating anions such as OTf^- or eventual coordinating solvent molecules are omitted from the notation of the Cu/CAGE complexes).

The ill-shaped nature of the voltammetric response can be due to the poor stability of the Cu^{I} complex. Cu^{I} complexes with amine ligands can participate in undesired reactions such as disproportionation to Cu^{II} and Cu^0 complexes. The generated Cu^0 deposits as metallic copper on the electrode surface, which is oxidized in the sharp anodic “stripping” peak at −0.36 V vs Fc^+/Fc.

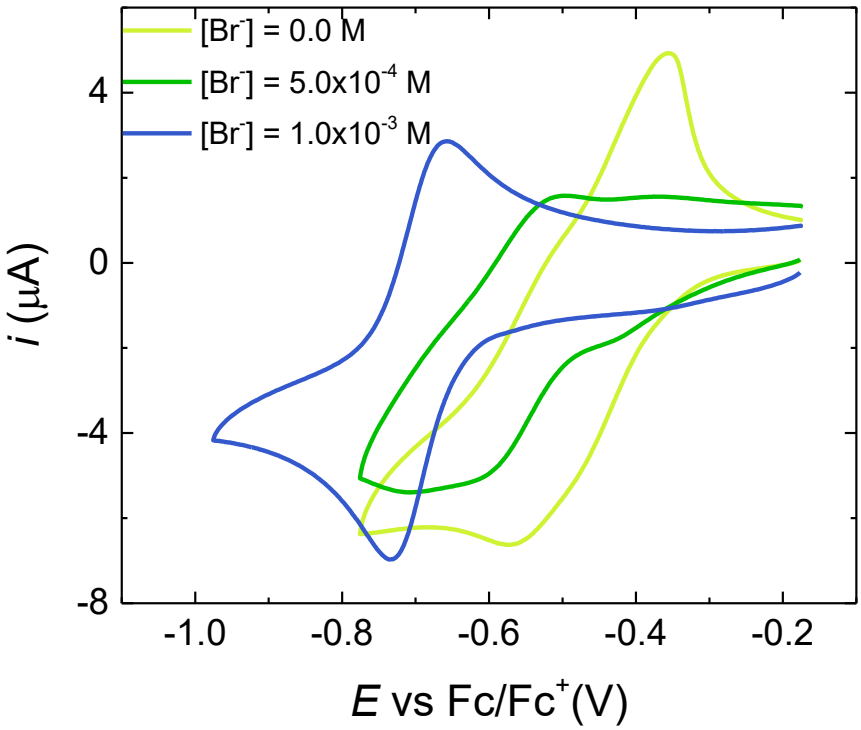

Figure 17. CV of 5×10^{-4} M $[Cu^{II}_2CAGE]^{4+}$, in the absence and in the presence of 5×10^{-4} M and 10^{-3} M *n*-Bu_4NBr at scan rate of 0.05 V/s, in DMF + 0.1 M n-Bu_4NPF_6 at T = 50 °C.

3.1.2 Effect of Bromide anions

A strategy to improve the stability of Cu complexes is to add halide anions to the solution, which can bind to the metal centres. Bromide anions are typically added during ATRP reaction, either by utilizing $CuBr_2$ as a source for Cu ions or deriving from the activation of carbon-bromine bonds of ATRP initiators.

Since $[Cu^{II}_2CAGE]^{4+}$ has two free axial coordination sites "inside" the cage, up to two bromide anions may bind to the Cu centres. To understand the impact of bromide ion coordination on the voltammetric response, a bromide source, specifically *n*-Bu_4NBr, was incrementally added to a concentration of 1 equivalent and, after that, 2 equivalents per $[Cu^{II}_2CAGE]^{4+}$ complex. Addition of Br^- resulted in a progressive shift of the voltammetric wave towards negative potentials, in line with the following complexation reactions taking place (the thermodynamic parameter of interest is listed in the same line):

$$[Cu^{II}_2CAGE]^{4+} + Br^- \rightleftharpoons [BrCu^{II}_2CAGE]^{3+} \qquad K^{II}_{1Br} \qquad (3.2)$$

$$[BrCu^{II}_2CAGE]^{3+} + Br^- \rightleftharpoons [Br_2Cu^{II}_2CAGE]^{2+} \qquad K^{II}_{2Br} \qquad (3.3)$$

Further additions of Br^- up to 3, 4, or 5 equiv. (Appendix B) compared to the Cu_2CAGE complex caused minimal variations in the CV and no further shifts towards negative potentials. This suggested that with 2 equivalents of Br^- per cage complex the $[Br_2Cu^{II}_2CAGE]^{2+}$was quantitatively formed and that no further Br^- could bind to the complex. Both the negative shift of potential and the presumed speciation of the $[Br_2Cu^{II}_2CAGE]^{2+}$ complex are consistent with the behaviour of tripodal amine-Cu complexes used as ATRP catalysts.[13,56]

The voltammetry of $[Br_2Cu^{II}_2CAGE]^{2+}$ (blue line in **Figure 17**) showed a well-defined and quasi-reversible peak couple with halfwave potential $E_{1/2}$ = -0.696 V vs Fc/Fc^+ and peak-to-peak separation ΔE = 0.077 V. The symmetric shape of the wave suggested that the generated Cu(I) complex was completely stable in the timescale of the CV experiment. Additionally, the presence of a single voltammetric wave indicates that the two Cu centers have little to no electronic interaction with each other, making them electrochemically equivalent and reducible at the same potential. This is consistent with the fairly large metal-to-metal distance that can be estimated at around 10 Å from the crystal structure of the CAGE ligand.[49]

The CV of $[Cu^{II}_2CAGE]^{4+}$ with C_{Br}-/C_{CAGE} = 1 (C_{Br}-/C_{Cu} = 1/2) showed a complicated pattern of waves that was however well compatible with the expected speciation of the complex. With a substoichiometric amount of Br^- with respect to the Cu centres, the bromide anions appear to distribute between the Cu centres producing an array of complexes with different speciation, including $[Cu^{II}_2CAGE]^{4+}$, $[BrCu^{II}_2CAGE]^{3+}$, and $[Br_2Cu^{II}_2CAGE]^{2+}$. By observing the trend in reduction potentials, the small shoulder at approximately -0.43 V vs Fc/Fc^+ can be attributed to the reduction of a small amount of $[Cu^{II}_2CAGE]^{4+}$. The most intense peak at -0.61 V vs Fc/Fc^+ can be attributed to the reduction of $[BrCu^{II}_2CAGE]^{3+}$, the predominant species in solution. The small shoulder at -0.70 V vs Fc/Fc^+ is instead associated to the reduction of a small amount of $[Br_2Cu^{II}_2CAGE]^{2+}$. The halfwave potential for the reduction of $[BrCu^{II}_2CAGE]^{3+}$ was assessed from the main voltammetric peak as $E_{1/2}$ = -0.56 V vs Fc/Fc^+. This is a rough estimate due to influence of multiple species and equilibra in solution.

Similarly, the standard reduction potential of $[Cu^{II}_2CAGE]^{4+}$ was roughly estimated at $E_{1/2}$ = -0.47 V vs Fc/Fc^+.

3.1.3 Comparison between $[Br_2Cu^{II}_2CAGE]^{2+}$ and $[BrCu^{II}TPMA]^+$

The CV of the $[Br_2Cu^{II}_2CAGE]^{2+}$ complex showed a quasi-reversible wave similar to other Cu amine catalysts, prompting a comparison with the established ATRP catalyst, $[BrCu^{II}TPMA]^+$. Voltammetry at the same Cu concentration (**Figure 18**) showed a smaller current intensity for the cage catalyst, indicating a lower diffusion coefficient due to its larger structure. The reduction potentials of both brominated complexes are very similar. This suggests that $[Br_2Cu^{I}_2CAGE]$ is a reductant as capable as $[BrCu^{I}TPMA]$, and therefore the two complexes may exhibit similar catalytic activity. Electrochemical parameters for **Cu/CAGE** and **Cu/TPMA** complexes are compared in **Table 1**, and further discussed in the next paragraphs.

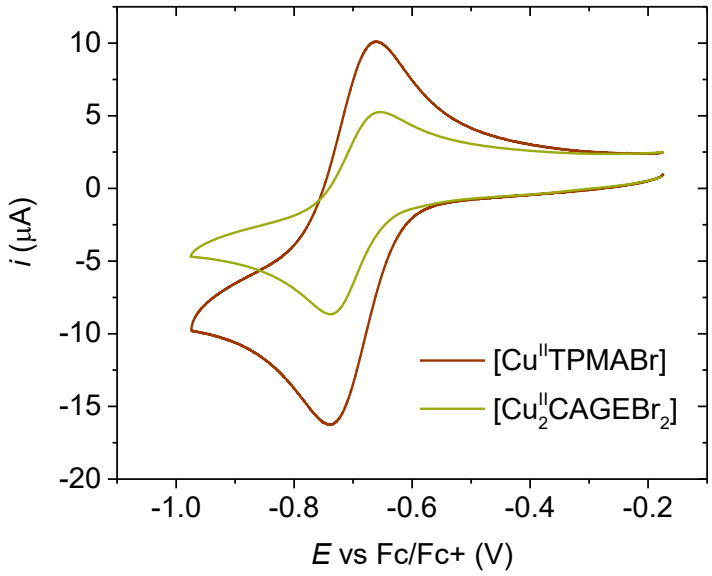

Figure 18. CV of 5×10^{-4} M $[Cu^{II}_2CAGE(Br)_2]^{2+}$ and 10^{-3} M of $[Cu^{II}TPMA(Br)]^+$ at scan rate of 0.1 V/s, in DMF + 0.1 M *n*-Bu_4NPF_6 at T = 50 °C, $[L]/[Cu^{2+}]/[Br^-]$ = 1/1/1 for $[CuTPMA]^{2+}$, 0.5/1/1 for $[Cu^{II}_2CAGE]^{4+}$.

Table 1. Electrochemical properties and Br^- affinity constants for copper complexes with TPMA and CAGE

Complex	$E_{1/2}$ V	$D\times10^6$ cm^2/s	$k^0\times10^3$ cm/s	log K^{II} Br M^{-1}	log K^{I} Br M^{-1}
$[Cu^{II}TPMA]^{2+}$	-0.599	[a]	[a]	5.62[b]	4.15[b]
$[BrCu^{II}TPMA]^{+}$	-0.693	5.82	9.50	/	/
$[Cu^{II}_2CAGE]^{4+}$	-0.465	1.05	[a]	6.53	3.57
$[BrCu^{II}_2CAGE]^{2+}$	-0.560	[a]	[a]	4.96	0.687
$[Br_2Cu^{II}_2CAGE]^{2+}$	-0.696	2.28	2.02	/	/

[a] not measured

[b] literature data[15]

3.1.4 Determination of equilibrium constants for Br^- addition to $[Cu^{II}_2CAGE]^{4+}$

Starting from the $[Cu^{II}_2CAGE]^{4+}$ complex, consecutive additions of Br^- lead to the formation of the $[BrCu^{II}_2CAGE]^{3+}$ and $[Cu^{II}_2CAGE]^{4+}$ complexes based on reactions (3.2) and (3.3).

In order to gather more information on the system, speciation of $[Cu^{II}_2CAGE]^{4+}$ in the presence of bromide anions, the association constant between the copper centres of the cage and the bromide ions (K^{II}_{2Br} and K^{II}_{2Br} **eq. 3.2** and **eq. 3.3**) were determined using UV-Vis spectroscopy. Since $[Br_2Cu^{II}_2CAGE]^{2+}$ is expected to be the main deactivator in ATRP processes, it is crucial to assess the stability of the brominated copper (II) form, which will provide the control of the polymerization through reversible deactivation of the growing radicals.

The method for the determination of the affinity constants was a spectrometric titration,[15] already utilized in previous works to determine the association constant of Br^- for the $[Cu^{II}TPMA]^{2+}$ catalyst. The procedure consisted of a titration of the $[Cu^{II}_2CAGE]^{4+}$ with bromine ions; for each addition the UV-Vis spectrum was collected. For a more accurate measure, a highly dilute solution was titrated in a 4 cm cuvette. The overall titration showed two distinct bands for the brominated and non-brominated complexes which were fitted (HypSpec2014) to calculate the association constants. **Figure 19** shows the experimental data and the theoretical fitting at two selected wavelengths.

From the spectrometric titration, it was clear that two bromide anions could successively bind to $[Cu^{II}_2CAGE]^{4+}$. Two distinct affinity constants were determined for the two Cu(II) ions, $\log K^{II}_{Br,a}$ = 6.53 and $\log K^{II}_{Br,b}$ = 4.96. The second bromine ion has a lower affinity for the

Cu(II)-CAGE. Interestingly, the affinity constant for $[BrCu^{II}TPMA]^+$ ($\log K^{II}_{Br}$ = 5.62) is intermediate between the two values recorded for $[Cu^{II}_2CAGE]^{4+}$ (**Table 1**).

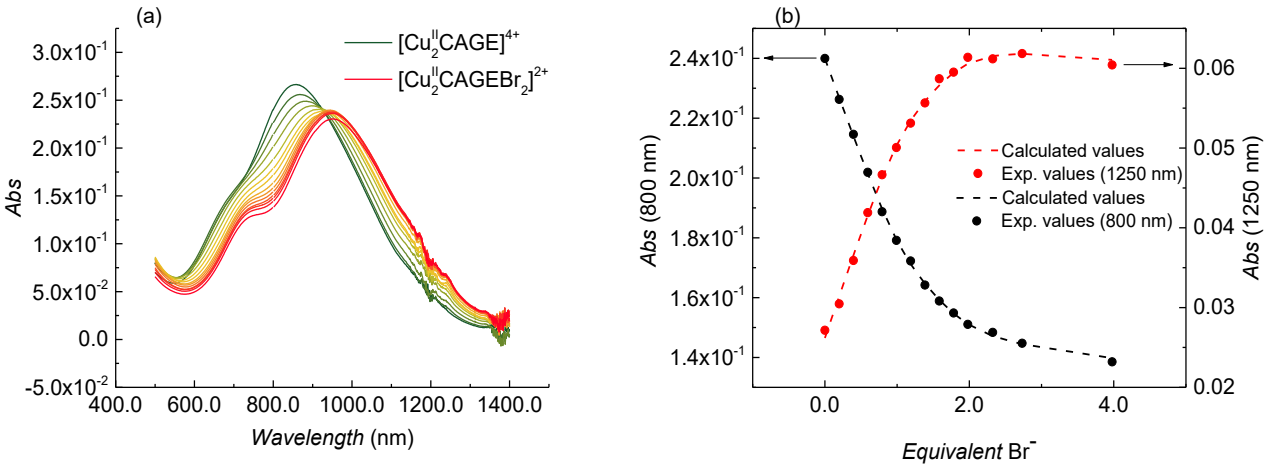

Figure 19. Absorbance spectra of a solution 10^{-4} M of $[Cu^{II}_2CAGE]^{4+}$ and 0.1 M of *n*-Bu_4NPF_6 in DMF at room temperature, after the progressive addition of *n*-Bu_4NBr up to four equivalents in respect to the concentration of cage centres. Measured in a cuvette with a 4 cm optical path length. (a) Complete spectra, (b) Experimental and fitted absorbance values at two selected wavelengths.

We can conclude that two bromide anions can consecutively bind to the $[Cu^{II}_2CAGE]^{4+}$. With such high affinity constants for the bromide anions, the $[Br_2Cu^{II}_2CAGE]^{2+}$ complex under typical polymerization conditions is mostly present in solution in its di-brominated form in the presence of one equiv. of bromide anions per Cu centre.

3.1.5 Determination of diffusion coefficients for the Cu-CAGE complexes

Given the known speciation of the $[Br_2Cu^{II}_2CAGE]^{2+}$ complex, several key electrochemical properties were determined, including the diffusion coefficients *D* and the electron transfer kinetic constants (k^0) and for the binary and ternary complexes $[Cu^{II}_2CAGE]^{4+}$ and $[Br_2Cu^{II}_2CAGE]^{2+}$. *D* is a measure of the mobility of the species, while k^0 is related to its electron transfer (ET) reactivity at the electrode. Both parameters will be further used in later sections to study quantitatively the reactivity of our **Cu/CAGE** catalyst.

The determination of *D* was achieved by performing a series of cyclic voltammetries at different scan rates (*v*), subtracting the capacitive current and then linearly fitting the cathodic peak current (I_p) to the square root of the scan rate to estimate the diffusion coefficient *D* (**Figure 20**) by applying the Randles-Sevcik equation:

$$I_p = 0.4463nFAC\sqrt{\frac{nFvD}{RT}} \tag{3.4}$$

where *n* is the number of exchanged electrons, and *A* is the electrode area equal to 0.07 cm^2, and *C* is the concentration of the analyte.

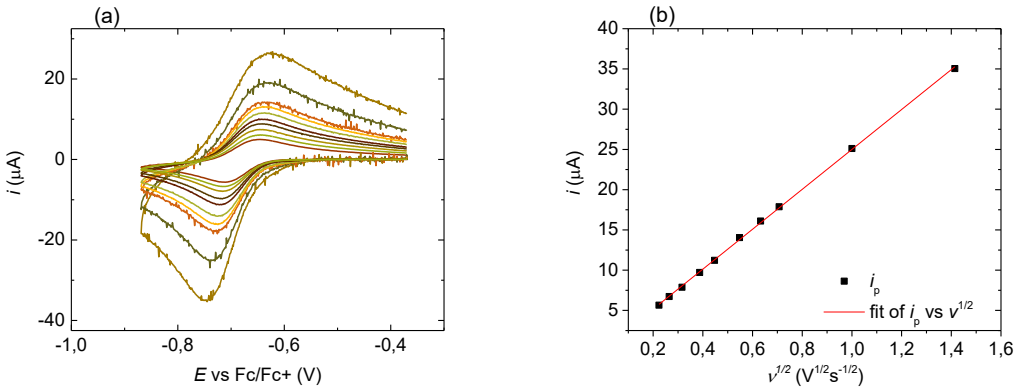

Figure 20. (a) Background subtracted CVs at increasing scan rate from 0.05 V/s to 2 V/s of a solution 5×10^{-4} M of $[Br_2Cu^{II}_2CAGE]^{2+}$, and 0.1 M of *n*-Bu_4NPF_6 in DMF at *T* = 50°C; (b) Linear fitting of the cathodic peak current against the square root of the scan rate for the CVs of (a) to find the diffusion coefficient.

Figure 20b shows a linear regression in i_p vs $v^{1/2}$ plot which was used for the calculation of *D* based on rearranging the Randles-Sevcik equation in the following form:

$$D = \frac{RT}{nF}\frac{1}{(0.4463nFAC)^2}\left(\frac{\partial i_p}{\partial\sqrt{v}}\right)^2 \tag{3.5}$$

The resulting data, summarized in **Table 1**, shows that the cage complex has a lower diffusion coefficient than that of the **Cu/TPMA** species, as expected, due to the much higher molecular weight of the cage system.

3.1.6 Determination of the standard rate constant for electron transfer (k^0) for $[Br_2Cu^{II}_2CAGE]^{2+}$

In the case of a quasi-reversible redox system, it is possible to determine k^0 using cyclic voltammetry. In these conditions, the shape of the peaks and the parameters that characterize them, such as i_p, E_p, etc., depend on α, the transfer coefficient, and a kinetic parameter Ψ. Specifically, the separation between the peak potentials $\Delta E_p = E_{pa} - E_{pc}$, which increases with the scan rate v, depends on the following parameter Ψ:

$$\Psi = \left(\frac{D_O}{D_R}\right)^{\alpha/2} \frac{k^0}{[(nF/RT)\pi D_O v]^{1/2}} \tag{3.6}$$

If we assume that $D_O = D_R$, **eq. 3.6** can be simplified to:

$$\Psi = \frac{k^0}{[(nF/RT)\pi D_O v]^{1/2}} \tag{3.7}$$

It is possible to derive the value of k^0 from the dependence of ΔE_p on $\log \Psi$. In the literature, a series of ΔE_p values as a function of Ψ, obtained from theoretical calculations, are reported. Plotting these data yields a working curve (**Figure 21a**) that can be used to determine k^0 by fitting the experimental ΔE_p data, a methodology that is referred to as the Nicholson method.[57]

The fitting operation is easier and more reliable if an equation describing the theoretical data is derived. To obtain this equation, the theoretical data were fitted to a fifth-degree polynomial which, as can be seen in **Figure 21a**, describes the data trend very well. The following polynomial equation was obtained to fit the theoretical ΔE_p values:

$$y = 0.00411x^5 - 8.63143 \cdot 10 - 4x^4 - 0.02649x^3 + 0.05387x^2 - 0.05274x + 0.08391 \tag{3.8}$$

where $y = \Delta E_p$ and $x = \log \Psi$. To determine k^0, a series of cyclic voltammograms for the Cu(II) complex (as in **Figure 20a**) were recorded at different scan rates, and from these, a series of ΔE_p values as a function of the potential scan rate, v, were obtained. For each v value, the parameter Ψ', defined as:

$$\Psi' = \frac{\Psi}{k^0} = \frac{1}{[(nF/RT)\pi D_O v]^{1/2}} \tag{3.9}$$

was calculated, which, by taking the logarithms, becomes:

$$\log \Psi' = \log \Psi - \log k^0 = \log\left\{\frac{1}{[(nF/RT)\pi D_O v]^{1/2}}\right\} \qquad (3.10)$$

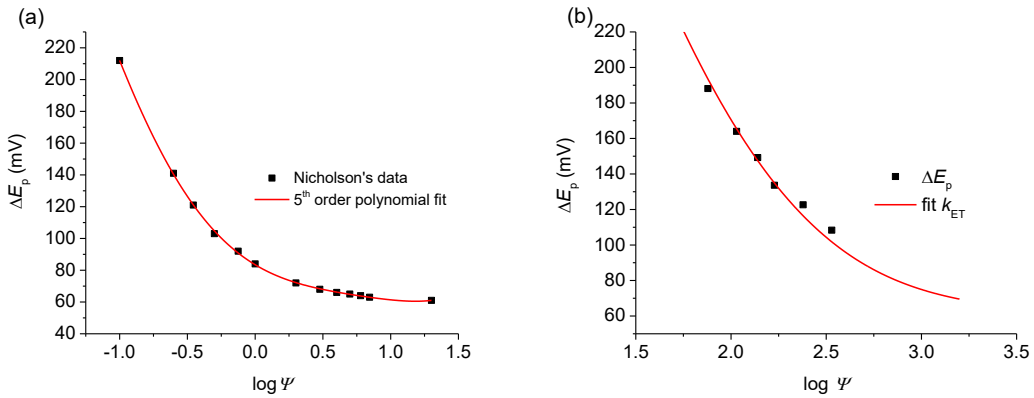

Figure 21 (a) Fitting of Nicholson's theoretical ΔE_p data with a fifth-degree polynomial, performed to obtain a theoretical curve. (b) Fitting of experimental ΔE_p for with the working curve.

By performing a non-linear regression based on **eq. 3.10** of the experimental data for ΔE_p against $\log\Psi$, $\log k^0$is obtained. In the regression, an independent variable $x = \log \Psi' + P$ is set, and fitting is performed by optimizing the constant $P = \log k^0$. Examples of fitting the experimental data to the working curve are shown in **Figure 21b**, which show acceptable agreement with the theoretical data. The k^0 values obtained for the complexes are summarized in **Table 1**.

The electron transfer rate constant is slightly lower for the $[Br_2Cu^{II}_2CAGE]^{2+}$ compared to $[BrCu^{II}TPMA]^+$, likely because the greater steric bulk of the macromolecular catalyst keeps the copper centres further from the electrode, shielding them from the electrode potential and consequentially slowing down the electron transfer (i.e. electron tunnelling) process.

In summary, we can conclude that the novel $[Br_2Cu^{II}_2CAGE]^{2+}$ behaves similarly to a typical Cu-amine complex, and readily coordinates Br^-. The two copper metals were reduced at the same potential, suggesting that they are sufficiently distant that no "electrochemical" communication was detected between them. The values of *D* and k^0 are slightly lower for the $[Br_2Cu^{II}_2CAGE]^{2+}$ complex compared to $[BrCu^{II}TPMA]^+$.

3.2 Application of the Cu/CAGE electrochemically mediated atom transfer radical polymerization

The main electrochemical and speciation properties of this novel **Cu/CAGE** architecture suggest that it could behave as a capable catalyst for electrochemically mediated ATRP.

3.2.1 Evaluation of the electrocatalytic activation of carbon-bromine bonds in a typical atom transfer radical polymerization initiator

In the first part of the study on the catalytic activity, the capability of the cage system to catalyse the reductive scission of the carbon-bromine bond in the ATRP initiator, thereby generating the propagating radicals, was tested. In particular, the voltammetric response in the presence of the ATRP initiator methyl 2-bromopropionate (which mimics the poly(methyl acrylate)-Br chain end) showed a change in the voltammetric response, indicative of a catalytic process (**Figure 22a**). The remarkable enhancement of the cathodic current and decrease of the anodic peak observed after the addition of the RBr initiator are caused by the consumption of the reduced copper(I) species to break the carbon-bromide bond, establishing the ATRP equilibrium (**Figure 22b**). This process re-oxidizes the copper species, reintroducing them into the catalytic cycle and allowing them to be reduced once again, causing the increase in the peak current. Also, the consumption of the same prevents copper(I) from being oxidized at the electrode, causing the notable decrease of the anodic peak current.

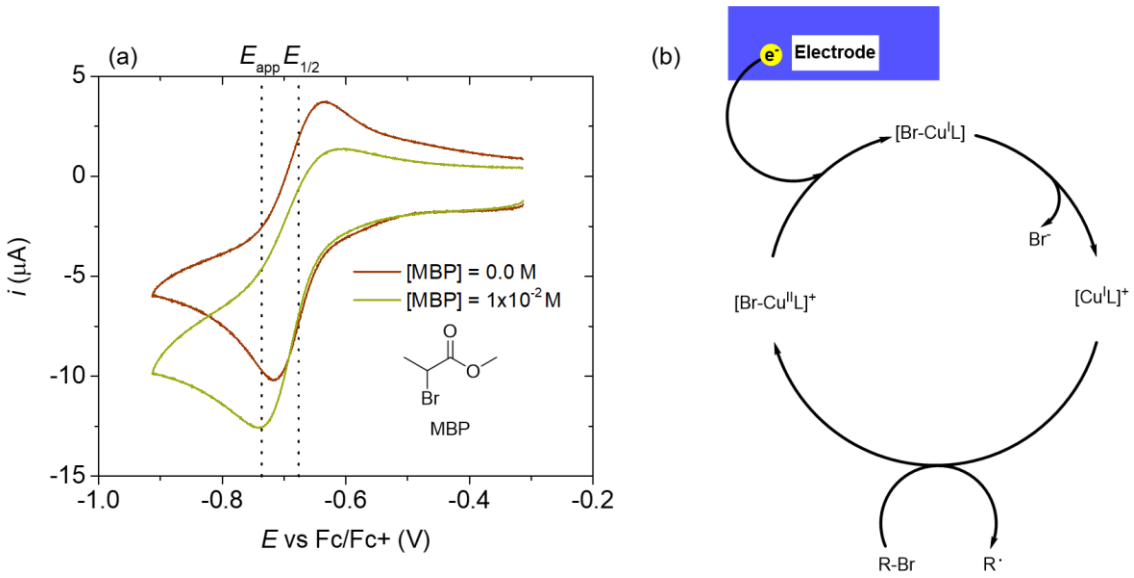

Figure 22 (a) CV at a scan rate of 0.1 V/s of 5×10^{-4} M of $[Cu^{II}_2CAGE(Br)_2]^{2+}$, 0.1 M of n-$Bu_4NPF_6$ in a mixture 1:3 = BA:DMF at T = 50 °C before and after the addition of 10^{-2} M MBP; (b) ATRP electrochemical catalytic cycle, representing the mechanism during the reduction of the copper catalyst.

3.2.2 eATRP of butyl acrylate in DMF catalysed by $[Br_2Cu^{II}_2CAGE]^{2+}$

After confirming that the $[Br_2Cu^{II}_2CAGE]^{2+}$ complex can perform electrocatalytic activation of the C-Br bond, ATRP of various commercial monomers was explored. The initial focus was on butyl acrylate (BA). In analogy to the simple TPMA molecule, it was hypothesized that the cage complex could effectively catalyse the electrochemically mediated ATRP (eATRP) of butyl acrylate, resulting in a controlled polymerization with predictable molecular weights and low dispersity.

In a typical experiment, the eATRP process was conducted in a 5-necked, jacketed electrochemical cell at a temperature of 50 °C in dimethylformamide (DMF), *n*-Bu_4NPF_6 0.1 M as a supporting electrolyte and at a concentration of copper of 10^{-3} M. BA was added to achieve a 25 % v/v concentration in DMF. A platinum mesh with a high surface area served as the working electrode during electrolysis to reduce the Cu^{II} catalyst to its active Cu^{I} state, while an Ag/AgI reference electrode and an aluminium wire in a 0.1 M solution of *n*-Bu_4NPF_6 in

DMF were used as the reference and counter electrodes, respectively. The ATRP initiator was added based on the target degree of polymerization (*DP*), which represents the number of monomer units constituting the polymer chain, using the formula:

$$DP = \frac{[\text{Monomer}]_0}{[\text{Initiator}]} \tag{3.11}$$

This is based on the assumption that all chains must start from the initiator molecules, meaning the number of chains is predetermined by the number of initiator molecules, assuming termination and other secondary processes are negligible. The applied potential E_{app} was chosen with respect to the half-wave potential of the catalyst, typically $E_{app} = E_{1/2} - 60$ mV for $[Br_2Cu^{II}_2CAGE]^{2+}$ and $E_{app} = E_{1/2}$ for $[BrCu^{II}TPMA]^{+}$. The application of a slightly more negative potential for the Cu-CAGE system was necessary to achieve a sufficient rate of polymerization (**Table 1**). Polymerization was triggered by application of the applied potential (market as a dotted line in **Figure 22a**).

Aliquots of the reaction mixture were periodically sampled to analyse the reaction mixture via Gel Permeation Chromatography (GPC) and NMR spectra. Key characteristics were determined for each sample, including the experimental number-average molecular weight (M_n), dispersity ($Đ$) and conversion. The M_n represents the statistical average molecular weight of all polymer chains in the sample, while $Đ$ quantifies the distribution of molecular weights and is calculated as M_w/M_n, where M_w is the weight-average molecular weight. M_w is a measure of the average molecular weight of a polymer, weighted by the mass of the molecule, giving greater significance to higher molecular weight species.

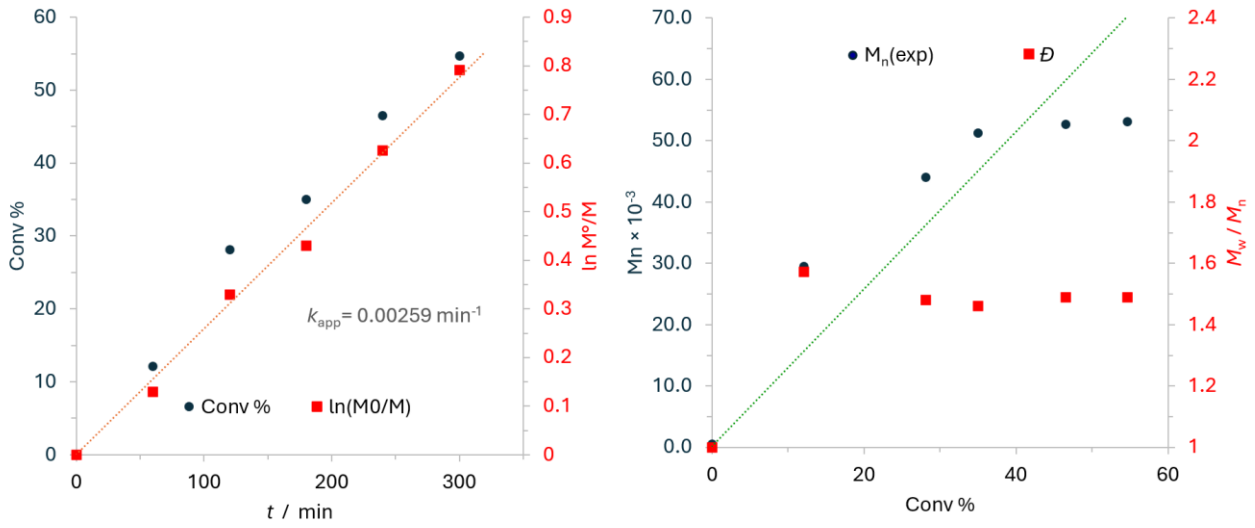

Figure 23. (a) Kinetics plot and (b) molecular weight and dispersity for the eATRP of BA in 1:3 = BA:DMF with 0.1 M (n-Bu)$_4$NPF$_6$, $[Cu^{II}_2CAGE(OTf)_2]^{2+}$= 5×10^{-4} M, and ($n$-Bu)$_4$NBr = 1×10^{-3} M so to obtain concentration ratios of [L]/[Cu^{2+}]/[Br$^-$] = 1/1/1 for $[CuTPMA]^{2+}$ and 0.5/1/1 for $[Cu^{II}_2CAGE]^{4+}$; [BA]:[EBiB] = 1000:1 at a T = 50 °C. The green line represents the theoretical M_n.

In the first experiment, butyl acrylate was used as a monomer with a target degree of polymerization (DP) of 1000. **Figure 23** shows the typical reaction profile of a polymerization carried out with the Cu-CAGE system. More in detail, the data **Figure 23a** indicates a steady increase in monomer conversion over time and linear profile indicating a first-order kinetic, thus a stable radical concentration. **Figure 23b** shows that the molecular weight (M_n) increased linearly with monomer conversion up to 35%, suggesting good control over the polymerization. After reaching 35% conversion, the experimentally observed M_n increases slowly. A possible hypothesis for this behaviour is that as the polymerization proceeds further, the reduced concentration of monomer increases the likelihood of parasitic chain transfer reactions, leading to a decrease in the average molecular weight. The resulting polymer had a dispersity of 1.49, at the boundary of what defines a well-controlled polymerization (dispersity < 1.5). Overall, the Cu-cage system proved to be a competent catalyst for ATRP. To further study its versatility, experiments varying the monomer, initiator, and target degree of polymerization were carried out to provide additional insights into the catalyst's performance.

3.2.3 Role of the degree of polymerization on butyl acrylate polymerization

After confirming the activity of the copper complexes in the eATRP of butyl acrylate, a relatively broad screening of monomers and initiators was performed, which are described in detail in **Appendix A**. Based on the results observed it was decided to focus on the eATRP of butyl acrylate to assess the potential correlation between the targeted polymer chain size and the maximum attainable molecular weight. This would provide valuable insights into the mechanistic aspects of the polymerization process when preparing polymers of different sizes with activation/deactivation within the confined environment of the cage. This study could be achieved by performing a series of polymerizations with increasing target degrees of polymerization (**Table 2**).

Table 2 Electrochemically mediated ATRP of BA at different target *DP* with $[Cu^{II}TPMA]^{2+}$ and $[Cu^{II}_2CAGE]^{4+}$

Catalyst	Entry [a]	Initiator	*DP*	*t*	Conv	$10^3 M_{n,th}$	$10^3 M_{n,exp}$	*Đ*	$k_{app} * 10^3$	Q_{exp}
				min	%				min^{-1}	C
Cu/CAGE	1	EBiB	170	300	97.4	21.1	17.9	1.5	10.2	0.73
	2	EBiB	250	300	97.0	31.8	29.4	1.46	14.6	1.2
	3	EBiB	400	300	97.7	50.5	39.3	1.45	14.0	1.14
	4	EBiB	600	300	83.5	61.0	34.0	1.36	6.12	1.04
	5	EBiB	1000	300	78.3	100.6	53.1	1.49	5.32	1.19
	6	MBP	2000	300	49.0	127.7	55.5	1.58	2.79	1.24
Cu/TPMA	7	EBiB[b]	1000	300	87.2	79.1	53.1	1.49	3.77	1.19
	8	MBP	2000	300	40.9	105	55.5	1.49	2.80	1.02

[a] General conditions: $[Cu^{2+}] = 10^{-3}$ M, T= 50°C, V_{tot} = 6 mL, [*n*-Bu_4NPF_6] = 0.1 M, [L]/$[Cu^{2+}]$/$[Br^-]$ = 1/1/1 for $[Cu^{II}TPMA]^{2+}$, 0.5/1/1 for $[Cu^{II}_2CAGE(Br)_2]^{2+}$, $E_{app} = E_{1/2}$ for Cu/TPMA, $E_{app} = E_{1/2\text{-}60mV}$ for Cu/CAGE

[b] $E_{app} = E_{1/2\text{-}60mV}$

The resulting data showed a decent control over the polymerizations exhibited by the cage catalyst over a relatively wide range of target *DP*, notably showing a trend of dispersity value decreasing to a minimum for the experiment at *DP* 600 (entry 4, **Table 2**), followed by an increase for the higher *DP*s targeted. This trend is also presented in **Figure 24**. The initial decrease is in agreement with the expected trends observed in literature, since as *DP* increases, dispersity should decrease[58]. Indeed, the equation to describe dispersity (M_w/M_n) of the resulting polymers, considering the absence of significant chain termination or transfer is proportional to experimental DP and inversely proportional to $[RX]_0$[58]:

$$\frac{M_w}{M_n} = 1 + \frac{1}{DP_n} + \frac{k_p[RX]_0}{k_{deact}[Cu^{II}]}\left(\frac{2}{p} - 1\right) \quad (3.12)$$

Here p is the conversion of the monomer, DP_n is the number average degree of polymerization and $[RX]_0$ is the initial concentration of initiator. This shows that the dispersity should decrease as the conversion increases and as the ratio of initiator over the deactivating specie copper (II) decreases, in other words, higher target *DP* should lead to smaller dispersity.

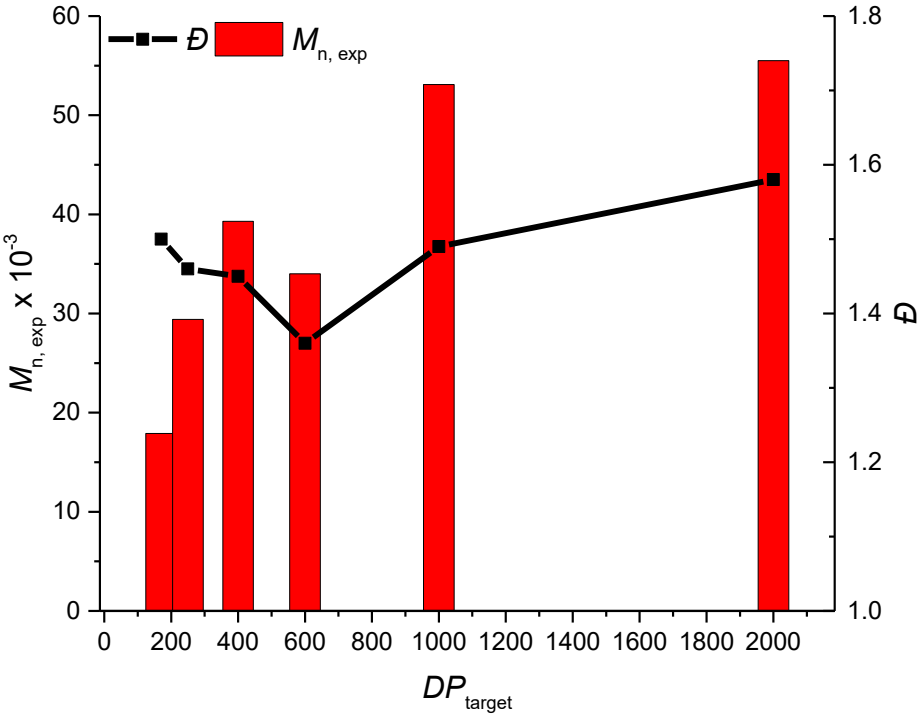

Figure 24. Significant trends for eATRP of BA catalysed by $[Cu^{II}_2CAGE(Br)_2]2+$ at various DPs.

Regarding the increase in dispersity above DP 600, there are two reasonable hypothesis for this behaviour.

The first hypothesis is that since the monomer to initiator ratio decreases as target *DP* increases, a smaller number of chains is actively growing at any given moment, propagation slows down likely increasing the probability of secondary reactions that involve the growing polymer chains such as termination or transfer[59–61]. This means that the dispersity of the obtained polymers is higher than predicted and can be accounted for in an alternative equation for the calculation of dispersity that includes the termination rate constant (k_t)[58]:

$$\frac{M_{\mathrm{w}}}{M_{\mathrm{n}}} = 1 + \frac{1}{DP_{\mathrm{n}}} + \frac{k_{\mathrm{p}}[\mathrm{RX}]_0}{k_{\mathrm{deact}}[\mathrm{Cu^{II}}]}\left(\frac{2}{p} - 1\right) + \left(\frac{k_{\mathrm{t}}k_{\mathrm{act}}[\mathrm{Cu^{I}}]_0}{4k_{\mathrm{p}}k_{\mathrm{deact}}[\mathrm{Cu^{II}}]_0}\right)p \tag{3.13}$$

This equation allows to account for termination reactions and the contribution of that term increases as monomer conversion gets larger, possibly explaining the data obtained.

The second hypothesis relates to the nature of the novel catalyst, which is a confined space, meaning that there could be an inherent size selectivity playing a role in these unexpected results.

3.2.4 Measurement of catalyst activity during polymerization

Having observed relatively poor control over the polymerization of butyl acrylate (BA) at high target degrees of polymerization (*DP*), it was hypothesized that this issue would stem from size selectivity of the confined space catalyst, where the increasing molecular weight of the growing chains affected the thermodynamic parameters (i.e. K_{ATRP}) and kinetics parameters (i.e. k_{act} and k_{deact}) of ATRP. To investigate this, experiments aimed at monitoring K_{ATRP}, k_{act}, and k_{deact} during the polymerization process were set up. The theoretical background on how to measure these parameters is explained next.

The monomer consumption is linked to K_{ATRP} via the following equation, which is derived by integrating the equation describing the rate of ATRP processes:[58]

$$ln\left(\frac{M_0}{M}\right) = k_{\mathrm{app}}t = K_{\mathrm{ATRP}}k_p[\mathrm{P_n - X}]\frac{[\mathrm{Cu^{I}}]}{[\mathrm{Cu^{II}}]}t \tag{3.14}$$

where k_p is the monomer propagation rate constant (available in the literature) and k_{app} is the apparent propagation rate that can be experimentally determined by the slope of the ln([M_0]/[M]) vs t plot (see e.g. in **Figure 23**). From **eq. 3.14** we can derive the ATRP equilibrium constant as:

$$K_{\mathrm{ATRP}} = \frac{k_{\mathrm{app}}}{k_{\mathrm{p}}[\mathrm{P_n - X}]}\frac{[\mathrm{Cu^{II}}]}{[\mathrm{Cu^{I}}]} \tag{3.15}$$

In essence, K_{ATRP} can be measured if the ratio between Cu^{II} and Cu^{I} can be determined during polymerization.

Further, K_{ATRP} is related to k_{act} by the following relation:

$$k_{\mathrm{act}} = K_{\mathrm{ATRP}} \times k_{\mathrm{deact}} \tag{3.16}$$

where k_{act} is the rate of activation of the C-Br bond catalysed by the copper(I) complexes, k_{deact} is the rate of deactivation of the growing radicals via formation of a C-Br bond, catalysed by the brominated copper (II) complexes. k_{deact} can be independently measured from dispersity values and from the concentration of [Cu^{II}]in agreement with **eq. 3.12**.

In summary, if K_{ATRP}, k_{act}, and k_{deact} can be measured during polymerization provided that the following experimental values are known: i) the polymerization rate, which can be easily obtained via the monomer conversion, ii) the dispersity values, which is obtained via GPC, and iii) [Cu^{II}], which can be measured as explained in the next paragraphs.

To investigate all the ATRP parameters, experiments aimed at monitoring the [Cu^{II}] concentration during the polymerization process using linear sweep voltammetry (LSV) were set up. The polymerizations were conducted under standard conditions (see **Table 3**) with the addition of a glassy carbon disk electrode in the reaction cell to collect LSV data at regular intervals. Figure 10a shows LSV recorded during polymerization. While the solution was mixed with a magnetic stirrer, two limiting (i.e. plateau) currents are observed at both cathodic and anodic potential values, which are proportional to the [Cu^{I}] and [Cu^{II}] concentration respectively (i.e. $I_{L,a}/I_{L,c}$ = [Cu^{I}]/[Cu^{II}]). The anodic ($I_{L,a}$) and cathodic ($I_{L,c}$) limiting currents were thus measured to determine the [Cu^{I}]/[Cu^{II}] ratio. Considering that the experiments start with a known amount of Cu^{II} catalyst [Cu^{II}]$_0$, the mass balance of the system is: [Cu^{II}]$_0$ = [Cu^{I}] + [Cu^{II}]). The resulting equation for [Cu^{II}] is thus:

$$[\mathrm{Cu^{II}}] = \frac{[\mathrm{Cu^{II}}]_0}{\left(\frac{I_{\mathrm{L,a}}}{I_{\mathrm{L,c}}} + 1\right)} \tag{3.17}$$

where $I_{L,a}$ and $I_{L,c}$ are the anodic and cathodic limiting currents respectively, [Cu^{II}]$_0$ is the total concentration of the copper centres.

By using this relation on a series of LSV recorded during the polymerization, **Figure 25b** shows that the concentration of Cu(II) continuously increases during the polymerization of poly(butyl acrylate) (PBA) catalyzed by Cu-CAGE, with a DP_T = 1000. From the [Cu^{II}] data in **Figure 25b**, k_{deact} and K_{ATRP} are obtained from the following relations (**eq. 3.18** and **3.19**), which are directly derived from **eq. 3.12** and **3.15**. The resulting K_{ATRP}, k_{act}, and k_{deact} during polymerization and are plotted in **Figure 25**. Some example values for t = 2h and t = 4 are displayed in **Table 3**.

.

$$\frac{1}{k_{\mathrm{deact}}} = \frac{\frac{M_{\mathrm{n}}}{M_{\mathrm{w}}} - 1 - \frac{1}{DP}}{\frac{1}{p} - 1} \times \frac{[\mathrm{Cu^{II}}]}{k_{\mathrm{p}} \times [\mathrm{RX}]} \tag{3.18}$$

$$K_{\mathrm{ATRP}} = \frac{k_{\mathrm{app}}}{k_{\mathrm{p}}} \times \frac{[\mathrm{Cu^{II}}]}{[\mathrm{Cu^{I}}]} \frac{1}{[\mathrm{RX}]} \tag{3.19}$$

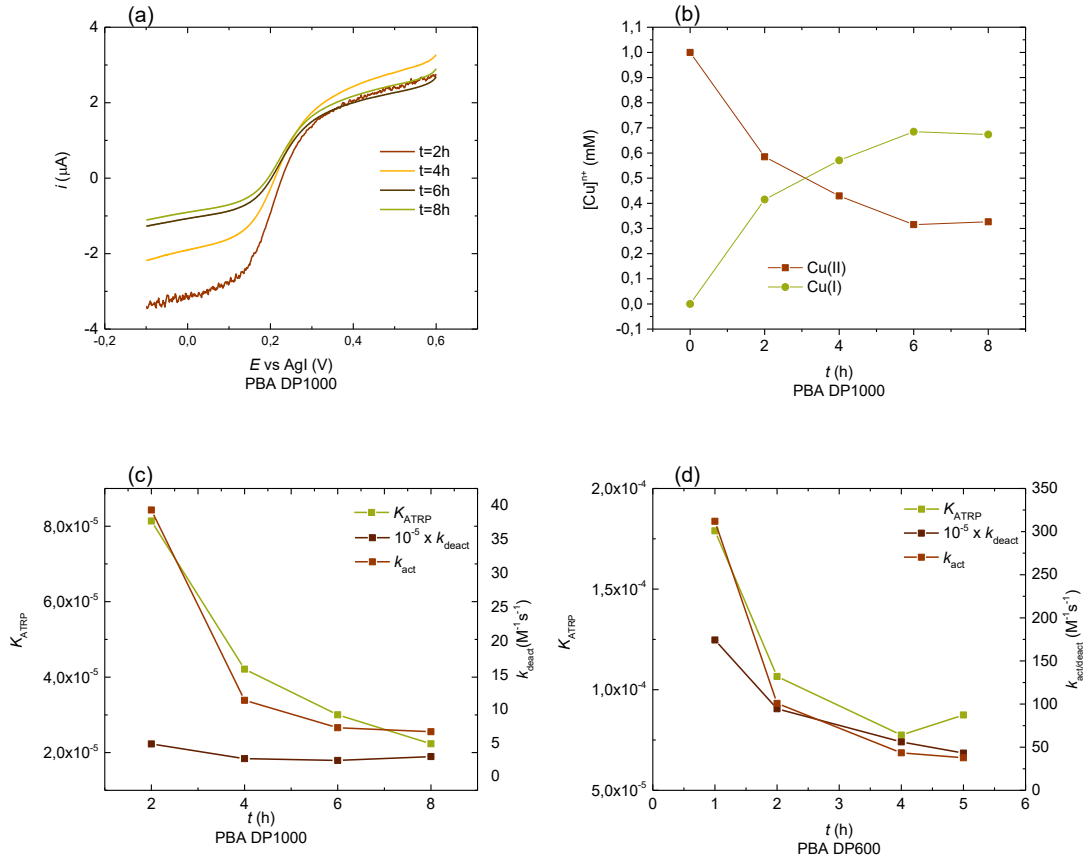

Figure 25 (a) LSV at 10 mV/s on GC electrode under magnetic stirring; (b) Cu(II) and Cu(I) concentrations trends during polymerization of PBA at target DP 1000 (conditions as in Table 4 entry 5); (c) calculated kinetic constant at different times for the ATRP of PBA at target DP 1000 (conditions as in Table 4 entry 5); (d) calculated kinetic constant at different times for the ATRP of PBA at target DP 600 (conditions as in Table 4 entry 4).

The results in **Figure 25c** showed that both values of k_{act} and K_{ATRP} diminished during polymerization, supporting the hypothesis that size control was a factor in the observed relatively poor control over polymerizations of BA high degrees of polymerization. In essence, these experiments suggested that larger polymers reacted more slowly within the confined

environment of the cage. Interestingly, the deactivation rate constant remained approximately stable, showing only a slight decline during the polymerization. This stability of k_{deact} indicates that further experiments are needed to understand the reasons behind this behaviour. Similar results were obtained for the monitoring a polymerization with DP_T = 600 (**Figure 25d**

Table 3 Kinetic and thermodynamic parameters measured during eATRP of BA with $[Cu^{II}CAGE]^{2+}$

Entry [a]	DP	Initiator		*t* = 2h			*t* = 4h		
			$10^3 k_{app}$	$10^{-5} K_{ATRP}$	k_{act}	$10^{-5} k_{deact}$	$10^{-5} K_{ARTP}$	k_{act}	$10^{-5} k_{deact}$
			min^{-1}		$M^{-1}s^{-1}$	$M^{-1}s^{-1}$		$M^{-1}s^{-1}$	$M^{-1}s^{-1}$
1	600	EBiB	3.09	10.7	101	94.6	7.75	43.5	56.1
2	1000	MBP	2.91	8.14	39.3	4.83	4.21	11.3	2.67

[a] General conditions: Solvent: DMF, [*n*-Bu_4NPF_6] = 0.1 M, *T* = 50 °C, $[Cu^{2+}] = 1\times10^{-3}$ M

3.3 Investigation of the reactivity of the Cu^I/CAGE complex with (macro)initiators and of increasing molecular weight

Having observed a drop in the activation kinetic constant as the polymerization progresses, the focus of the experiments shifted toward the exploration of the hypothesized size selectivity of the confined environment within the cage. The approach utilized to effectively probe on a possible size-selectivity was to test the variation in the ATRP activation rate constant with initiators having the same chain-end reactivity but increasing molecular weight.

Initially, the synthesis of acrylate based macroinitiators (MIs) was considered, but the literature concerning acrylate oligomerization via ATRP (to obtain bromine functionalized chain-ends) was scarce. It was then decided to synthesize styrene oligomers, as the propagation rate constant for this monomer is much lower than that of acrylates, making it easier to obtain shorter chains with well-defined molecular weights. Furthermore, ATRP of relatively short chained polystyrene was already reported, allowing easier development of a synthetic procedure.[62]

The properties of the styrene-based (macro)initiators are listed in **Table 4**. Bromoethylbenzene, which mimics polystyrene of DP 1, is commercially available, while higher molecular weight $PSty_nBr$ macroinitiators were synthetizes as explained below.

Table 4 Properties of the styrene based (macro) initiators.

Initiator	DP	$M_{n,\,NMR}$	$Đ$	α	$10^{-6}D$ (cm^2/s)	% C-Br Functionality
BEB	1	185.1[a]	1	0.382	11.8	80
$PSty_4Br$	3.6	466.8	1.03	0.294	8.90	92
$PSty_7Br$	6.6	786.6	1.07	-[b]	-[b]	94
$PSty_{14}Br$	14	1667	1.17	0.282	2.58	81
$PSty_{15}Br$	15	1783	1.15	0.258	5.51	77

[a] Formula molecular weight

[b] Not measured

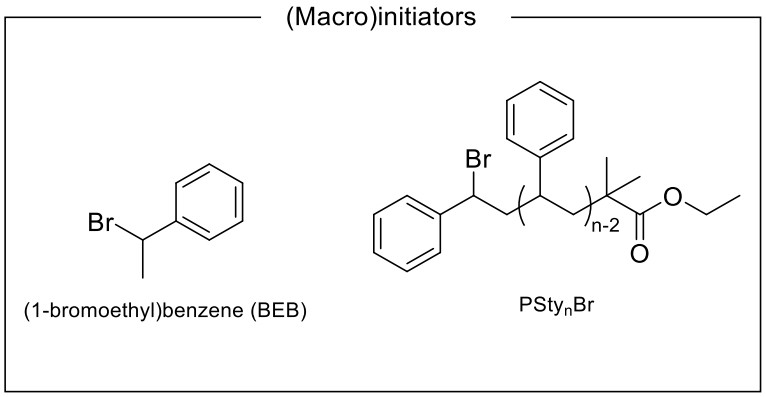

3.3.1 Synthetic approach

The synthesis of the macroinitiators (MIs) was carried out by normal ATRP following this general approach:

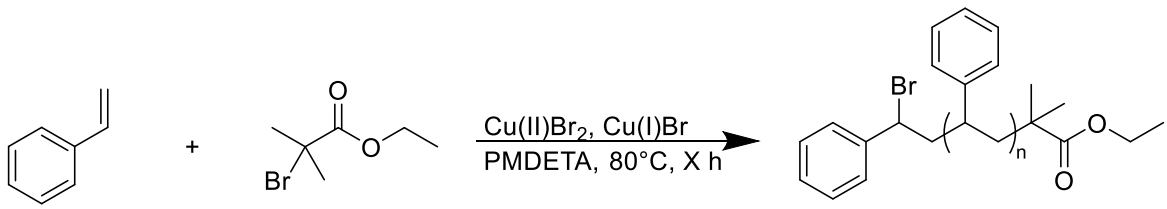

All the syntheses happened in bulk styrene, at 80 °C, using PMDETA as a ligand for the copper, forming the complex Cu/PMDETA, a commonly used ATRP catalyst. According to traditional normal ATRP procedure, copper(I) is used in a large excess, leading to a concentration of 0.3 M, while copper(II) is present in a concentration of 1.3×10^{-3} M. The ATRP

was conducted for 60 minutes to 3 hours, depending on the targeted *DP* of the reaction ([Monomer]/[Initiator]) and the targeted *DP* of the MI, since to avoid termination and other secondary processes the reaction was conducted stopping at relatively low conversions. The resulting product was purified by re-precipitated in methanol three times and then dried in rotavapor at 50 °C and full vacuum.

A different purification procedure was used to obtain $PSty_{3.6}Br$ and $PSty_{6.6}Br$. Initially, a relatively polydisperse sample of average *DP* 4.2was synthesized using the aforementioned method. The GPC trace of this sample is shown in **Figure 27** and shows different peaks and shoulders indicating the presence of PSty oligomers of different MWs. Subsequently, various separations were performed to isolate two different polymeric fractions within this sample ($PSty_{3.6}Br$ and $PSty_{6.6}Br$). Instead of precipitating the raw $PSty_{4.2}Br$ mixture after the alumina filtration, it was first filtered over a silica column to remove the styrene with a 99:1 hexane:ethyl acetate mixture as a washing solution. The obtained polymer was then separated in an automated silica column (Biotage®), and two fractions were collected and isoalted: the second one containing and the last one (tail) (**Figure 27**). These were selected in order to achieve sufficient moelcular weight separation between the isolated fractions.

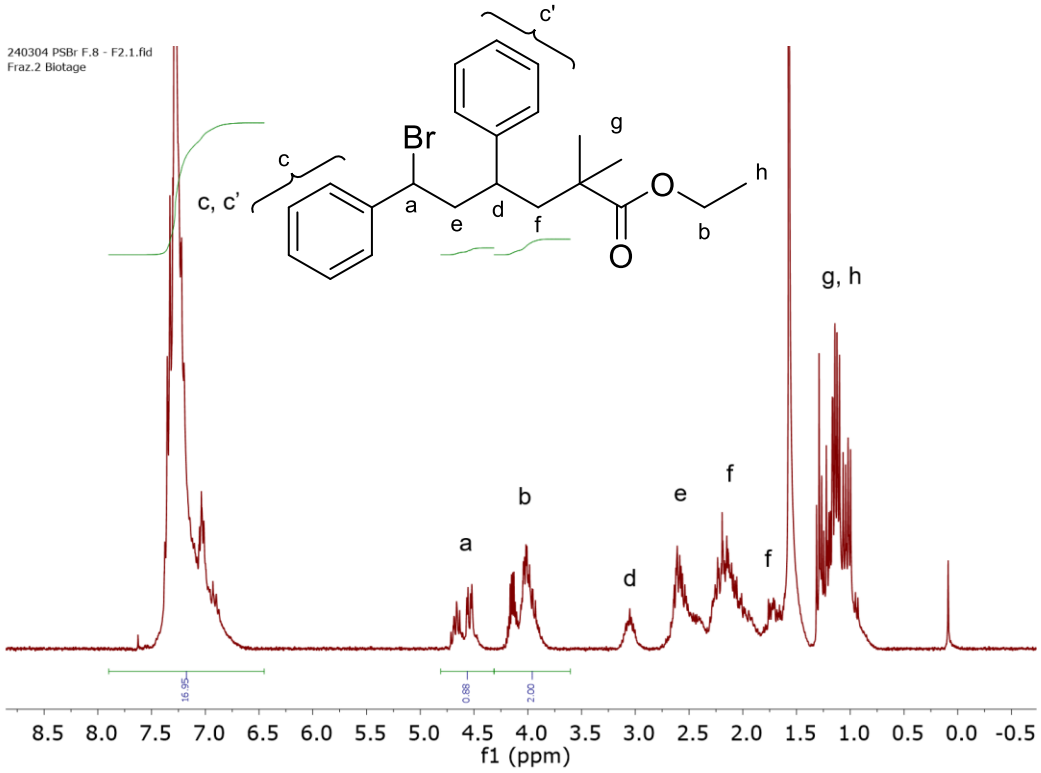

Figure 26 NMR spectrum and peak assignation of $PSty_{3.6}Br$.

The resulting fractions were characterized by ^{1}H-NMR (an example is shown in **Figure 26**) and GPC analysis. The experimental degree of polymerization was determined as the ratio of the area under the peaks of the aromatic protons (c, c'), normalized for their number for repetitive styrene unit, over the area of the signal for the α hydrogen respective to the brominated carbon(a). The extra signal included in **eq. 3.20** ($S_{5.5\text{ppm}}$) represents one of the vinylic protons on the styrene (monomer) and is useful to correct the formula in case trace residues of styrene remained in the macroinitiator.

$$DP_{\text{exp}} = \frac{\frac{S_{6.5-7\text{ppm}}}{5} - S_{5.5\text{ppm}}}{S_{4.6\text{ppm}}} \tag{3.20}$$

where $S_{x\ \text{ppm}}$ represents the area under the curve of the NMR peak found at a chemical shift of x ppm, the integer numbers are instead used to normalize the peak integral for the number of protons constituting it. The chain-end functionality was instead calculated as the ratio between the area of the peak of the proton of the brominated carbon (a) over that of the methylene protons of the ethyl acetate group of the initiator fragment (b).

$$Br^{-}func = \frac{S_{4.6}}{\frac{S_{4.0}}{2}} \tag{3.21}$$

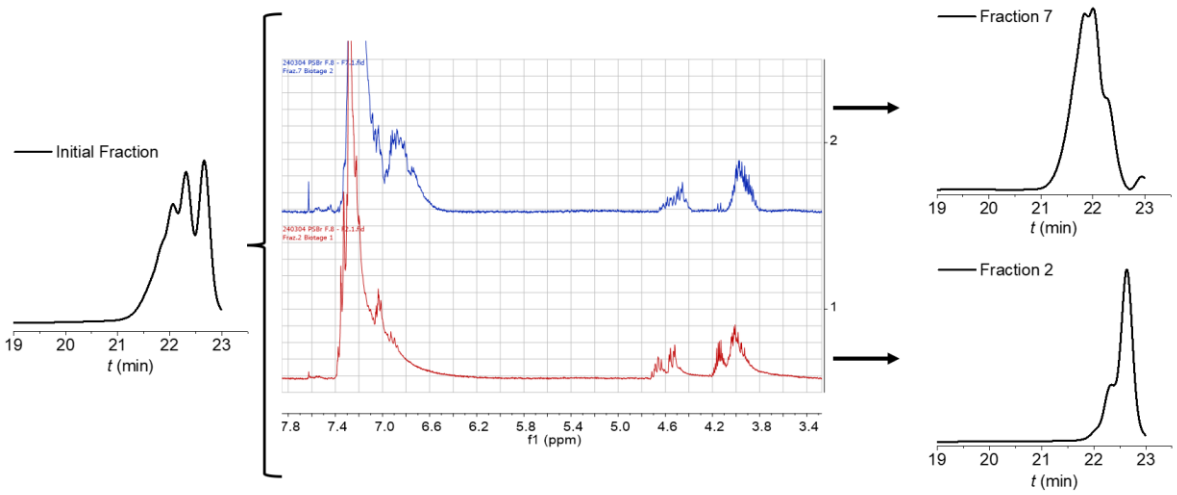

Figure 27 GPC trace for the initial fraction obtained from filtration over silica; NMR spectra of the head and tail fractions (referred only to the fractions containing oligomeric product) obtained from the Biotage® column with 2 being the first useful eluted fraction, containing the $PSty_4Br$ mixture and 7 being the last one, containing the $PSty_{6.6}Br$ mixture; GPC traces for the selected fractions 2 and 7 ($PSty_{3.6}Br$ and $PSty_{6.6}Br$).

^{1}H-NMR of all fractions collected during the separation of the MI mixture provided some interesting insights into the composition of the samples. During the silica separation, residual styrene was eluted first, likely because it is more mobile and less polar than the brominated and acrylated oligomers. The shorter polymeric chains were eluted next, as the bromide functionality makes them slightly more polar and thus interact better with silica if compared with styrene. As the chain length increases their mobility decreases, likely explaining why longer elution times rendered higher molecular weight chains.

The resulting oligomeric mixtures had a narrow molecular weight distribution according to the GPC analysis and a high chain-end functionality according to the NMR spectra, making them extremely promising for the application in the following studies as well-defined MIs. In

the next sections, the procedure to study the activation reaction of the initiators with the **Cu/CAGE** and **Cu/TPMA** systems is explained.

3.3.2 Determination of the diffusion coefficients of the (macro)initiators

The diffusion coefficient for the initiators was estimated through a slightly different version of the method described previously for the **Cu/CAGE** and **Cu/TPMA** systems.

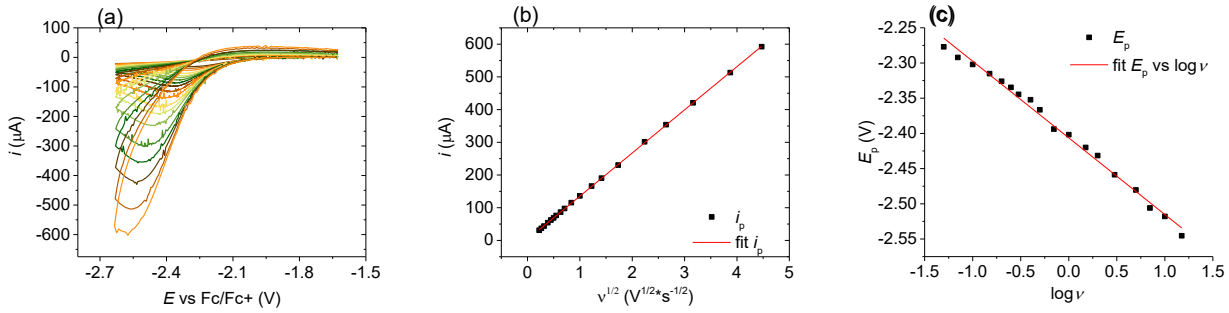

Figure 28 Determination of the diffusion coefficient for $PSty_{3.6}Br$: (a) CVs at a scan rate from 0.05 to 20 V/s of 2×10^{-3} M $PSty_{3.6}Br$ in a solution of 0.1 M *n*-Bu_4NPF_6 in DMF; (b) linear fitting of peak current intensity over square root of the scan rate; (c) linear fitting of peak potential over the logarithm of scan rate.

The Randles-Sevcik equation must be adjusted for this system since the direct reduction of the carbon-bromide bond is an irreversible two electron process, while the previously discussed equation refers to electrochemically reversible systems. The following two ETs are associated with the single irreversible peak of the MIs:

$$RX + e^- \leftrightarrows R^\bullet + X^- \tag{3.22}$$

$$R^\bullet + e^- \rightleftarrows R^- \tag{3.23}$$

The ensuing radical $R^\bullet$ is more easily reduced that the starting material RX, making the overall process an irreversible two-electrons reduction.

The adjusted formula linking peak current to *D* for irreversible ETs is:

$$I_p = (2.99 \times 10^5) nAC\sqrt{\alpha D v} \tag{3.24}$$

where α is the transfer coefficient, a dimensionless parameter that relates the variation of Gibbs free energy for an electron transfer reaction to the activation energy of the cathodic process. It is estimated by plotting the shift in cathodic peak potential (E_p) against the

logarithm of the scan rate (*v)*, which for an irreversible electron transfer process forms a linear relationship following the equation:

$$\frac{\partial E_{\mathrm{p}}}{\partial \log v} = -1.15 \times \frac{RT}{\alpha F} \tag{3.25}$$

this allows an easy determination of α through cyclic voltammetry. Plotting the values of E_p vs log*v* for the reduction of the MIs (**Figure 28**) showed indeed a linear trend from which α could be determined. The values of α were in the range 0.2 - 0.4, which is in line for an ET involving the concerted reduction of a carbon-halogen bond. The diffusion coefficient was estimated from the linear trend of the i_p vs $v^{1/2}$ plot via the Randles-Sevcik equation for irreversible processes resulting in the data reported in **Table 4**.

3.3.3 Voltammetry of $[Br_2Cu^{II}_2CAGE]^{2+}$ and $[BrCu^{II}TPMA]^{+}$ in the presence of the (macro)initiators

Having prepared a series of initiators of different molecular weight, a series of experiments was conducted to investigate their reactivity with the copper complexes. The first test was the comparison between the catalytic properties of the **Cu/CAGE** catalyst and that of **Cu/TPMA** on the electrocatalysis of the monomolecular initiator 1-bromoethylbenzene (BEB) and on that of $PSty_{15}Br$. The setup was similar to that of most other cyclic voltammetries but, with the idea of studying only the carbon-halogen bond cleavage, the radical trap TEMPO was added in the electrolytic solution. This compound makes the ATRP activation stap irreversible by trapping the radicals forming after the activation of the initiator.

The overall catalytic mechanism underlying the process is presented in **Figure 29**. The radical trap, signified by the letter T, takes part in the radical termination reaction and causes the peak catalytic current to increase due to the reoxidation of copper(I) to copper(II), while the peak anodic current decreases due to the same process. The radical trap was added in large excess, typically 5 to 20 times more concentrated than the catalyst. The mechanism, for the sake of completeness, reports also the cycle involving the non-brominated copper complex, this has a small contribution to the total catalytic effect in DMF due to the very high binding constant of bromide to the metal centres in this solvent.

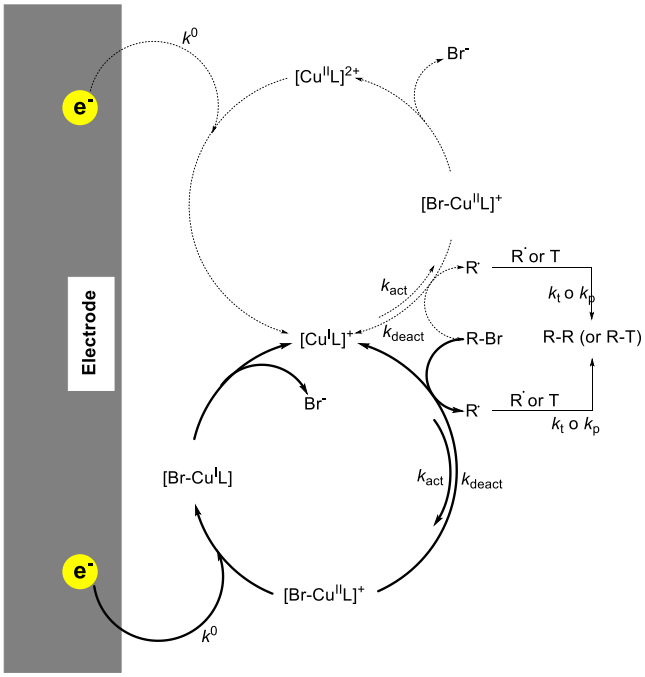

Figure 29 Mechanism of ATRP activation at the electrode, where R-Br, T and L represent respectively the initiator, the radical trap TEMPO and the ligand forming the catalyst (CAGE or TPMA).

The obtained CVs (**Figure 29**) show a remarkable difference between $[BrCu^{II}TPMA]^+$ and $[Br_2Cu^{II}_2CAGE]^{2+}$, especially after the addition of $PSty_{14}Br$, the high molecular weight macroinitiator.

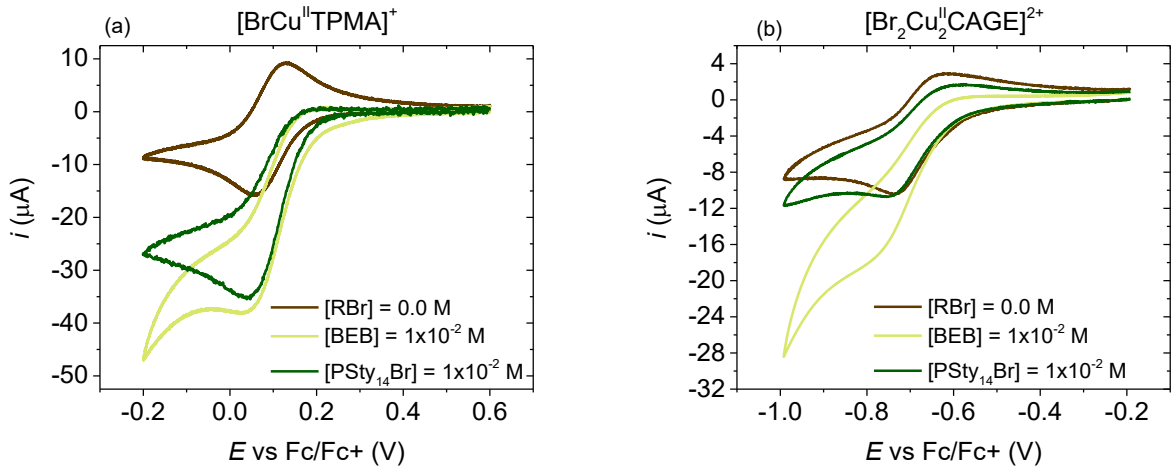

Figure 30 CVs of 5×10^{-4} M $[Br_2Cu^{II}_2CAGE]^{2+}$ (a) and 10^{-3} M of $[Cu^{II}TPMA(Br)]^+$ (b), at a scan rate of 0.1 V/s, in DMF + 0.1 M *n*-Bu_4NPF_6 at T = 50 °C and in presence of excess radical trap TEMPO. The dark green curve was recorded after the addition of 10 equiv. of $PSty_{14}Br$, while the light green scan was collected after the addition of 10 equiv. of BEB, in a different experiment with the same conditions.

The activity of an electrocatalytic system can be determined from the peak current enhancement, that is the ratio between the peak current in the absence and in the presence of initiator. Using this we can calculate the degree of catalysis (i_p/i_p^0) for every combination of catalyst-initiator, which are reported in **Table 5**.

The $[BrCu^{II}TPMA]^+$ catalysts displayed similar reactivity with the BEB and the $PSty_{14}Br$, with similar i_p/i_p^0 values. Conversely, the $[Br_2Cu^{II}_2CAGE]^{2+}$ catalysts showed markedly diminished reactivity with $PSty_{14}Br$.

These results confirm that the confined environment of the cage catalyst has different properties than those of the standard catalyst **Cu/TPMA**, the main one being observed seemingly being dimensional selectivity towards small molecular weight species.

Table 5 Cathodic peak current ratio between catalytic and non-catalytic cyclic voltammetries (i_p/i_p^0)

	$[BrCu^{II}TPMA]^+$	**$[Br_2Cu^{II}_2CAGE]^{2+}$**
BEB	2.43	2.13
$PSty_{14}Br$	2.41	1.03

Preliminary esperiments (not reported here) suggest that the reactivity of $[Br_2Cu^{II}_2CAGE]^{2+}$ scales with the DP of the (macro)initiators.

4 CONCLUSIONS

In this work, the novel cage catalyst $[Cu^{II}_2CAGE]^{4+}$ was characterized with the intention of exploring its electrochemical properties and, more specifically, the possibility of its application in electrochemically mediated atom transfer radical polymerization (eATRP).

The speciation of the confined-space complex was first investigated through a combination of cyclic voltammetry and UV-Vis based titrations. $[Cu^{II}_2CAGE]^{4+}$ could bind two bromide anions forming the stable $[Br_2Cu^{II}_2CAGE]^{2+}$ complex. The two copper centres appeared to be independently reduced at the working electrode, demonstrating absence of electronic interactions between the two.

The behaviour of $[Br_2Cu^{II}_2CAGE]^{2+}$ was consistent with that of the comparative reference model, provided in the form of the well-established $[BrCu^{II}TPMA]^{+}$ catalyst, which shares similar electrochemical properties, including the similar standard reduction potential and electron transfer rate constants. However, the diffusion coefficients differed because of the significantly different molecular weight of the two catalysts. In essence, the electrochemical behaviour of $[Br_2Cu^{II}_2CAGE]^{2+}$ resembled that of two fused, but independent, $[BrCu^{II}TPMA]^{+}$ complexes.

After studying the electrochemical behaviour of the **Cu/CAGE** catalyst, we turned to its application in eATRP. Cyclic voltammetry with a typical ATRP initiator (MBP) confirmed the electrocatalytic C-Br activation by the **Cu/CAGE** complex, paving the way for its further exploration in eATRP.

Performing eATRP of poly(butyl acrylate), testing the catalyst's ability to initiate and control the reversible deactivation radical polymerization, confirmed the effectiveness of the **Cu/CAGE** catalyst. A wide screening of eATRP of various monomers and initiators was successively performed (Appendix A), showing that the catalyst was able to work in a wide range of conditions, from which the polymerization of butyl acrylate was chosen as the more convenient option for further studying of the process.

The eATRP of butyl acrylate at various target *DP*s showed an intriguing trend of diminishing polymerization control when increasing the targeted molecular weight of the final polymer, prompting further exploration of the causes of these trends. For this reason, the kinetic constants of ATRP activation/deactivation were monitored over time during the polymerization of butyl acrylate, showing a remarkable drop in the kinetics of activation at higher

polymerization times, which correlates with higher molecular weight of the growing chains. This was a first indication of a possible effect of the confined environment provided by the **Cu/CAGE** complex over its reactivity.

With the objective of further exploring the size selectivity hypothesis, ATRP initiators with the same end-chain functionality but increasing molecular weight were then synthesized via normal ATRP. The catalytic activity of the **Cu/CAGE** complex with the synthesized initiators was tested, showing a drastic drop in catalytic activation for the higher molecular weight initiator over that of the small-molecule initiator with the same structure. For comparison, the same analysis was performed with the **Cu/TPMA** system, which confirmed a remarkable difference between the two catalysts, where **Cu/TPMA** showed negligible effect of initiator size on its catalytic activation compared to **Cu/CAGE**. These observations can be justified by a dimensional selectivity provided by the confined space environment of the **Cu/CAGE** complex, although further studies are required to elucidate the mechanisms and entity of this effect.

Future experiments will focus on providing a more accurate quantitative analysis of the size selectivity phenomenon. This can be achieved within the framework established in this thesis, by analyzing CVs at various scan rates in the presence of different synthesized macroinitiators. Additionally, this unique size selectivity effect should be leveraged for the preparation of new materials, enabling the synthesis of polymers with novel architectures and applications.

5 EXPERIMENTAL SECTION

5.1 Materials and reagents

Solvents

N,N-Dimethylformamide (DMF, Carlo Erba, HPLC isocratic grade 99.9%). Chloroform-d (CDCl 3 , Sigma-Aldrich, 99.8% atom % D).

Catalyst

Copper(II) bromide ($CuBr_2$, Sigma-Aldrich, 99%), Tris(2-pyridilmethyl)amine (TPMA, Koei chemical, CAS 16858-01-8). Cu_2CAGE (Synthesized as reported in the section 1.5, MW = 2432 g/mol).

Monomers

Butyl acrylate (BA, Sigma-Aldric, (stabilised) ≥99%), Methyl acrylate (MA, Sigma-Aldrich, (stabilised) ≥99%), Methyl methacrylate (MMA, Sigma-Aldrich, (stabilised) ≥99%), Styrene (Sty, Sigma-Aldrich, (stabilised) ≥99%), Poly(ethylene glycol) methyl ether methacrylate ($OEOMA_{500}$, Sigma-Aldrich, stabilised, M_n = 500), Isobornyl acrylate (iBoA, Sigma-Aldrich, technical grade).

Bromide source

Tetrabutylammonium bromide (TBABr, Sigma-Aldrich, ≥98%) It was purified by recrystallization by adding Et_2O as counter solvent to a saturated EtOAc solution and dried in vacuum at 60 °C for 3 days.

Supporting electrolyte

Tetrabutylammonium hexafluorophosphate (*n*-Bu_4NPF_6, Sigma-Aldrich, ≥99%). It was purified by recrystallization from an EtOH/H_2O 1:1 solution and dried in vacuum for one day.

Other chemicals

Methanol (MeOH, Sigma-Aldrich, ACS reagent, ≥ 99.8%), Ferrocene (Fc, Acros Organics, 98%), Dichloromethane (DCM, Sigma-Aldrich, ≥99%), Ethanol (EtOH, Sigma-Aldrich, ≥99.5%), Acetone (Sigma-Aldrich, suitable for HPLC ≥99.9%) tetrabutylammonium iodide (*n*-Bu_4NI, Sigma-Aldrich, ≥99%), tetrabutylammonium tetrafluoroborate (*n*-Bu_4NBF_4, Sigma-Aldrich, ≥99%).

5.2 Instrumentation

Working electrode (WE):

(i) Glassy carbon disk electrode (GC, r = 1.5 mm) for cyclic voltammetries. Before every electrochemical measurement, the GC electrode's surface is polished with a 0.25 µm diamond paste for 30-90s and cleaned by sonicating 2-5 minutes in absolute ethanol. Before inserting it in the electrochemical cell it is carefully rinsed with acetone.

(ii) Platinum mesh for polymerizations. Before every polymerization experiment, the platinum mesh was burned red using a blow torch. It was then activated through repeated CV scans (100-200 scans typically) between -0.67 V to 0.91 V vs $Hg/HgSO_4$ in a 0.5 M H_2SO_4 aqueous solution.

Reference electrode (RE):

$AgI_{(s)}$ coated silver wire immersed in a solution of *n*-Bu_4NI 0.1 M in DMF. The AgI coating was produced via galvanostatic electrodeposition (0.4 mA/cm^2, KI 0.1 M + HNO_3 0.1 M) for 45 minutes. The separated cell containing the *n*-Bu_4NIsolution was prepared from a glass tube with a porous frit (G3) partially filled with Agar-Agar gel. The Agar gel was heated with a thermic gun to remove bubbles and even the filling level and then vacuumed through the porous frit to make the Agar adhere to the frit. The silver wire is held in place thanks to a rubber cap closing the tube.

The potential of the RE couple is not stable and tends to drift. For this reason, the ferrocene/ferrocenium (Fc/Fc^+) couple is used as internal reference. At the end of every electrochemical experiment, a small amount of Fc is added to the electrolytic solution and its oxidation halfwave potential is measured via CV. The potential measured during the experiments (vs Ag/AgI) is scaled versus the Fc/Fc^+ couple by subtracting the halfwave potential of the ferrocene's oxidation to the potentials measured against the Ag/AgI couple.

Counter electrode (CE):

(i) Platinum wire for the CVs.

(ii) Sacrificial aluminium wire in separated cell for the polymerization experiments. The electrode is prepared in a glass tube with a porous frit, partially filled with Agar-Agar gel following the same procedure illustrated for the preparation of the

RE. The separated cell is then filled with a 0.1 M solution of *n*-Bu_4NBF_4 in DMF and an aluminium wire is dipped in the solution and locked in position with a rubber cap on the tube.

5.2.1 Potentiostats

Four potentiostats were used in this work: (i) Autolab PGSTAT30 (eco-Chemie, Utrecht, Netherlands), connected to the software GPES; (ii) Princeton Applied Research Model 273A Potentiostat/Galvanostat; (iii) Autolab PGSTAT204 (Eco-Chemie, Utrecht, Netherlands), connected to the software NOVA 2.1); (iv) Ivium V99738, connected to IviumSoft 4.1109 software.

5.2.2 Gel permeation chromatography (GPC)

Instrument: Agilent infinity 1260, equipped with two columns (Agilent PLgel 5 μm MIXED-C 300 × 7.5 mm) connected in series and thermostated at 60 °C. The stationary phase is constituted of reticulated polystyrene-divinylbenzene, the mobile phase is a DMF solution (1×10^{-2} M LiBr), set at a 1 mL/min flow and at the exit of the column a refractive index detector is set and kept at 50 °C. The calibration of the instrument was made on the retention times of polymethylmethacrylate standards (Agilent Easivial), fitted on a third order polynomial equation.

The sample's preparation consisted in a dilution of the raw product with DMF, bringing the polymer's concentration to 1 mg/mL, followed by a filtration over neutral alumina to remove all the solid particles.

Gel permeation chromatography is a chromatographic technique based on the separation of molecules taking advantage of their different hydrodynamic radius. The separation happens inside the chromatographic columns, where a stationary phase is immobilized, and the analyte is eluted with the mobile phase through the stationary one. Higher hydrodynamic radius species are excluded by the immobilized phase's porosity and have lower retention times. Conversely, smaller hydrodynamic radius species have higher retention times due to the multiple passageways that are available through the stationary phase's porosity.

5.2.3 Nuclear magnetic resonance (NMR) spectrometer

Bruker 200 equipped with a QNP probehead, for one-dimensional routine spectra: Used for the determination of monomer conversion in the eATRPexperiments.

Bruker 400 Avance III HD, with Topspin 3.5 software, equipped with a ^{1}H-^{13}C ATM-z grad probehead: Used for the analysis of the macroinitiators, as discussed in section 3.3.1.

5.3 Experimental procedures

5.3.1 Electrochemical cell

A 5 necked, jacketed electrochemical cell (50 mL) was used in all the electrochemical experiments. The experimental setup also included three electrodes (WE, RE and CE as discussed above), a rubber septum and a plastic cap to close the remaining neck. The rubber septum is used to set up an argon bubbler to remove the oxygen from the electrolytic solution. The bubbler was set up using two single-use hypodermic needles, one long and one short, so the long one was dipped in the solution to bubble argon and the other was used to let the gas escape the cell. The cell was also equipped with a magnetic stir bar and thermostated at 50 °C with a heated water bath circulator.

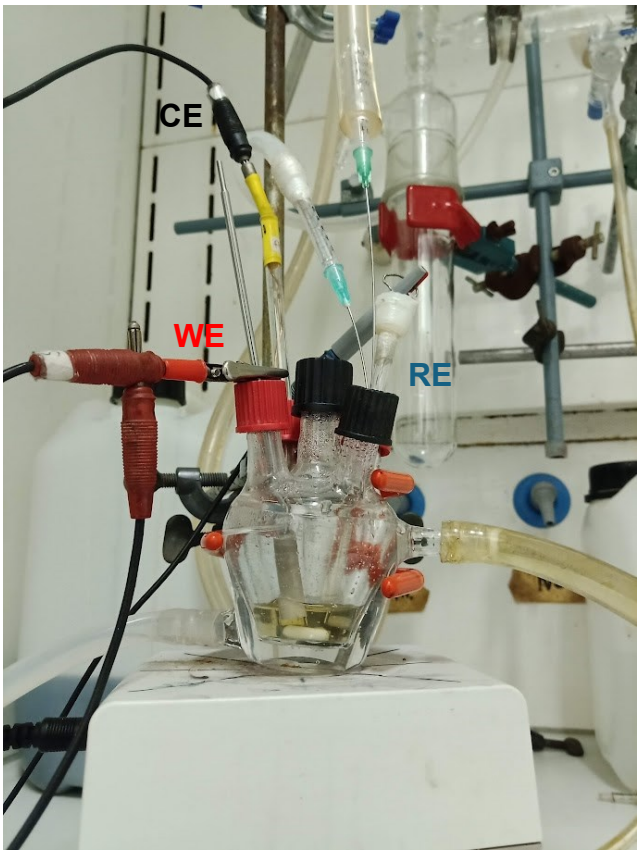

Figure 31 Typical CV experimental setup, with WE: glassy carbon electrode; CE: platinum wire electrode; RE: Ag/AgI separated cell electrode

5.3.2 Cyclic voltammetry

Cyclic voltammetry allows to obtain a wide range of information on a redox process. The voltammetric analysis consists in the application of a linear potential scan applied at the working electrode while measuring the current flowing through the amperometric circuit. After the first scan, reaching the apex potential, the scan is reversed, keeping the speed constant and collecting valuable data on the reversibility of the redox process. A typical reversible redox process, like:

$$O + e^- \rightleftharpoons R \tag{5.1}$$

assuming the starting solution contains only the oxidated specie (O), shows a cathodic peak, scanning towards progressively more negative potentials, associated with the reduction of the oxidated specie. Once the scan's direction gets reversed, the reduced specie (R) undergoes oxidation, showing the anodic peak. These peaks are characterized by a peak potential (E_p) and a peak current intensity (i_p). Another very useful parameter is the halfwave potential,

which is a very good approximation of the redox potential of the couple, and it is found following the equation:

$$E_{1/2} = \frac{E_{\mathrm{p,c}} + E_{\mathrm{p,a}}}{2} \tag{5.2}$$

where the subscript under E_p signifies the cathodic (c) and anodic (a) nature of the peak.

The peak intensity of the current measured at the electrode in a still solution is correlated with many parameters and its described by the Randles-Sevcik equation:

$$i_p = 0.4463nFAC\sqrt{\frac{nFvD}{RT}} \tag{5.3}$$

where n is the number of transferred electrons, *F* is the Faraday constant, *A* is the area of the electrode in cm^2, *C* is the concentration of analyte in mol/L, *v* is the scan rate in V/s, *D* is the diffusion coefficient of the analyte in cm^2/s, *R* is the universal gas constant and *T* is the temperature in K.

5.3.3 eATRP

The electrochemically mediated ATRP was conducted in a 5-necked, jacketed electrochemical cell equipped with a magnetic stir bar and the three electrodes setup (WE, CE, RE), with the platinum mesh electrode as working electrode and the aluminium wire in separated cell as the counter electrode and in addition the GC working electrode to perform the preliminary CVs. 0.232 g (5.99×10^{-4} mol) of supporting electrolyte (*n*-Bu_4NPF_6) was added to the cell, followed by the addition of 4.5 mL of DMF. 20 mL of the chosen monomer were then filtered over basic alumina to remove the stabilizer and 1.5 mL of the purified monomer were added to the electrochemical cell. The electrolytic solution was then stirred vigorously and argon was bubbled through it for 20-30 minutes using the setup described in section 5.3.1.

The catalyst was then added (Cu_2CAGE 7.30×10^{-3} g (2.5×10^{-6} mol); 120 µL CuTPMA was added from a 0.05 M stock solution) followed by 1.93×10^{-3} g of bromide source (*n*-Bu_4NBr, 5×10^{-6} mol). A cyclic voltammetry of the solution was then performed in order to calculate the $E_{1/2}$ of the catalyst's redox couple, used to determine the potential applied in the polymerization ($E_{app} = E_{1/2} - 60$ mV for the Cu_2CAGE catalyst and $E_{1/2}$ for the CuTPMA). The ATRP initiator was added based on the target degree of polymerization (DP), using the formula:

$$[\text{Initiator}] = \frac{[\text{Monomer}]_0}{DP} \tag{5.3}$$

where $[\text{Monomer}]_0$ is the concentration of monomer added at the beginning.

The chosen potential is then applied for 3-8 hours, depending on various conditions like catalyst, target *DP* and monomer choice.

5.3.4 Normal ATRP (macroinitiators' synthesis)

The normal ATRP synthesis of the macroinitiators (MIs) followed the general structure of the $PSty_{15}Br$ preparation, presented as follows:

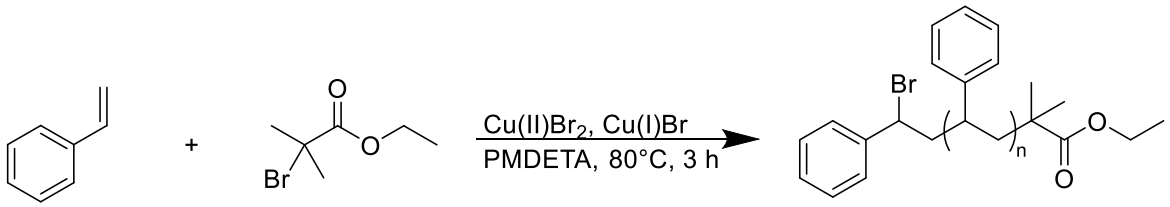

About 150 mL of styrene were filtered over basic alumina to remove the stabilizer. 15 mL (0.131 mol) of styrene were put into a dried 100 mL Schlenk flask equipped with a stir bar and degassed through argon bubbling for about 20 minutes. 400 µL (1.94 mmol) of bis(2-dimethylaminoethyl)methylamine (PMDETA) and 400 µL (2.72 mmol) of ethyl α-bromoiso-butyrate (EBIB) were added to the degassed styrene and the slightly yellow tinted solution was degassed through three cycles of freeze-pump-thaw to completely remove the oxygen from the system. In a second dried 100 mL Schlenk flask, equipped with a stir bar, 314 mg (2.19 mmol) of CuBr and 21 mg (0.0095 mmol) of $CuBr_2$ were added. This Schlenk flask was degassed through three consecutive vacuum pulling and argon refilling.

The styrene solution was then transferred via a transfer canula to the CuBr and $CuBr_2$ flask. The obtained dispersion (green solution, black particles) was once again degassed through three freeze-pump-thaw cycles. The flask was then punt in an 80 °C oil bath under mild stirring. After three hours the flask was cooled to room temperature and the reaction quenched by adding 20 mL of dichloromethane and filtering the formed solution over neutral alumina to remove the copper salts and to expose the solution to air. The flask and alumina column were washed two times with 20 mL of dichloromethane to ensure that no oligomer remained in the column.

Table 6 Different conditions applied to the synthesis of the macroinitiators. All the other conditions follow the procedure reported above.

Macroinitiator	Reaction time (min)	EBIB (mL)	EBIBI (mol)
$PSty_4Br+PSty_7Br$	60	1.2	8.18×10^{-3}
$PSty_{14}Br$	180	0.4	2.72×10^{-3}
$PSty_{15}Br$	180	0.4	2.72×10^{-3}

5.3.5 Macroinitiators purification

Two distinct procedures were followed for the purification of the longer chains ($PSty_{14}Br$ and $PSty_{15}Br$) and shorter chains ($PSty_4Br$ and $PSty_7Br$) and are described below:

- **$PSty_{14}Br$ and $PSty_{15}Br$:** The obtained colourless solution was distilled at a rotary evaporator until a slightly yellow tinted oily residue was left at 50 °C water temperature and full vacuum. 50 mL of methanol (MeOH) were added to the residue and a white suspension was formed. The dispersion was precipitated overnight in the freezer at -15 °C. The obtained product was then precipitated in methanol, filtered and precipitated again, repeating the procedure for a total of 3 times. Lastly, the product was dried in rotavapor at full vacuum and 50 °C for at least an hour after the complete removal of the solvent (It's recommended to closely observe and regulate temperature and vacuum until most or all of the solvent is removed to prevent formation of highly voluminous foams).
- **$PSty_{3.6}Br$ and $PSty_{6.6}Br$:** After filtration over the neutral alumina column the resulting solution was first filtered over a short silica column and washed with a 99:1 hexane/ethyl acetate mixture to elute most of the styrene. The silica, now embedded with styrene oligomers, was collected and dried through a rotary evaporator. The resulting powder was then separated in an automated silica column (Biotage®), eluting with hexane/ethyl acetate 99:1 and gradually decreasing the ratio to 80:20. The first fraction containing product and the last one were then characterized as $PSty_{3.6}Br$ and $PSty_{6.6}Br$ macroinitiator mixtures.

REFERENCES

(1) *The IUPAC Compendium of Chemical Terminology: The Gold Book*, 4th ed.; Gold, V., Ed.; International Union of Pure and Applied Chemistry (IUPAC): Research Triangle Park, NC, 2019. https://doi.org/10.1351/goldbook.

(2) Rudin, A.; Choi, P. Ionic and Coordinated Polymerizations. In *The Elements of Polymer Science & Engineering*; Elsevier, 2013; pp 449–493. https://doi.org/10.1016/B978-0-12-382178-2.00011-0.

(3) Yamada, B.; Zetterlund, P. B. General Chemistry of Radical Polymerization. In *Handbook of Radical Polymerization*; Matyjaszewski, K., Davis, T. P., Eds.; Wiley, 2002; pp 117–186. https://doi.org/10.1002/0471220450.ch3.

(4) *Handbook of Radical Polymerization*, 1st ed.; Matyjaszewski, K., Davis, T. P., Eds.; Wiley, 2002. https://doi.org/10.1002/0471220450.

(5) Szwarc, M. 'Living' Polymers. *Nature* **1956**, *178* (4543), 1168–1169. https://doi.org/10.1038/1781168a0.

(6) Webster, O. W. Living Polymerization Methods. *Science* **1991**, *251* (4996), 887–893. https://doi.org/10.1126/science.251.4996.887.

(7) Braunecker, W. A.; Matyjaszewski, K. Controlled/Living Radical Polymerization: Features, Developments, and Perspectives. *Prog. Polym. Sci.* **2007**, *32* (1), 93–146. https://doi.org/10.1016/j.progpolymsci.2006.11.002.

(8) Minisci, F. Free-Radical Additions to Olefins in the Presence of Redox Systems. *Acc. Chem. Res.* **1975**, *8* (5), 165–171. https://doi.org/10.1021/ar50089a004.

(9) Pintauer, T.; Matyjaszewski, K. Atom Transfer Radical Addition and Polymerization Reactions Catalyzed by Ppm Amounts of Copper Complexes. *Chem. Soc. Rev.* **2008**, *37* (6), 1087. https://doi.org/10.1039/b714578k.

(10) Wang, J.-S.; Matyjaszewski, K. Controlled/"living" Radical Polymerization. Atom Transfer Radical Polymerization in the Presence of Transition-Metal Complexes. *J. Am. Chem. Soc.* **1995**, *117* (20), 5614–5615. https://doi.org/10.1021/ja00125a035.

(11) Kato, M.; Kamigaito, M.; Sawamoto, M.; Higashimura, T. Polymerization of Methyl Methacrylate with the Carbon Tetrachloride/Dichlorotris- (Triphenylphosphine)Ruthenium(II)/Methylaluminum Bis(2,6-Di-Tert-Butylphenoxide) Initiating System: Possibility of Living Radical Polymerization. *Macromolecules* **1995**, *28* (5), 1721–1723. https://doi.org/10.1021/ma00109a056.

(12) Tang, W.; Matyjaszewski, K. Effects of Initiator Structure on Activation Rate Constants in ATRP. *Macromolecules* **2007**, *40* (6), 1858–1863. https://doi.org/10.1021/ma062897b.

(13) Isse, A. A.; Gennaro, A. Electrochemistry for Atom Transfer Radical Polymerization. *Chem. Rec.* **2021**, *21* (9), 2203–2222. https://doi.org/10.1002/tcr.202100028.

(14) Braunecker, W. A.; Tsarevsky, N. V.; Gennaro, A.; Matyjaszewski, K. Thermodynamic Components of the Atom Transfer Radical Polymerization Equilibrium: Quantifying Solvent Effects. *Macromolecules* **2009**, *42* (17), 6348–6360. https://doi.org/10.1021/ma901094s.

(15) Fantin, M.; Tognella, E.; Antonello, A.; Lorandi, F.; Calore, E.; Macior, A.; Durante, C.; Isse, A. A. Effects of Solvent and Monomer on the Kinetics of Radical Generation in Atom Transfer Radical Polymerization. *ChemElectroChem* **2024**, *11* (6), e202300662. https://doi.org/10.1002/celc.202300662.

(16) Lorandi, F.; Matyjaszewski, K. Why Do We Need More Active ATRP Catalysts? *Isr. J. Chem.* **2020**, *60* (1–2), 108–123. https://doi.org/10.1002/ijch.201900079.

(17) Gennaro, A.; Magenau, A. J. D.; Strandwitz, N. C.; Matyjaszewski, K. Electrochemically Mediated Atom Transfer Radical Polymerization. *Science* **2011**, *332* (6025), 81–84. https://doi.org/10.1126/science.1202357.

(18) Chmielarz, P.; Fantin, M.; Park, S.; Isse, A. A.; Gennaro, A.; Magenau, A. J. D.; Sobkowiak, A.; Matyjaszewski, K. Electrochemically Mediated Atom Transfer Radical Polymerization (eATRP). *Prog. Polym. Sci.* **2017**, *69*, 47–78. https://doi.org/10.1016/j.progpolymsci.2017.02.005.

(19) Lorandi, F.; Fantin, M.; Isse, A. A.; Gennaro, A. Electrochemically Mediated Atom Transfer Radical Polymerization of N-Butyl Acrylate on Non-Platinum Cathodes. *Polym. Chem.* **2016**, *7* (34), 5357–5365. https://doi.org/10.1039/C6PY01032F.

(20) Ardkhean, R.; Fletcher, S. P.; Paton, R. S. Ligand Design for Asymmetric Catalysis: Combining Mechanistic and Chemoinformatics Approaches. In *New Directions in the Modeling of Organometallic Reactions*; Lledós, A., Ujaque, G., Eds.; Topics in Organometallic Chemistry; Springer International Publishing: Cham, 2020; Vol. 67, pp 153–189. https://doi.org/10.1007/3418_2020_47.

(21) Kumar, A.; Sun, S.-S.; Lees, A. J. Directed Assembly Metallocyclic Supramolecular Systems for Molecular Recognition and Chemical Sensing. *Coord. Chem. Rev.* **2008**, *252* (8–9), 922–939. https://doi.org/10.1016/j.ccr.2007.07.023.

(22) Leenders, S. H. A. M.; Gramage-Doria, R.; De Bruin, B.; Reek, J. N. H. Transition Metal Catalysis in Confined Spaces. *Chem. Soc. Rev.* **2015**, *44* (2), 433–448. https://doi.org/10.1039/C4CS00192C.

(23) Carmo Dos Santos, N. A.; Lorandi, F.; Badetti, E.; Wurst, K.; Isse, A. A.; Gennaro, A.; Licini, G.; Zonta, C. Tuning the Reactivity and Efficiency of Copper Catalysts for Atom Transfer Radical Polymerization by Synthetic Modification of Tris(2-Methylpyridyl)Amine. *Polymer* **2017**, *128*, 169–176. https://doi.org/10.1016/j.polymer.2017.09.018.

(24) Anderegg, G.; Hubmann, E.; Podder, N. G.; Wenk, F. Pyridinderivate Als Komplexbildner. XI. Die Thermodynamik Der Metallkomplexbildung Mit Bis-, Tris- Und Tetrakis[(2-pyridyl)Methyl]-aminen. *Helv. Chim. Acta* **1977**, *60* (1), 123–140. https://doi.org/10.1002/hlca.19770600115.

(25) Abdel-Magid, A. F.; Carson, K. G.; Harris, B. D.; Maryanoff, C. A.; Shah, R. D. Reductive Amination of Aldehydes and Ketones with Sodium Triacetoxyborohydride. Studies on Direct and Indirect Reductive Amination Procedures [1]. *J. Org. Chem.* **1996**, *61* (11), 3849–3862. https://doi.org/10.1021/jo960057x.

(26) Bravin, C.; Badetti, E.; Licini, G.; Zonta, C. Tris(2-Pyridylmethyl)Amines as Emerging Scaffold in Supramolecular Chemistry. *Coord. Chem. Rev.* **2021**, *427*, 213558. https://doi.org/10.1016/j.ccr.2020.213558.

(27) Porras Gutiérrez, A. G.; Zeitouny, J.; Gomila, A.; Douziech, B.; Cosquer, N.; Conan, F.; Reinaud, O.; Hapiot, P.; Le Mest, Y.; Lagrost, C.; Le Poul, N. Insights into Water Coordination Associated with the Cu^{II}/Cu^{I} Electron Transfer at a Biomimetic Cu Centre. *Dalton Trans* **2014**, *43* (17), 6436–6445. https://doi.org/10.1039/C3DT53548G.

(28) Otter, C. A.; Hartshorn, R. M. Preparation and Photochemistry of Cobalt(Iii) Amino and Amino Acidato Complexes Containing Tripodal Polypyridine ligandsElectronic Supplementary Information (ESI) Available: Synthetic, Spectroscopic and Crystallographic Details. See Http://Www.Rsc.Org/Suppdata/Dt/B3/B311809f/. *Dalton Trans.* **2004**, No. 1, 150. https://doi.org/10.1039/b311809f.

(29) Jenkins, H. A.; Klempner, M. J.; Prokopchuk, E. M.; Puddephatt, R. J. Dimethyl(Hydrido)Platinum(IV) Chemistry Related to Methane Activation: The Effect of a Tetradentate Ligand. *Inorganica Chim. Acta* **2003**, *352*, 72–78. https://doi.org/10.1016/S0020-1693(03)00148-8.

(30) Benazzi, E.; Begato, F.; Niorettini, A.; Destro, L.; Wurst, K.; Licini, G.; Agnoli, S.; Zonta, C.; Natali, M. Electrocatalytic Hydrogen Evolution Using Hybrid Electrodes Based

on Single-Walled Carbon Nanohorns and Cobalt(II) Polypyridine Complexes. *J. Mater. Chem. A* **2021**, *9* (35), 20032–20039. https://doi.org/10.1039/D1TA03645A.

(31) Natali, M.; Badetti, E.; Deponti, E.; Gamberoni, M.; Scaramuzzo, F. A.; Sartorel, A.; Zonta, C. Photoinduced Hydrogen Evolution with New Tetradentate Cobalt(II) Complexes Based on the TPMA Ligand. *Dalton Trans.* **2016**, *45* (37), 14764–14773. https://doi.org/10.1039/C6DT01705C.

(32) Chan, S. L.-F.; Lam, T. L.; Yang, C.; Yan, S.-C.; Cheng, N. M. A Robust and Efficient Cobalt Molecular Catalyst for CO 2 Reduction. *Chem. Commun.* **2015**, *51* (37), 7799–7801. https://doi.org/10.1039/C5CC00566C.

(33) Upper, D. THE UNSUCCESSFUL SELF-TREATMENT OF A CASE OF “WRITER’S BLOCK”1. *J. Appl. Behav. Anal.* **1974**, *7* (3), 497–497. https://doi.org/10.1901/jaba.1974.7-497a.

(34) Chan, S. L.-F.; Lam, T. L.; Yang, C.; Lai, J.; Cao, B.; Zhou, Z.; Zhu, Q. Cobalt(II) Tris(2-Pyridylmethyl)Amine Complexes [Co(TPA)X]+ Bearing Coordinating Anion (X = Cl−, Br−, I− and NCS−): Synthesis and Application for Carbon Dioxide Reduction. *Polyhedron* **2017**, *125*, 156–163. https://doi.org/10.1016/j.poly.2016.09.049.

(35) You, L.; Pescitelli, G.; Anslyn, E. V.; Di Bari, L. An Exciton-Coupled Circular Dichroism Protocol for the Determination of Identity, Chirality, and Enantiomeric Excess of Chiral Secondary Alcohols. *J. Am. Chem. Soc.* **2012**, *134* (16), 7117–7125. https://doi.org/10.1021/ja301252h.

(36) Kiggen, W.; Vögtle, F. Functionalized, Oligocyclic Large Cavities — A Novel Siderophore. *Angew. Chem. Int. Ed. Engl.* **1984**, *23* (9), 714–715. https://doi.org/10.1002/anie.198407141.

(37) Zhang, G.; Mastalerz, M. Organic Cage Compounds – from Shape-Persistency to Function. *Chem Soc Rev* **2014**, *43* (6), 1934–1947. https://doi.org/10.1039/C3CS60358J.

(38) Lehn, J.-M. Dynamic Combinatorial Chemistry and Virtual Combinatorial Libraries. *Chem. – Eur. J.* **1999**, *5* (9), 2455–2463. https://doi.org/10.1002/(SICI)1521-3765(19990903)5:9<2455::AID-CHEM2455>3.0.CO;2-H.

(39) Mastalerz, M. Shape-Persistent Organic Cage Compounds by Dynamic Covalent Bond Formation. *Angew. Chem. Int. Ed.* **2010**, *49* (30), 5042–5053. https://doi.org/10.1002/anie.201000443.

(40) Schouwey, C.; Scopelliti, R.; Severin, K. An Imine-Based Molecular Cage with Distinct Binding Sites for Small and Large Alkali Metal Cations. *Chem. – Eur. J.* **2013**, *19* (20), 6274–6281. https://doi.org/10.1002/chem.201300098.

(41) Bravin, C.; Mason, G.; Licini, G.; Zonta, C. A Diastereodynamic Probe Transducing Molecular Length into Chiroptical Readout. *J. Am. Chem. Soc.* **2019**, *141* (30), 11963–11969. https://doi.org/10.1021/jacs.9b04151.

(42) Lin, Z.; Sun, J.; Efremovska, B.; Warmuth, R. Assembly of Water-Soluble, Dynamic, Covalent Container Molecules and Their Application in the Room-Temperature Stabilization of Protoadamantene. *Chem. – Eur. J.* **2012**, *18* (40), 12864–12872. https://doi.org/10.1002/chem.201200602.

(43) Boaler, P. J.; Piskorz, T. K.; Bickerton, L. E.; Wang, J.; Duarte, F.; Lloyd-Jones, G. C.; Lusby, P. J. Origins of High-Activity Cage-Catalyzed Michael Addition. *J. Am. Chem. Soc.* **2024**, *146* (28), 19317–19326. https://doi.org/10.1021/jacs.4c05160.

(44) Cook, T. R.; Stang, P. J. Recent Developments in the Preparation and Chemistry of Metallacycles and Metallacages via Coordination. *Chem. Rev.* **2015**, *115* (15), 7001–7045. https://doi.org/10.1021/cr5005666.

(45) Chen, S.; Chen, L.-J. Metal–Organic Cages: Applications in Organic Reactions. *Chemistry* **2022**, *4* (2), 494–519. https://doi.org/10.3390/chemistry4020036.

(46) Takezawa, H.; Shitozawa, K.; Fujita, M. Enhanced Reactivity of Twisted Amides inside a Molecular Cage. *Nat. Chem.* **2020**, *12* (6), 574–578. https://doi.org/10.1038/s41557-020-0455-y.

(47) Gramage-Doria, R.; Hessels, J.; Leenders, S. H. A. M.; Tröppner, O.; Dürr, M.; Ivanović-Burmazović, I.; Reek, J. N. H. Gold(I) Catalysis at Extreme Concentrations Inside Self-Assembled Nanospheres. *Angew. Chem. Int. Ed.* **2014**, *53* (49), 13380–13384. https://doi.org/10.1002/anie.201406415.

(48) Cullen, W.; Takezawa, H.; Fujita, M. Demethylenation of Cyclopropanes via Photoinduced Guest-to-Host Electron Transfer in an M_6L_4 Cage. *Angew. Chem. Int. Ed.* **2019**, *58* (27), 9171–9173. https://doi.org/10.1002/anie.201904752.

(49) Bravin, C.; Badetti, E.; Scaramuzzo, F. A.; Licini, G.; Zonta, C. Triggering Assembly and Disassembly of a Supramolecular Cage. *J. Am. Chem. Soc.* **2017**, *139* (18), 6456–6460. https://doi.org/10.1021/jacs.7b02341.

(50) Acharyya, K.; Mukherjee, P. S. Organic Imine Cages: Molecular Marriage and Applications. *Angew. Chem. Int. Ed.* **2019**, *58* (26), 8640–8653. https://doi.org/10.1002/anie.201900163.

(51) Joyce, L. A.; Maynor, M. S.; Dragna, J. M.; Da Cruz, G. M.; Lynch, V. M.; Canary, J. W.; Anslyn, E. V. A Simple Method for the Determination of Enantiomeric Excess and Identity of Chiral Carboxylic Acids. *J. Am. Chem. Soc.* **2011**, *133* (34), 13746–13752. https://doi.org/10.1021/ja205775g.

(52) Zonta, C.; Begato, F.; Penasa, R.; Wurst, K.; Licini, G. Combining Imine Condensation Chemistry with [3,3] Diaza-Cope Rearrangement for One-Step Formation of Hydrolytically Stable Chiral Architectures. *Angew. Chem. Int. Ed.* **2023**, *62* (30), e202304490. https://doi.org/10.1002/anie.202304490.

(53) Chin, J.; Mancin, F.; Thavarajah, N.; Lee, D.; Lough, A.; Chung, D. S. Controlling Diaza-Cope Rearrangement Reactions with Resonance-Assisted Hydrogen Bonds. *J. Am. Chem. Soc.* **2003**, *125* (50), 15276–15277. https://doi.org/10.1021/ja0387554.

(54) Kim, H.-J.; Kim, H.; Alhakimi, G.; Jeong, E. J.; Thavarajah, N.; Studnicki, L.; Koprianiuk, A.; Lough, A. J.; Suh, J.; Chin, J. Preorganization in Highly Enantioselective Diaza-Cope Rearrangement Reaction. *J. Am. Chem. Soc.* **2005**, *127* (47), 16370–16371. https://doi.org/10.1021/ja055776k.

(55) Begato, F.; Penasa, R.; Licini, G.; Zonta, C. Chiroptical Enhancement of Chiral Dicarboxylic Acids from Confinement in a Stereodynamic Supramolecular Cage. *ACS Sens.* **2022**, *7* (5), 1390–1394. https://doi.org/10.1021/acssensors.2c00038.

(56) Fantin, M.; Isse, A. A.; Matyjaszewski, K.; Gennaro, A. ATRP in Water: Kinetic Analysis of Active and Super-Active Catalysts for Enhanced Polymerization Control. *Macromolecules* **2017**, *50* (7), 2696–2705. https://doi.org/10.1021/acs.macromol.7b00246.

(57) Nicholson, R. S. Theory and Application of Cyclic Voltammetry for Measurement of Electrode Reaction Kinetics. *Anal. Chem.* **1965**, *37* (11), 1351–1355. https://doi.org/10.1021/ac60230a016.

(58) Krys, P.; Matyjaszewski, K. Kinetics of Atom Transfer Radical Polymerization. *Eur. Polym. J.* **2017**, *89*, 482–523. https://doi.org/10.1016/j.eurpolymj.2017.02.034.

(59) Nikitin, A. N.; Hutchinson, R. A.; Buback, M.; Hesse, P. Determination of Intramolecular Chain Transfer and Midchain Radical Propagation Rate Coefficients for Butyl Acrylate by Pulsed Laser Polymerization. *Macromolecules* **2007**, *40* (24), 8631–8641. https://doi.org/10.1021/ma071413o.

(60) Ahmad, N. M.; Charleux, B.; Farcet, C.; Ferguson, C. J.; Gaynor, S. G.; Hawkett, B. S.; Heatley, F.; Klumperman, B.; Konkolewicz, D.; Lovell, P. A.; Matyjaszewski, K.; Venkatesh, R. Chain Transfer to Polymer and Branching in Controlled Radical

Polymerizations of *n* -Butyl Acrylate. *Macromol. Rapid Commun.* **2009**, *30* (23), 2002–2021. https://doi.org/10.1002/marc.200900450.

(61) Plessis, C.; Arzamendi, G.; Leiza, J. R.; Schoonbrood, H. A. S.; Charmot, D.; Asua, J. M. A Decrease in Effective Acrylate Propagation Rate Constants Caused by Intramolecular Chain Transfer. *Macromolecules* **2000**, *33* (1), 4–7. https://doi.org/10.1021/ma991205z.

(62) Sarbu, T.; Lin, K.-Y.; Ell, J.; Siegwart, D. J.; Spanswick, J.; Matyjaszewski, K. Polystyrene with Designed Molecular Weight Distribution by Atom Transfer Radical Coupling. *Macromolecules* **2004**, *37* (9), 3120–3127. https://doi.org/10.1021/ma035901h.

(63) De Bon, F.; Carlan, G. M.; Tognella, E.; Isse, A. A. Exploring Electrochemically Mediated ATRP of Styrene. *Processes* **2021**, *9* (8), 1327. https://doi.org/10.3390/pr9081327.

6 APPENDIX

6.1 Appendix A

6.1.1 Effect of monomer choice on key polymerization parameters

The polymerization of several monomers catalysed by $[Br_2Cu^{II}_2CAGE]^{2+}$ was studied, including acrylates, methacrylates and styrene. For comparison similar experiments performed with the thoroughly studied "standard" catalyst $[BrCu^{II}TPMA]^{+}$ are reported (**Table 10**).

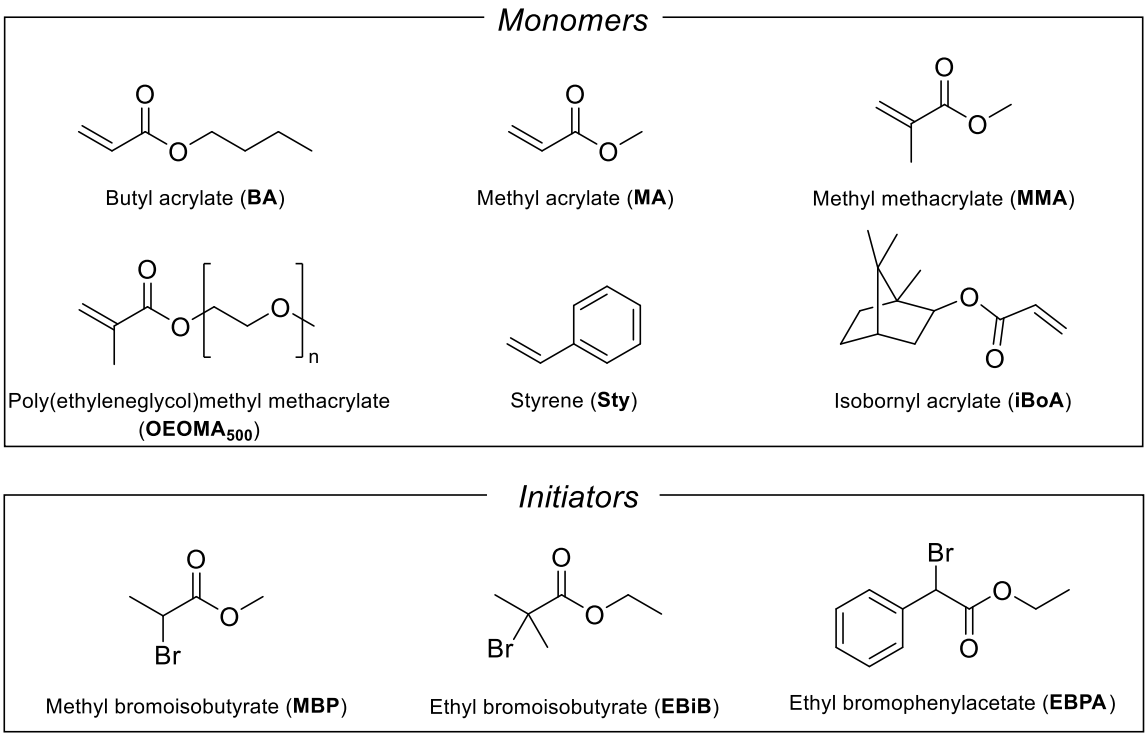

Table 7. Electrochemically mediated ATRP of various monomers with $[Cu^{II}TPMA]^{2+}$ and $[Cu^{II}CAGE]^{2+}$.

Monomer	Entry	Ligand	E_{app} V	t min	DP	$Conv$ %	$10^3 M_{n,th}$	$10^3 M_{n,exp}$	$Đ$	$10^3 k_{app}$[a] min^{-1}	Q_{exp} C
BA	1	CAGE	$E_{1/2\text{-}60mV}$	300	1000	78.3	100.6	53.1	1.49	5.3	1.19
	2	TPMA	$E_{1/2}$	300	1000	87.2	79.1	53.1	1.49	3.8	1.19
MA	3	CAGE	$E_{1/2\text{-}60mV}$	300	600	86.5	44.7	37.9	1.45	9.3	1.23
	4	TPMA	$E_{1/2}$	270	600	61.0	30.2	23.9	1.11	7.5	0.54
MMA	5	CAGE	$E_{1/2\text{-}60mV}$	300	300	59.5	15.1	13.6	1.27	3.1	2.56
	6	TPMA[b]	$E_{1/2+60mV}$	720	467	77.0	36	45.9	1.12	1.8	8.93
$OEOMA_{500}$	7	CAGE	$E_{1/2\text{-}60mV}$	300	300	-[d]	-[d]	100.2	2.22	-[d]	1.20
	8	TPMA	$E_{1/2\text{-}60mV}$	240	300	-[d]	-[d]	82.8	1.66	-[d]	1.53
Sty[e]	9	CAGE	$E_{1/2\text{-}60mV}$	1380	600	5.8	3.5	4.2	1.11	1.2	/
	10	TPMA[c]	$E_{1/2}$	240	580	11	6.7	5.6	1.33	0.48	7.7
iBoA	11	CAGE	$E_{1/2\text{-}60mV}$	360	-[d]	-[d]	15.1	13.6	1.27	-[d]	0.94

General conditions: Solvent: DMF, T = 50 °C, Monomer:DMF = 25:75 v/v, V_{tot} = 6 mL, [Monomer]/[Initiator] = DP, $[L]/[Cu^{2+}]/[Br^-]$ = 1/1/1 for $[CuTPMA]^{2+}$, 0.5/1/1 for Cu/CAGE, Initiator: ethyl α-bromoisobutyrate

[a] the slope of the $\ln([M_0]/[M])$ vs t plot

[b] literature data[23], T = 25°C, V_{tot} = 15mL

[c] literature data[63], T = 80°C, V_{tot} = 10mL

[d] not measured

[e] Sty:DMF = 50:50 in v/v

The **Cu_2CAGE** catalyst seems to be capable of performing eATRP of a variety of monomers, although the achieved degree of control and polymerization rates seems generally slightly worse than those obtained with **CuTPMA.**

6.1.2 Role of the polymerization initiator

Different ATRP initiators were evaluated for the polymerization of butyl acrylate (BA) and methyl methacrylate (MMA) using the $[Br_2Cu^{II}_2CAGE]^{2+}$ catalyst.

Table 8 Electrochemically mediated ATRP of BA and MMA using various initiators with [CuIITPMA]2+ and [CuIICAGE]2+

Monomer	Entry	Initiator	Ligand	*t* min	*DP*	*Conv* %	$10^3 M_{n,th}$	$10^3 M_{n,exp}$	*Đ*	$10^3 k_{app}$ min^{-1}	Q_{exp} C
BA	1	MBP	CAGE	480	1000	87.3	112.1	58.5	1.57	5.23	1.35
	2	MBP	TPMA	300	2000	40.9	105	55.5	1.49	2.80	1.02
	3	EBiB	CAGE	300	1000	78.3	100.6	53.1	1.49	5.32	1.19
	4	EBiB	TPMA	300	1000	87.2	79.1	53.1	1.49	3.77	1.19
	5	EBPA	CAGE	180	300	<5	/	/	/	/	1.72
MMA	6	EBiB	CAGE	300	300	59.5	15.1	13.6	1.27	3.08	2.56
	7	EBPA	CAGE	300	200	<5	/	/	/	/	/
	8	EBPA[b]	TPMA	720	467	77	36	45.9	1.12	1.83	8.93

a General conditions: $[Cu^{2+}] = 10^{-3}$ M, T = 50 °C, V_{tot} = 6 mL, $[(n\text{-}Bu)_4NPF_6]$ = 0.1 M, $[L]/[Cu^{2+}]/[Br^-]$ = 1/1/1 for $[CuTPMA]^{2+}$, 0.5/1/1 for $[Cu^{II}_2CAGE]^{4+}$, $E_{app} = E_{1/2}$ for $[CuTPMA]^{2+}$, $E_{app} = E_{1/2\text{-}60mV}$ for $[Cu^{II}_2CAGE]^{4+}$.

b literature data[23], T = 25 °C, $E_{app} = E_{1/2+60mV}$, V_{tot} = 15 Ml

The **Cu_2CAGE** catalyst appears to initiate both the commonly used EBIB and MBP initiators, although the most active EBPA results problematic, maybe due to a too high reactivity leading to secondary reactions, possibly with the other copper centre within the cage.

An higher apparent rate of initiation was also observed for the **Cu_2CAGE** although it might be caused by the different conditions required to perform eATRP with this catalyst, namely the much more negative applied potential.

6.2 Appendix B

6.2.1 Cyclic voltammetries of Cu_2CAGE at varying concentration of bromide anions

The **Cu_2CAGE** was titrated by adding *n*-Bu_4NBr in discrete steps of concentration to study its behaviour in the presence of bromide anions.

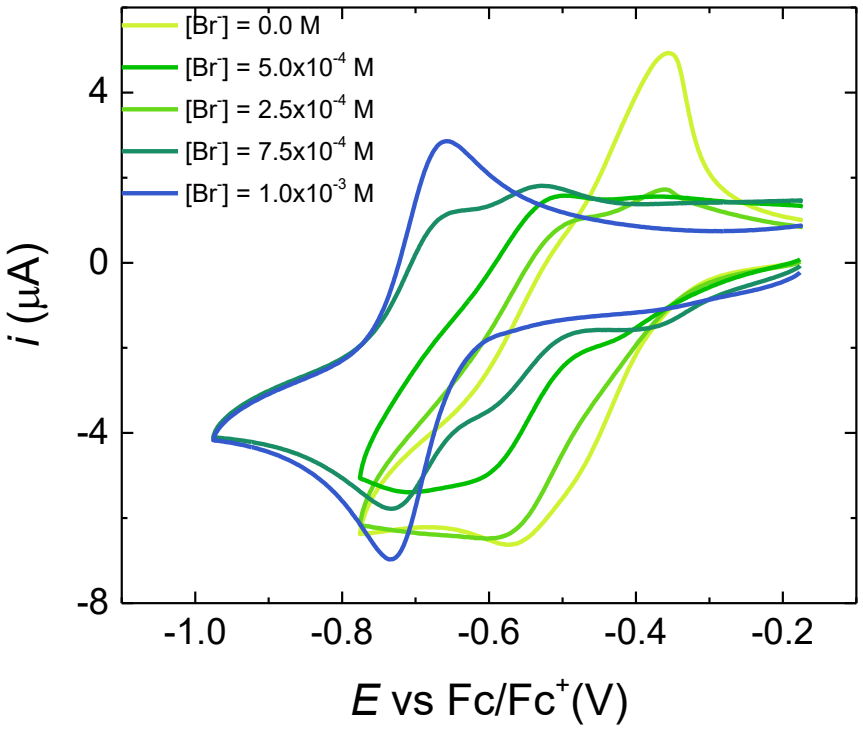

Figure 32 Cyclic voltammetry of $[Cu^{II}_2CAGE]^{4+}$ at increasing *n*-Bu_4NBr concentration

The results show, as discussed in section 3.1.2, a gradual shift from the voltammetry of the "empty" **Cu_2CAGE** (light green curve) to that of the dibrominated complex (blue curve)

The experiment was extended to observe the behaviour of the **Cu_2CAGE** complex in an excess of bromide ions.

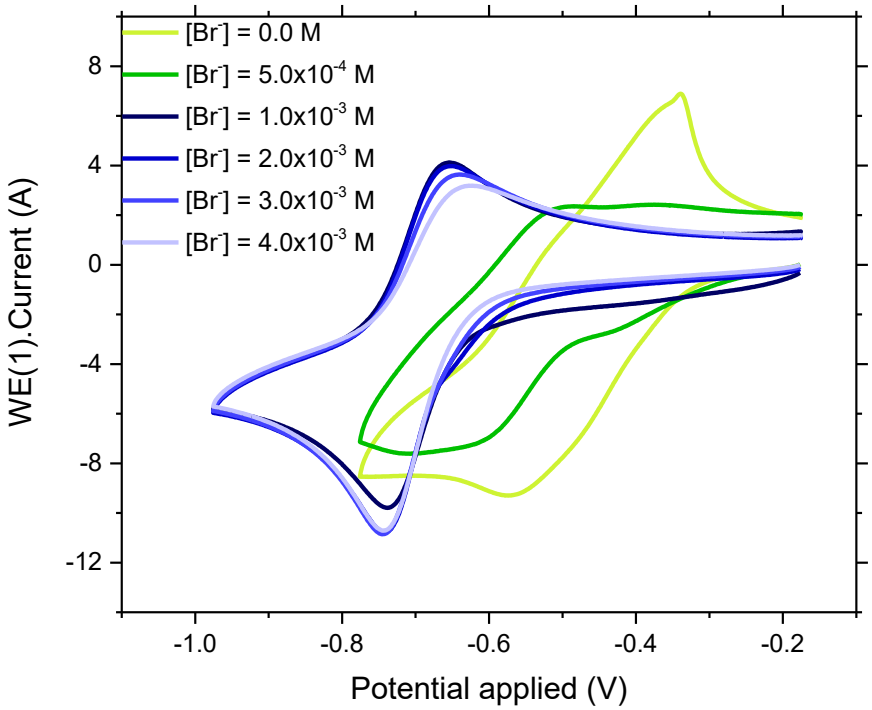

Figure 33 Cyclic voltammetry of $[Cu^{II}_2CAGE]^{4+}$ at increasing *n*-Bu_4NBr concentration

As mentioned in section 3.1.2, an excess of bromide anions concentration leads to no further shift in the redox potential of the couple.